

AALTO UNIVERSITY
School of Engineering
Department of Engineering Design and Production

Teemu Halmeaho

Magnetic bearing as switched reluctance motor

**Thesis submitted in partial fulfillment of the requirements for the degree of
Master of Science in Technology**

Espoo, August 7, 2012

Supervisor: Professor Petri Kuosmanen
Instructor: Kari Tammi, D.Sc. (Tech.)

AALTO UNIVERSITY SCHOOLS OF TECHNOLOGY PO Box 11000, FI-00076 AALTO http://www.aalto.fi		ABSTRACT OF THE MASTER'S THESIS	
Author: Teemu Halmeaho			
Title: Magnetic bearing as Switched Reluctance Motor			
School: School of Engineering			
Department: Department of Engineering Design and Production			
Professorship: Machine Design		Code: Kon-41	
Supervisor: Professor Petri Kuosmanen			
Instructor: Kari Tammi, D.Sc. (Tech.)			
<p>Abstract:</p> <p>The goal of this work was to research the similarities between active magnetic bearings and switched reluctance motor and particularly research the chances for converting magnetic bearing into switched reluctance motor. In addition, ways to cope with the widely reported problems the motor type has were studied. The test environment consisted of test rig, previously used for testing control methods for magnetic bearing. In addition to this, MATLAB Simulink simulation models were built to help the designing of the test setup. The test setup had two alternative controllers, an original magnetic bearing controller, modified to work as a motor controller and a new CompactRIO-based controller that was used for comparing different speed control and commutation methods. New rotor designs were engineered to work with the prototype motor that used unmodified magnetic bearing stator. This setup was tested for obtaining the output torque and maximum speed of the motor together with the accuracy to follow set values. Test results of simulations and test setup were inside the error margins, showing the use of simulations beneficial in design process of this type of a motor. The tests revealed differences between the control methods, suggesting using the advanced angle controller and adjustable commutation angles.</p>			
Date: 7.8.2012	Language: English		Number of pages: 86 + 12
Keywords: magnetic bearing, reluctance motor, speed control, machine design, simulation			

AALTO-YLIOPISTO PL 11000, 00076 AALTO http://www.aalto.fi		DIPLOMITYÖN TIIVISTELMÄ	
Tekijä: Teemu Halmeaho			
Työn nimi: Aktiivinen magneettilaakeri vaihtoreluktanssimoottorina			
Korkeakoulu: Insinööritieteiden korkeakoulu			
Laitos: Koneenrakennustekniikan laitos			
Professori: Koneensuunnitteluoppi		Koodi: Kon-41	
Työn valvoja: Professori Petri Kuosmanen			
Työn ohjaaja: Tekniikan tohtori Kari Tammi			
<p>Tiivistelmä:</p> <p>Työn tavoitteena oli tutkia yhteneväisyyksiä aktiivimagneettilaakerien ja vaihtoreluktanssimoottorin välillä. Tutkimus keskittyi erityisesti arvioimaan mahdollisuuksia muuntaa magneettilaakeri vaihtoreluktanssimoottoriksi. Lisäksi tutkittiin keinoja ratkaista ongelmia, joita tämän tyyppisessä sähkömoottorissa on raportoitu olevan. Testiympäristö koostui roottorikoelaitteesta, jota on aikaisemmin käytetty magneettilaakerin säätöjärjestelmän tutkimuksessa. Lisäksi rakennettiin MATLAB Simulink simulointimalli, jota käytettiin moottorin säätöjärjestelmän suunnittelun apuna. Testilaitteessa oli kaksi vaihtoehtoista säätöjärjestelmää; alkuperäinen magneettilaakerin ohjain muokattuna toimimaan moottorin ohjaimena sekä uusi CompactRIO -järjestelmään perustuva säätöjärjestelmä. Jälkimmäistä käytettiin erilaisten nopeus- ja kommutointitapojen vertailuun keskenään. Prototyypimoottorin staattori oli sama, jota käytettiin magneettilaakerin kanssa. Roottori suunniteltiin sopimaan juuri tähän käyttötarkoitukseen. Tätä koelaitetta testattiin vääntömomentin ja maksiminopeuden selvittämiseksi. Lisäksi suoritettiin testejä, joissa tutkittiin kykyä seurata nopeuden asetusarvoa. Simuloimalla saadut tulokset olivat hyvin lähellä koelaitteella saatuja tuloksia osoittaen simuloinnin käytön olevan hyödyllistä tämän tyyppisen moottorin suunnittelussa. Säätömenetelmät suoriutuivat vaihtelevalla menestyksellä testeistä. Suositeltava säätömenetelmä oli edistyskulman säädin, joka käytti hyväkseen säädettäviä kommutointikulmia.</p>			
Päivämäärä: 7.8.2012		Kieli: englanti	Sivumäärä: 86 + 12
Avainsanat: magneettilaakeri, reluktanssimoottori, nopeussäätö, koneensuunnittelu, simulointi			

Foreword

The work in this Master's Thesis was carried out at VTT, Technical Research Centre of Finland, Industrial Systems, in Electrical Product Concepts team of Smart Machines knowledge center. I wish to thank former Technology Manager of smart machines Pekka Koskinen for giving me the chance to work at VTT in the first place. I am also grateful to current Technology Manager Johannes Hyrynen for giving me the opportunity to carry on working in this great team.

I wish to thank Professor Petri Kuosmanen, the supervisor of this thesis, and Res. Prof. Tammi, the instructor of the thesis. I greatly appreciate the wisdom of both of you.

I would like to express my gratitude towards M.Sc. (Tech) Tuomas Haarnoja, who co-instructed this work with Res. Prof. Tammi. In addition to this, he had notable contribution on FEM modeling part of this work together with the design and manufacturing of an electrical converter circuit needed in this work. I wish to thank also Mr. Timo Lindroos for milling the rotor parts despite his busy schedule. I also thank other colleagues who helped me during this work.

I wish to thank my family and friends, specially my parents-in-law Dr. Kirsi-Marja Oksman-Caldentey and Dr. Javier Caldentey for sharing me their scientific perspective of life and giving guidance throughout this work. The most of everyone I wish to thank my beautiful wife Tania for standing by me not just during this thesis but also for the whole time of my studentship. For my ten months old son Nico, I am grateful for tearing only a few pages of the drafts.

Espoo, 7.8.2012

Teemu Halmeaho

Table of Contents

Abstract

Tiivistelmä

Foreword

Nomenclature

1	Introduction.....	1
1.1	Background	1
1.2	Research problems	3
1.3	Aim of the research	3
1.4	Limitations	4
1.5	Methods of research	4
1.6	Own contribution	5
2	Magnetic bearings and Switched Reluctance Motor	6
2.1	Magnetic bearings	6
2.2	Electric motors in general	8
2.3	SRM compared to other electric motors	11
2.4	Physical characteristics behind SRM.....	13
3	State of the art	17
3.1	Research on SRM	17
3.2	Control theory for basic SRM operation.....	19
3.2.1	Mathematical model	20
3.2.2	Power electronics and controller.....	26
3.3	Solutions for problems with SRM	30
3.3.1	Torque ripple.....	30
3.3.2	Radial vibration.....	31
3.3.3	Noise	33
3.3.4	Bearingless SRM	34
4	Materials & methods	37
4.1	Test environment	37
4.1.1	Simulations of the model	39

4.1.2	Test setups.....	40
4.2	Test planning.....	45
4.2.1	Rotor designs	45
4.2.2	Steps of the tests	46
4.3	Estimations for error	49
4.3.1	Error in mathematical methods.....	49
4.3.2	Error in test setup	49
5	Results	51
5.1	Deceleration measurements to obtain resistance torque	51
5.2	Acceleration measurements to obtain torque values.....	51
5.2.1	Acceleration from 240 rpm to 420 rpm using the AMB controller	52
5.2.2	Acceleration from 0 rpm to 250 rpm using different control methods in the cRIO	54
5.2.3	Acceleration from 240 rpm to 420 rpm using different control methods in the cRIO	57
5.2.4	Acceleration in simulations	59
5.3	Step and sweep response measurements.....	63
5.3.1	Sweep response with AMB.....	63
5.3.2	Step response with cRIO.....	65
5.4	Maximum speeds	69
5.4.1	Using AMB.....	69
5.4.2	Using cRIO	71
6	Discussion	73
6.1	Conclusions from test results.....	73
6.2	Applications for SRM.....	76
6.3	Future work.....	77
7	Summary.....	79
	References.....	81

Appendices

Appendix A: Specific Simulink model

Appendix B: Simplified Simulink model

Appendix C: Simulink model converted to LabVIEW

Appendix D: Real-time part of the LabVIEW VI used for controlling the SRM

Appendix E: FPGA part of the LabVIEW VI used for controlling the SRM

Appendix F: Error budget for pure mathematical model error

Appendix G: : Error budget for difference between the simulation model and the test setup

Nomenclature

Abbreviations

AALZ	Advanced Angle controller using the Linearized motor model
AAAL	Advanced Angle controller Assuming Linear behavior of the motor
AMB	Active Magnetic Bearing
AC	Alternating Current
AVC	Active Vibration Control
BEV	Battery Electric Vehicle
BLDC	Brushless Direct Current Motor
BSRM	Bearingless Switched Reluctance Motor
CCAA	Current Controller using Adjustable Angles
CCCA	Current Controller using Constant Angles
cRIO	Compact Reconfigurable Input Output
DC	Direct Current
FEM	Finite Element Method
FPGA	Field Programmable Gate Array
HEV	Hydrogen Electric Vehicle
MBS	Multi Body Simulation
PWM	Pulse-Width Modulation
SRM	Switched Reluctance Motor

Symbols

θ	Rotational angle
----------	------------------

θ_{off}	Ending angle of commutation
θ_{on}	Starting angle of commutation
θ_m	Advanced angle
μ_0	Permeability of air
ω	Rotational speed
B	Flux density
F	Force
f	Frequency
I, i	Current
L	Inductance
L_a	Inductance when rotor and stator poles are aligned
L_u	Inductance when rotor and stator poles are un aligned
m	Number of phases
n	Rotational speed
N_p	Number of rotations in coil
N_{par}	Number of coils connected in parallel
N_r	Number of rotor poles
N_{ser}	Number of coils connected in series
P_{in}	Input power
P_{out}	Output power
p	Number of magnetic pole pairs
T	Nominal torque
T_{avg}	Average torque
T_{peak}	Maximum torque

W_{motor}	Energy supplied for motor
V	Voltage
W	Energy transformed into mechanical energy

1 Introduction

1.1 Background

The use of magnetic bearings (here referred to as active magnetic bearings, abbreviated AMBs) in rotating machines brings advantages compared to traditional bearings. AMBs use an active magnetic force control to levitate rotor inside stator, leaving an air gap between the rotor and the stator. They have some good inherent properties, such as low friction (Nordmann & Aenis, 2004), possibility to control and monitor the rotor movement (Schweitzer, 2002), almost maintenance-free operation and stability at high speeds (Matsumura, et al., 1997). These good qualities can be found also in switched reluctance motors (SRMs), since their working principles are similar. In addition, there are other good electric motor qualities in SRMs, such as low production costs (Cao, et al., 2009) through ease of manufacture (Cameron, et al., 1992) with plain stator construction and robust rotor structure (Li, et al., 2009).

SRM is an electric motor where both rotor and stator have salient structure. When simplified, this means both of them having poles. The stator poles are wound forming coils. The rotor is a simpler part. It does not have any windings on it. The material used in the rotor is soft iron, being passive component compared to for example brushless direct current motor, which has permanent magnets in the rotor.

When the opposite stator coils are excited, the rotor tends to move to a position, where the reluctance is least and therefore the magnetic flux passing through the rotor is at maximum. When the next adjacent stator coil pair is activated, the rotor rotates to the next aligned position to minimize the air gap between the active poles of the stator and the rotor. The switching frequency between adjacent coils determines the rotation speed of the motor. More generally, the speed n is defined by the switching frequency f between the magnetic pole pairs p

$$n = \frac{f}{p}. \quad (1)$$

The switching is done electronically using the feedback information of the rotor angle to correctly do the timing of the on and off switching of the coils.

A stator of an AMB resembles the one in the SRM. The rotor is as simple as it can be imagined: a cylindrical rod. The working principle to produce radial force with the AMB is also based on activating the coils to generate the magnetic flux that pierces the rotor. Depending on the layout of the poles in the stator, the flux can go all the way to the opposite half of the rotor, when the difference of magnetic fluxes in opposite sides of the rotor defines the magnitude of the radial force. This happens only if at least two separate opposite magnets are in active at the same time. The magnetic flux can alternatively penetrate slightly when only one magnet instead of two is excited. In both cases, the radial force is produced.

The history of SRMs goes more than hundred years back. This is because it has close relation to synchronous reluctance motor, step motor and inductance motor, at least it had in 19th century. Nowadays they do not have that much in common except their electromagnetic similarities. They all have power control methods of their own and their structures are different (Toliyat & Kliman, 2004). The current form of SRM started to shape in the 1960s and continued to develop up to the 1980s. Fundamental problems were found and solutions suggested (Cai, 2004). The main problems in implementing these solutions were the lack of computation power and sufficiently good electronics. In addition, not all of the flaws were found at that time because of the limitations of measuring technology. Due to advances in computer science, control engineering and electronics since the late 1990s, it has been possible to cope with the awkward nature of SRMs. However, even today SRMs have not got that much of usage as a power source. Although some applications have been around since the early years of SRM, it has not skyrocketed at any time. The most recent application has been in the vacuum-machine industry. In the near future, however, there may be an opportunity for low cost electric motors such as the SRM. The trend in the price of permanent magnets has been upward for some time, which hikes up the material costs of many other competing electric motor types.

The interest on the subject of this master's thesis aroused from the fact that SRMs can become increasingly popular in a short time. The work was done at VTT's Electrical Product Concepts team, where AMBs have been researched before (Tammi, 2007). Tammi (2007) focused on studying a control system for the radial vibration attenuation of the rotating shaft. The test arrangements involved a test rig, which was also used as a base for this study. In practice, only minor physical modifications are needed for converting a magnetic bearing into a motor. Replacing the cylindrical rotor with a branched one and using a slightly different control method should get the rotation started. Nevertheless, to make it behave properly, a little more is needed. The nonlinear character of the SRM produces torque ripple (Cai, 2004). The nonlinearity is a result of doubly-salient structure where magnetic flux is a function of the angular position of the rotor. In addition, acoustic noise is generated by the vibration of the stator. The vibration is born from the radial forces acting between the rotor and the stator (Wu & Pollock, 1995). The aerodynamic resistance is the other reason for the acoustic noise. The balance in loudness between these two noise sources depends on the construction of the motor. Usually the stator vibration is the dominant one. The stator vibration can be forced or born when system excited with the natural frequency of the system. Another radial vibration problem is the movement of the rotor shaft. This movement can be also divided into forced and natural frequency of the system-originated vibration. All these issues mentioned will be under discussion during the whole work.

The most interesting design for SRM is the one where the bearing function is combined with the motor function. This hybrid system can be achieved by using two separate stators or by combining both functions in one stator. In practice, the latter alternative needs a more complex stator design or at least a more sophisticated control algorithm (Takemoto, et al., 2001). The ultimate engineering goal for making a good SRM-driven mechanical system would be to build this kind of hybrid system that outputs smooth torque with a properly attenuated stator vibrations combined to shaft movement

attenuation. In addition, traditional mechanical bearings could be replaced or at least reduced to one.

1.2 Research problems

As an outcome of this section, a scope for the research is formed. The bottom question was whether it is possible to convert an AMB to SRM simply by replacing the rotor and updating the control algorithm. As mentioned earlier, the nonlinear nature is a major source for most of the problems SRM has. This is why even the simplest motor functions and their design process can be considered as a challenge. Modeling of SRM's operation precise enough to give an approximation of its performance was under the lens. In addition, one problem was how difficult it is in practice to implement a closed-loop system to control the rotation speed of the physical system. Answers to these questions are given as extensive way as possible. The other SRM problems are torque ripple and radial vibrations. The vibration in the stator also evokes acoustic noise. The main source for the vibration is the radial force between the rotor and stator (Cameron, et al., 1992). In addition, the air resistance of the rotor poles produces some noise (Fiedler, et al., 2005). A literature review is given to enlighten the possible ways to cope with these three. In this research, prospects for the multifunctional hybrid SRM system that can include vibration attenuation with bearing function in addition to motor function is considered.

The main purpose of this research was to gain knowledge on SRM. This was reasonable because generally engineers do not know this type of electric motors. In addition, the ones who know it have a bit negative attitude against them, and it has been reported that even misleading claims are made in research papers (Miller, 2002). This is because SRM needs a more modern approach compared to the other electric motors. It has issues that need mechanical-, control-, computer - and electrical engineering skills to be understood and solved. Depending on the issue, a different skill is needed but to understand the relations between them, an engineer needs at least some experience in all of the mentioned fields.

1.3 Aim of the research

As said, the aim of the research was to gain knowledge on SRM. The more precise actions were namely: to get an understanding how to solve most of the problems of SRM, simulating SRM operation, resurrecting the previously used AMB test device and converting the AMB into SRM. At first, it was researched if the rotor has any rotation at all using the modified AMB control system. With the original AMB controller, the rotor rotates in a magnetic field without any feedback from the angular position. After successfully completing this, a new control system with both hardware and software is put up to replace the old one. With this, a closed loop commutation is implemented using the feedback information of the angular position measurements. In addition, two different speed control methods are implemented. One being traditional current-limiting PI controller and another more sophisticated including also a high-resolution commutation method to optimize the controllability of SRM.

1.4 Limitations

About the boundary conditions that affect reaching the goals of the research is discussed next. Two main factors were limiting this research. Firstly, the scope of the Master's Thesis in general was actually quite narrow for researching something that is not well known in engineering society. Especially in this case where multi-disciplinary knowledge is needed, as discussed earlier, there will be a lot of groundwork to be done. Secondly, the stator of the original magnetic bearing test device could not be modified because it was an original prototype of a previous AMB study. Considering these limitations, several aspects are worth discussing. In the stator, there were Hall sensors sticking out in every pole and a safety plate bearing protecting the sensors from having physical contact with the rotor. The construction was not very compact, which meant that there was a rather large air gap between the stator and the rotor. Most probably, this is dramatically reducing the output torque of the motor. Although the safety plate may come in use if something goes wrong. Another thing considering the stator was the coupling of the poles. There were eight poles connected as adjacent pairs forming four magnets. This defined the number of rotor poles to be two. The scope of Master's Thesis gave mainly a limit for the time resources available. This affected to the research problems that were chosen to be part of this particular research. Not all of the SRM flaws were possible to include to the scope in same scale as the others. In practice this meant finding an answer to some of the SRM problems only in a form of a literature review.

1.5 Methods of research

This section presents actions making it possible to reach the goals in the environment, where previously mentioned boundary conditions stand. The research can be divided into three phases, which were executed partially in parallel to support each other. Still, the preceding phases worked as a foundation for the subsequent tasks. The starting point was theoretical approach that produced a mathematical model to describe the behavior of SRM. In addition, there is given an insight into methods to cope with the other SRM problems than just the ones that are faced with commutation and speed control. In the second phase, based on the mathematical model, a simulation model was created using MATLAB Simulink. This model is converted into LabVIEW simulation model to be later modified into LabVIEW real-time control system. The final phase was the physical test setup. This began with tests using the original AMB controller. Later, the test setup is updated to work with controller that consists of LabVIEW and CompactRIO (cRIO), a reconfigurable embedded control and monitoring system.

Another purpose for simulations was to get a better understanding of SRM, especially how to control it, and to get a more specific estimate of its performance capabilities. If it is possible to build accurate enough model, it can be used to estimate what actions should be done to increase the performance of the SRM in the test setup. Simulation results are also an interesting point of comparison.

The main research method was the physical test setup. As explained earlier, the test rig used to be a test environment for magnetic bearing. This made it convenient for SRM usage. Due to restrictions that did not allow modifying the stator, the motor type was

defined to be a 2-phase $4/2$ motor, which means that there are two different states during one revolution and four poles in the stator and two poles in the rotor. This type of SRM is one of the simplest constructions there are, so it suited well for basic testing. With the test setup, a series of tests were performed. In tests, the focus was on performance analysis. In addition to $4/2$ type motor, an $8/6$ (eight stator poles and six rotor poles) was also inspected when theoretical aspects were considered. This was because $8/6$ is a 4-phase motor, which brought some interesting aspects when control strategies were considered.

1.6 Own contribution

Everything mentioned in the work was entirely done by the author except the design and manufacturing of an SRM inverter, FEM models and manufacturing of the rotors. The scientific contribution this work has to offer is firstly, the corrections done for the method expressing the SRM torque, presented by (Li, et al., 2009). This was proven right by unit comparison. In addition, after the editing the results started to agree with other methods to calculate the SRM torque. Secondly, built-in MATLAB Simulink block describing the dynamics of SRM was corrected to output speed in the same units the block description stated. This was proven using author's own Simulink model to describe the equation of the motion, which was the faulty part of the block. Thirdly, it was verified experimentally that eight-pole AMB stator does not convert into eight-pole SRM stator to be used together with six-pole rotor converting the AMB to $8/6$ SRM. Instead, the eight-pole AMB stator was verified to convert into four-pole SRM stator forming a $4/2$ SRM.

2 Magnetic bearings and Switched Reluctance Motor

2.1 Magnetic bearings

In this section, the history of magnetic bearings and working principles are enlightened. The concept of a magnetic bearing is actually more recent than that of SRM's. The reason for this might be that the advantages compared to traditional bearings were not needed in any way before, because there were other non-ideal components involved. When thinking of the original version of the magnetic bearing, a passive magnetic bearing, not so many benefits can actually be found. Before any actual concepts of magnetic bearings were introduced, it was shown that stable levitation using permanent magnets is not possible in free space where all three rotational and transitional degrees of freedom should be covered by the magnets (Earnshaw, 1842). The first approaches to design a magnetic bearing were in the 1930s and the studies at that time were more or less theoretical. It was only in the 1980s when the active magnetic bearing studies begun intensively. Before that the lack of good enough electronic components and computers were limiting the research enthusiasm. In the 1990s, the state of the art was in the level where the commercial products could be launched. (Matsumura, et al., 1997), (Schweitzer & Maslen, 2009)

The first applications were in the area of turbo-machinery and, it remains as a main area of usage. Other popular applications are, for example, machine tools, medical devices and different kind of pumps. In general, magnetic bearings can fit well in applications that have either high rotation speed or demanding operation environment. There are also three special ways of using AMBs: bearingless motor, unbalance control and self-diagnosing smart machine. Some of the applications mentioned may be using these techniques as a part of their operation. These techniques can be seen as intelligent ways of using the active magnetic bearings. (Matsumura, et al., 1997), (Schweitzer & Maslen, 2009)

The term bearingless motor is widely used, but actually, it is a self-bearing motor. This kind of motor has rotor and stator constructions where the motoring and bearing functions are combined. The setup where a torque producing stator and another stator that produces supporting forces are distinct is not considered as a self-bearing motor. Although, if the stator is constructed to be only one actuator with separate windings, but the rotor has two portions of different geometries, it can be classified as self-bearing. The key in here is the compact structure. In fact, the latter example has suffered in compactness compared to ideal case where the motoring winding can be used also for the bearing function and separate rotor portions are not needed. The ideal case has a performance problem, because the rotor and stator constructions are trade-offs between the output torque and the support capacity of the bearing. There is also an advanced way to support the shaft by the means of unbalance control. The key is to keep the eccentricity of the shaft rotation in minimum, in addition for supporting the rotor against the gravity. The self-bearing motor can be constructed to include the unbalance control also. Induction motors controlling the eccentricity have been studied in (Laiho, et al., 2009) and (Laiho, et al., 2011). With self-diagnosing smart machine, the unexpected system changes can be found before any severe malfunctions. For example,

the bearing can detect if the force needed to support the shaft is increased significantly, which can be a sign of a sudden failure of some component in the system. The three special techniques mentioned have self-explanatory benefits. Other properties that make AMBs desirable to certain use are: contactless operation, rotor can be run fast without losing its balance, low bearing losses, adjustable dynamics and low maintenance costs with high life time (Schweitzer & Maslen, 2009).

The operation principle of the active magnetic bearing can be described as contactless support of the shaft. In addition to support, AMB suspends and guides the rod (Chiba, et al., 2005). The actuator is normally constructed so that there are magnets in four perpendicular directions forming orthogonal coordinate system. This way it is possible to produce both positive and negative force in each direction separately. Electromagnet is composed of two adjacent wound poles that are connected in series forming a horseshoe magnet (Figure 1). This way the total number of poles is eight. Each magnet is independent of each other, therefore four force components can be operated separately. The higher the number of poles gets, more costs will be born. This is why a three pole AMB has been studied by (Chen & Hsu, 2002). The control system Chen & Hsu used was more complex than what is needed with eight-pole version.

The simplest AMB control method uses only one magnet to produce one pulling force component. Hence, if a force component pointing straight up would be needed, as it is the case in situation of Figure 1, only the upmost horseshoe magnet would be activated. The excited magnet produces a pulling force that tries to minimize the length of the air gap. According to (Schweitzer, 2002), the radial force of Figure 1 produced by one horseshoe magnet, is defined as

$$F = \frac{1}{4} \mu_0 n^2 A \frac{i^2}{s^2} \cos \alpha . \quad (2)$$

Here μ_0 is the permeability of air, n is the number of rotations in one coil, A is the cross-sectional area of the coil, i is the winding current, s is the air gap length and α is the glancing angle of the pole. While the air gap decreases, the pulling force increases causing non-linear behavior as seen from the equation (2), where the air gap length s is inversely quadratic. The feedback measurements of the air gap length are provided for the controller to calculate the forces to minimize the unwanted deflection (Chiba, et al., 2005). In addition, the current also causes non-linear control behavior. This is why sometimes AMBs are controlled using opposite magnet pairs. If both of the magnets are fed with the same current, they should produce opposite force components with equal magnitude both trying to pull the rotor away from the center point. The resultant force is zero, but if the control current of one of these two magnets is raised above the preload bias current, the resultant force will point towards the magnet excited with higher current. The F/i plot should be linearized around suitable operating point to provide longest possible operation range. Hence, value of the bias current will be the start of the linearized slope.

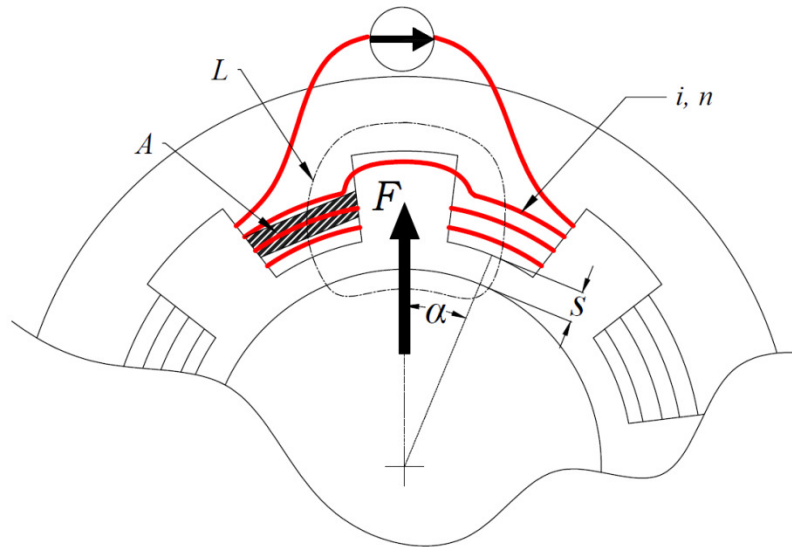


Figure 1. Illustrative figure of one horseshoe magnet of AMB pulling the rotor.

2.2 Electric motors in general

A short review of different electric motor types is given in this chapter. There is more than just one way to divide electric motors into different categories. Here, the division is done by distinguishing different commutation methods. As a result, four categories for electric motors were formed. The main reason for using this kind of method was the demand to find a category also for SRM. The method was adapted from (Yeadon & Yeadon, 2001). The four compartments are direct current motors, alternating current induction motors, synchronous machines and electronically commutated motors. The latter is the one that includes the SRM. Most of the divisions used in handbooks do not include SRM at all; it is rather described as a special type of an electric motor. This review was done especially from the motor control and commutation point of view. The commutation is needed to pass the current to the rotor and to change the direction of rotation. Normally the change of direction is done at every 180 mechanical degrees to maintain the torque production during one revolution. The review can be seen useful because the SRM is not well known and it makes a point to compare it to more widely used electric motors to estimate its potential uses.

The brushed direct-current motor is considered as the simplest electric motor from the control-engineering point of view. It has a linear speed-voltage ratio and torque-current ratio. The stator consists of permanent or electromagnets forming field wiring that is fed with direct current. The armature winding is located on the rotor. The commutator feeds alternating current for the armature winding. The commutation is managed via brushes that have a tendency to sparkle and wear out during time. The biggest problem with the brushed DC motor is the frequent need for maintenance concerning the brushes. To solve this problem, a brushless DC motor (BLDC) has been developed. This motor type

will be described with the electronically commutated motors. (Toliat & Kliman, 2004), (Yeadon & Yeadon, 2001)

The AC induction motor is the most popular electric motor at least in the industrial -use, some say it is the most used in home and business also. It has wound stator poles to produce magnetomotive force that causes torque. The rotor has a squirrel cage structure that is used for catching the current induced by the rotating magnetic field produced on stator windings. This way a torque-producing magnetic field is formed in the rotor. Induction motors can be broken down to single-phase and polyphase motors. Single-phase motor uses single-phase power and poly-phase motors use multiphase, usually three-phase power. The latter is usually available only in industrial sites. This is why in home and business the induction motors are normally single-phase type. In single-phase motor, the rotating magnetic field is not born unlike in its multiphase brother. To produce the rotating field, there are multiple methods depending on the application where the single-phase motor is used. The difference between these methods is how they get the rotation started. In the applications that do not require high starting torque, a shading coil can be used. In this method, a time lag is produced in the flux that passes through the shading coil causing an initial rotating magnetic field. This field is enough to start rotating the rotor. When the rotor speeds up, the main rotating magnetic field is produced by the rotor. Another version of single-phase motor is a split-phase induction motor. Common version of this type is to use a capacitor in series together with a startup winding, which is separate from the main winding. This method provides higher starting torque than the shading coil method. (Toliat & Kliman, 2004), (Yeadon & Yeadon, 2001)

Synchronous machines have a lot in common with induction motors. Although in synchronous motors, the phase between the magnetic fields of the rotor and the stator is synchronous, in induction motors the fields are not in the same phase, but the inducing field is leading the induced field by the slip factor describing the tendency to have phase difference. This is why induction machines are also known as asynchronous machines. Three synchronous motor working principles can be found to be distinct from each other: reluctance, hysteresis and permanent magnet. All of these have stator construction that is almost identical with the induction motor stator. Different rotor types define different working principles. The synchronous reluctance motor has a damper winding in the rotor to help with starting the motor, if used in direct on-line. The winding is adapted from the induction motor and the motor actually works as an induction motor until the synchronous speed is reached. When the motor runs at synchronous speed, the pole winding is being exploited. Alternative way for direct on-line is to use frequency converter that enables to run the motor in synchronous all along, from start to top speed. The damper winding is no longer needed when a frequency converter is introduced. The second category in synchronous motors is hysteresis motors. The key in hysteresis motor is the rotor that is manufactured from such steel, which has hysteresis properties to make the magnetization lag behind the applied field. It is because of the phase shift between the induced magnetization in the rotor and the magnetic field in the stator that makes the motor to start. In time, the rotor catches up the stator field and the phase shift goes to zero making the motor run at synchronous speed. Again, the pole winding is excited to keep up the synchronous speed. The third

version, permanent magnet synchronous machine, resembles the brushless DC machine. They both have permanent magnets inside the rotor and an electronically controlled stator. Although the BLDC uses electronic commutation more than just to get the rotation started. Another way to start up the motor is to use unevenly distributed stator poles with a return spring. These kind of unidirectional motors are suitable only for modest applications. In synchronous speed, the magnets lock into the rotating magnetic field produced in the stator. All the synchronous motor types mentioned so far are so called non-excited machines. There are also DC-excited machines that use slip rings and brushes to carry the current for the rotor. (Toliat & Kliman, 2004), (Yeadon & Yeadon, 2001)

The most interesting and challenging group of motors in control engineering point of view is the electronically commutated motors. They are all DC-powered and commutated electronically instead of mechanical. This group contains the brushless direct current motor, the step motor and the switched reluctance motor. The key to work with the electronically commutated motors is to have information of the rotation angle. This information is used to trigger the magnetic fluxes on and off. The angle is normally measured but in the case of step motor, there is no feedback. This is because with step motors the angle can be determined from the previously fed pulses. In all of these three motors, there can be found a clear structural consistency that is derived from the commutation method that is used; the windings are located on the stator instead of the rotor. This results in salient pole cross-section in the rotor. (Toliat & Kliman, 2004), (Yeadon & Yeadon, 2001)

The brushless DC motor has permanent magnets inside the rotor. It has linear current-to-torque and speed-to-torque relationships. Compared to the traditional brushed DC motor, the brushless improves some poor properties. Downsides are the additional costs and complexity. (Yeadon & Yeadon, 2001)

Step motors come in three structures: variable-reluctance, permanent magnet-rotor and hybrid permanent magnet. The rotation of the step motors is best described as stepping. Every step is a stationary state, and one revolution can be composed of more than several hundred steps. The operating principle is close to SRM, but the main difference is the stationary states. If step motor is fed with a frequency converter trying to rotate the motor so fast, that it cannot find the stationary states, it loses the steps. This actually reduces the speed of the motor, because the following steps do not match the rotor position. The same thing happens with a critical load; the motor fails to produce enough torque. For these reasons, step motors are used only in applications that have known loads and need positioning only at moderate speed. In variable reluctance step motor, the toothing in the rotor and in the stator poles is dense to create many steps. This way the positioning is accurate. Although there are many common features in variable reluctance step motor and SRM, the SRM is designed to operate in different applications. The fact that SRM is lacking the dense toothing of the poles is the key difference. In SRM, there are no stationary states, so the position angle feedback is required for the commutation. In principle, the positioning applications are not impossible for SRM, but using it in such a way does not take the full advantage of SRM's capabilities. It is the non-linear character what makes the positioning difficult.

Other electric motors can perform such task better because of the linear nature. A more suitable application for SRM is in traditional electrical power to mechanical power conversion where good acceleration and high speed is needed. In the following chapters, detailed descriptions of the SRM working principles are presented. (Toliat & Kliman, 2004), (Yeadon & Yeadon, 2001)

2.3 SRM compared to other electric motors

To sum up the similarities of SRM compared to other electric motors, three motor types were taken into comparison. As stated earlier, SRM can be thought as a special case of a variable reluctance stepper motor. Actually, the right way to put it would be vice versa, because SRM was discovered first. Nevertheless, stepper motors are known more widely so it makes sense to keep them as a reference. In theory, the constructions are the same, despite the pole toothing in some stepper motors. The rotation of SRM is continuous unlike in stepper motors. This means they have control methods of their own and different optimal use. The relation to brushless direct current motor is the active phase-to-phase rotation of the magnetic flux at discrete rotor angles that are programmed to the controller. This is true only in the case of BLDC that has square wave input. The third motor type, synchronous reluctance motor, may sound like a close relative to SRM, but has nothing to do with it. In older publications, a variable reluctance motor can be found. This actually means SRM, not the step motor and it was used confusingly especially in the United States for some period.

The roots of SRM are there where the first electric motors were invented. The working principle is simple, so it was not hard to discover the motor after the concept of electric motor in general was proposed. The most significant difference between the earliest structures and today's design is in commutation method. The first versions used mechanical switches instead of electrical transistors. The mechanical switching produced inaccurate and slow magnetic flux switching. This meant low torque and slow rotation speed. The first application was to propel a locomotive in 1838. The speed was 4 miles per hour. (Byrne, et al. 1985) Effective operation of SRM calls for fast electronics and motor controller that is configured for the specific motor setup. It was in the 1960s when it was possible to use electronic components to control the SRM. In practice, the first controllers for actual prototypes and products were created in the 1970s and 1980s. These first versions had only the necessary functionalities to use SRM as a power source with speed control. The compensation of the unwanted side effects was not in interest at that time. It was challenging enough to implement the fundamental functionalities using computers and software of the time. At that time, the design process of SRM was heavier than nowadays. To verify the geometry of the rotor and the stator, finite element analysis is needed. Now the FEM software can be run on an ordinary PC, but 30 years ago, the situation was something else. The commutation logic in the motor controller also needs to be simulated first to obtain the optimal angles for the wanted performance nature. Because these analyses were not available when the first versions were designed, engineers needed to rely on the theoretical examination. In the 1990s, the computer science was advanced enough to make possible deeper analyses when designing motors. At that time, the design process of SRM reached the point where the motor was ready to be used in many applications. The only problem was that

it was too late. The other electric motor types were already infiltrated into the industry. Because those others had simpler nature, it took less work to streamline the design and the engineering process. The fact that SRM does not bring any significant improvements compared to competing motors makes it unwanted as a substitutive technology, especially when compared to induction motor. Ten years later the interest towards this motor type woke up again and at this moment is receiving considerable attention by the scientists involved with electric motors. Now the interest is on compensating the unwanted side effects that is evoked by the working principle. Addition to this, the focus is on combining the magnetic bearing to the motor, forming a bearingless motor.

The interest towards this motor type arises from the inherent good qualities. On the other hand, many not so good properties are characteristic to this motor type. As mentioned earlier, in the past the rivals for the SRM had shorter and faster path to commercial use as a power source. The reason for this is these specific unwanted properties. Some of them relate to the motor itself and others are more related to controller. The most relevant pros and cons have already been analyzed or will be analyzed further in the work. Therefore, only summary of them is presented here in a Table 1.

When analyzing the qualities in Table 1, description for optimal application for SRM can be found by combining these pros and cons. The manufacturing cost structure of SRM is biased towards high initial costs because of high design expenses coming from controller that needs to be tuned for specific motor. In addition, this motor type is yet missing network for sub-contractor manufacturers, unlike every other type electric motor. On the other hand, the manufacturing costs coming from materials and assembly are low. Hence, specific for optimal application area should be large production numbers and a natural tendency to accept the motor and the controller as a package where they are integrated together by the same manufacturer. Because the rivals of the SRM have so strong status in all possible industries, it makes sense to aim for newish application area that does not yet have a standard practice. The most promising target is an electric vehicle. SRM could be a power source both in Battery Electric Vehicle (BEV) and in Hydrogen Electric Vehicle (HEV), which are the two most vital technologies for the vehicle of the future. When alternatives for the electric motor role in electric cars are reviewed, there are usually at least these three contenders: induction motor, brushless DC-motor and SRM. The SRM has an average to good success in reviews (Larminie & Lowry, 2003), (Chan, 2007), (Xue, et al., 2008). According to (Rahman, et al., 2000), SRM was described having potential for performance superior to brushless DC-motors and induction motors when these three were compared for electric vehicle applications. The main decrease of points seems to come from the complex control method and from the unusualness that may lead to higher costs than with induction motor. At the same time, the commonly mentioned positive aspects for vehicle propulsion are the first nine positive aspects listed in Table 1. The end verdict of the reviews usually states that selecting between these motor types is not the most crucial thing when designing an electric vehicle, because there are also many other engineering challenges that need to be taken into account.

Table 1. The pros and cons of SRM (Miller, 1993), (Miller, 2002), (Larminie & Lowry, 2003), (Takemoto, et al., 2001), (Rahman, et al., 2000).

Positive properties	Negative properties
+ Robust and rugged construction	– Torque ripple
+ Almost maintenance free	– Noise
+ Low material costs	– Stator vibrations
+ Low manufacturing costs	– Complex control method
+ Good heat conductivity because windings are on the stator	– Controller needs to be tuned for specific motor design
+ Low inertia allows high acceleration	– Small air gap needed
+ Efficiency can be maintained over wide range of torque and speed	– Angular position feedback required
+ Possibility to operate in high temperatures	– Not well known technology
+ Operation as generator possible	– Limited sub-contractor network available
+ Possibility to build bearingless motor	
+ High-speed operation possible	
+ No sparking tendency, so usage in the explosion hazard environment possible	

2.4 Physical characteristics behind SRM

Plain description of SRM's nature has already been given in previous chapters. Next, the subject is examined more thoroughly. The cross-sectional view of SRM is presented in Figure 2. Even though the figure is a conceptual drawing, it actually does not differ that much from the actual appearance of SRM. The real rotor geometry is exactly as it is drawn; no windings or permanent magnets are present. The air gap in the drawing is exaggerated; the thumb rule for the air gap length is 0.5% of the outer diameter of the rotor (Miller, 1993). Still, having smaller air gap length than 0.25 mm may lead to mechanical problems with tolerances. The reason why so small length is recommended is the low permeability of air and high permeability of iron. The magnetic flux tends to choose the path that has the lowest magnetic reluctance. The word reluctance occurs also in the name of SRM. It means magnetic resistance and is inversely proportional to the permeability of the material. If the air gap between the rotor pole and the stator pole is too long, the flux does not reach out over the air gap to meet the rotor lowering the flux density. The flux density is a product of current i and inductance L . The rate of change in inductance related to angular position θ determines the available torque (Miller, 2001)

$$T = \frac{1}{2} i^2 \frac{dL}{d\theta}. \quad (3)$$

Thus too large air gap means poor output torque. Then, having a smaller air gap leads to more noisy construction because of the non-uniform structure. In Figure 2, the rotor is aligned with the stator coils AA'. If the direction of rotation is anticlockwise, the next coil pair to be activated is BB'. When BB' is excited the AA' is turned out. To get the maximum torque simultaneous coil pair activation can be used. Hence before the rotor is aligned with the AA' the BB' can be switched on to get higher torque. More about the commutation strategies will be discussed later.

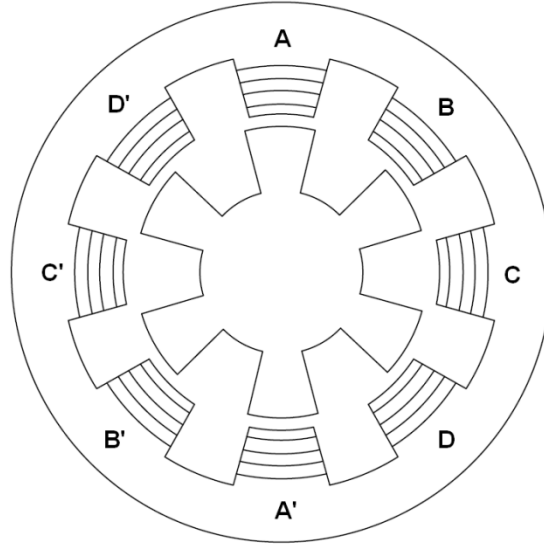


Figure 2: Cross-section of 8/6 Switched Reluctance Motor

The number of poles in the rotor and in the stator defines the number of phases. The ratio between these three aspects determines the basic type of the motor. The simplest version of SRM is shown in Figure 3. This kind of 2/2 setup, having two rotor and stator poles, has some problems. It has only one phase, so the torque has extremely high ripple. Most of the time coils cannot be excited to prevent the negative torque that would slow down the rotation speed. In addition to poor torque, the motor cannot be started in arbitrary angles, because the change in inductance is zero during wide range of the resolution. In practice, the 4-phase 8/6 setup shown in Figure 2 has turned out to be the most sensible layout. It was one of the first configurations used in commercial products (Miller, 2002). The main problem in 2-phase motor is the lack of self-starting. Performance is also lower than in 4-phase situation. When using a rotor that has specially designed pole shapes the 2-phase motor can be started from any given angle, but it has a downside of limiting the direction of rotation to only one direction. This special rotor construction has secondary poles forming a stepping between the main pole and the secondary. In chapter 4.2.1 Rotor designs, is described a rotor design that utilizes the stepping to enable the arbitrary starting angle. In 3-phase motors, the 12/8 setup is sometimes used for its simpler power electronics. In 3-phase motor, there has to be more poles in the stator and rotor to get the same number of strokes, which makes the motor more expensive. In addition, there may be problems with producing enough

torque to get the motor started in arbitrary angles. The number of strokes is the product of number of phases and number of poles in the rotor. So the number of strokes is equal in both 4-phase 8/6 and in 3-phase 12/8. With high stroke number, the torque ripple is lower. In 2-phase version, the setup should be 8/12 to get the same number of strokes.

To sum up, the 4-phase 8/6 has the advantage of self-starting capability at any position to both directions with high number of strokes achieved with low number of poles. Miller (2002) has done a review of worthwhile pole and phase combinations. The phase numbers of five and higher are not recommended by Miller due to increased costs in controller that need to have more channels. He also told that high pole numbers should be avoided because of unsatisfactory inductance ratio.

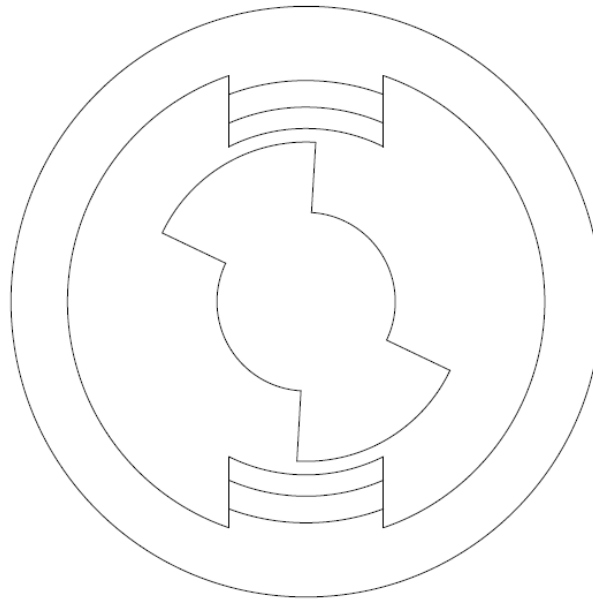


Figure 3: Cross-section of 2/2 SRM

The windings are connected as pairs, and in Figure 2, they are signed with the same letter, for example AA' forming one pair. The opposite coils of one coil pair are switched on at the same time but usually they are connected in series to manage with fewer electrical components. This is the principal difference in AMB and SRM winding because with AMB the adjacent instead of opposite coils are connected together. The current in excited windings generates magnetic flux in the iron core of the stator. Usually this flux goes through the rotor to the opposite iron core on the other side of the stator that was also excited. The flux can also just pierce the rotor pole returning to the same stator pole it left. The magnetic flux can be represented with swarm of lines describing flux density, like those presented in Figure 4. From the picture, also the return flow of the flux in the back iron of the stator and flux in the interface between the rotor and the stator can be seen. The flux is obtained from FEM-model calculations. Because the coils are activated alternately the flux is not constant or even continuous between two sequential phases. When more than one pole pair is excited, the fluxes

produced by separate coils change the density and path of the flux piercing the rotor. In addition, during one coil pair activation the flux is also non-linear with respect to rotation angle because of the continuously changing air gap length.

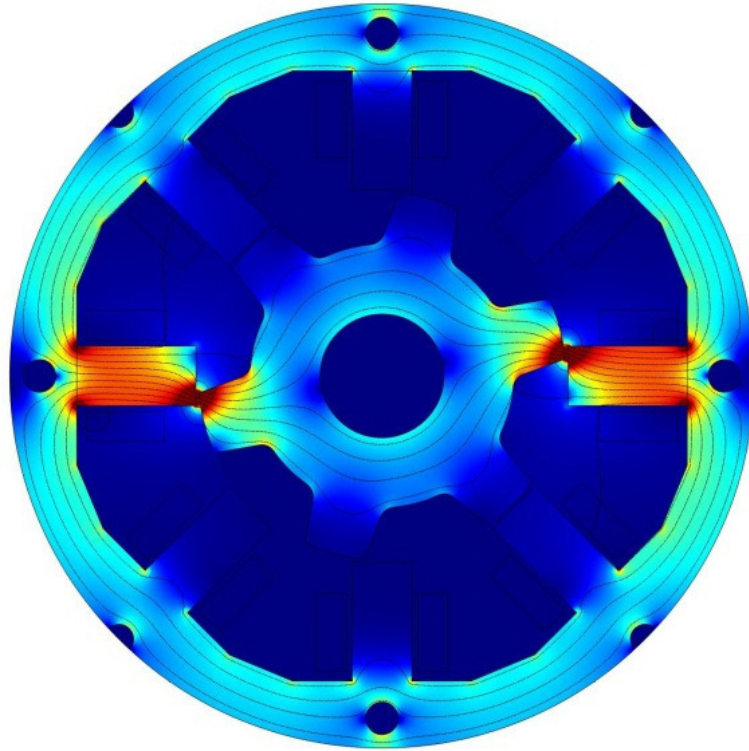


Figure 4: Magnetic fluxes in 8/6 SRM. (Haarnoja, 2012)

3 State of the art

3.1 Research on SRM

A short review of the past research on SRM is given in this section. The review is divided into seven categories regarding the research scope. The first category is a principal study such as this Master's Thesis. Others are research of the torque ripple, radial vibration, noise, bearingless switched reluctance motor, sensorless control and finally applications. This division categorizes extensively the papers published regarding the SRM. Usually the research scope is defined to be one of these topics. However, some studies handle multiple issues due to close relation of issues to each other. In here is referred into only part of the overall research done on a certain topic. However, for every research can be found at least one suchlike study on the same time. As in research in general, the studies can be divided into verifying assumptions and into resolving problems. In the first case, the research concentrates on finding relations between phenomenon and in the later figuring out methods to cope with something that does not have a general solution yet. Studies from both of these categories are reviewed next. The methods for resolving the SRM problems will be looked more thoroughly in chapter 3.3.

The research of basic SRM operation concentrates mainly on describing the production of main output component of a motor: torque. At first is determined a mathematical model to describe the production of torque. Usually, this model is a mechanical model describing mechanical torque, but sometimes an equivalent electrical circuit is formed leading into electromagnetic torque. The basic research is either general know how or it is more concentrated on something specific basic function such as improving the power intensity of the motor. This Master's thesis handles mostly commutation and speed control, which is the most essential part of electric motors. This topic was the first focus when electronic control of SRM was included in research. The time before SRM was not controlled electronically using microprocessors is not included in this review, nor was the research too intense anyway at the time. One of the first papers that fulfill the scope was published by (Bose, et al., 1986). It was a thorough study of SRM in general which also included a working prototype of the motor. This kind of basic research was in interest especially in the early 90s (Miller & McGlip, 1990), (Materu & Krishnan, 1990), (Stefanovic & Vukosavic, 1991) and ten years later when SRM was found again, now as interesting subject for modern control engineering (Miller, 2002), (Rfajdus, et al., 2004), (Chancharoensook & Rahman, 2002), (Ho, et al., 1998), (Chancharoensook & Rahman, 2000), (Soares & Costa Branco, 2001), (Barnes & Pollock, 1998). Even today, papers are published regarding optimization using the newest methods (Jessi Sahaya Shanthi, et al., 2012), (Petrus, et al., 2011), (Hannoun, et al., 2011), (Pop, et al., 2011).

Torque ripple has been interesting as a research object since the 1990s. Especially finding a solution for the ripple has been scope for many researchers. The interest lasted for about ten years and it still can be found as a secondary object in many studies. As a summary can be said that only a little can be done to torque ripple if decrease in performance is not acceptable. Even though the lower performance can be tolerated, the

ripple remains high. It seems torque ripple has earned its place as part of SRM's nature. The methods for the reduction have relied mostly on control engineering (Russa, et al., 1998), (Mir, et al., 1999), (Cajander & Le-Huy, 2006), (Henriques, et al., 2000), although mechanical properties of the rotor have been also considered (Lee, et al., 2004).

The radial vibration is a problem just by itself, and in addition, it produces acoustic noise. However, the noise is treated as an individual problem in here. The radial vibration is same kind of principal problem of SRM as is the torque ripple. This is why the vibration was also an interesting matter at the same time in the 1990s. To reduce the vibration level, different approaches has been suggested. First ways used at the 90s were to affect to power control of SRM by controlling transistor switching in an intelligent way (Wu & Pollock, 1995). This method has been research subject recently in (Liu, et al., 2010). Another way to cope with vibrations is to use mechanical means and more precisely by using optimal stator construction. This has been under investigation by (Cai, et al., 2003) and (Li, et al., 2009). The most popular radial vibration attenuation subject has been to operate with bearingless SRM. The BSRM combines functionality of an active magnetic bearing with the SRM's motor function. This way it is possible to cancel the vibration before it is even actually born.

The acoustic noise is usually an indication of vibration. Thus if the vibration can be attenuated, the noise should also decrease. This is true if the noise source is entirely vibration born, not aerodynamic as it sometimes is. Many researches that have set topic on finding solution for noise in SRM are concentrating on finding a way to cope with the vibration (Wu & Pollock, 1995), (Cameron, et al., 1992). This is why the noise topic has gathered interest at the same time as the vibration studies. In (Fiedler, et al., 2005) was shown aerodynamic noise to be the dominant source in some cases. Fiedler, et al. (2005) proposed solutions for aerodynamic problems that were simple when compared to what is needed to solve problems in radial vibration.

Bearingless SRM can be used for solving the radial vibration problem, which may also generate noise. First studies that also included prototypes were published in the start of 21st century (Takemoto, et al., 2001). Today, this remains as the most interesting subject when SRM is considered. Many studies are approaching BSRM by using separate coils for radial force and motoring (Takemoto, et al., 2001), (Cao, et al., 2009), (Guan, et al., 2011), but it is also possible to use simpler construction (Chen & Hofmann, 2010), (Morrison, et al., 2008). The advantage of using this kind of simpler topology is the lower costs in manufacturing. It seems that there are different ways to implement the BSRM, and it is likely that not all the ways are yet researched.

One trend in SRM is to design sensorless motors. These types of motors are not using any external probes or such to produce feedback information of the system. This kind of setup is reasonable, because the sensors are expensive (Bass, et al., 1987), the motor suffers in compactness with them (Cheok & Ertugrul, 2000) and there is an increased chance of malfunction when sensors are used (Ray & Al-Bahadly, 1993). The simplest way for sensorless operation is to forget the closed loop control and feed the stator with square wave signal that corresponds the motor phases. The problem is how to make sure

the rotor does not fall out from the phase and catches the rotating magnetic field at start up. When the first attempts were made in the end of 1980s, the sensorless action was implemented in this way but complemented with current measurements from the some point of the power electronics circuit (Bass, et al., 1987). This kind of method was still researched ten years later, although with more sophisticated usage of the feedback current information (Gallegos-Lopez, et al., 1998). In 1993, the state of the art in sensorless control of SRM was reviewed and the verdict was that none of the techniques of the time was good enough to be used in actual products (Ray & Al-Bahadly, 1993). Since that, the trend has been more towards fuzzy control (Cheok & Ertugrul, 2000) and neural networks (Mese & Torry, 2002), (Hudson, et al., 2008), where the angular position is deduced from measured current or flux. In addition, specific analytical models are also used, which may lead into extremely heavy computing requirements (Hongwei, et al., 2004). Hongwei, et al. (2004) calculated the feedback information from the rate of change in measured inductance. A more recent review of the sensorless methods is given by (Ehsani & Fahimi, 2002) stating the techniques are now on a level that is more implementable. But then again, if SRMs are manufactured in means of mass production the variation in parameters that are used in sensorless methods are so high that self-tuning controller needs to be used. In addition, Ehsani & Fahimi (2002) pointed out that these parameters are used also with normal SRMs. This said the self-tuning should be used regardless of the feedback method. In practice, this would mean using neural networks in every controller designed for any given SRM, especially since aging of materials also affect into these parameters.

The final category is the applications. SRM is not mentioned in many studies where alternatives for something certain application are reviewed. However, electric and hybrid cars are one common interest amongst researchers when applications for SRM are considered. Alternatives for electrical propulsion motor are reviewed in both (Chan, 2007) and (Xue, et al., 2008). The approach is only theoretical, but they both suggest SRM over other types of electric motors. In addition, tests that are more specific were done for prototype of SRM attached on actual car by (Rahman, et al., 2000). Rahman states that SRM produces better performance than brushless direct current motor or induction motor when used as a power source of a car. In reviews for electric car motors, these two motor types are included in most cases together with permanent magnet motors. Another SRM included automotive application is a combined starter and generator. The reason for popularity in car related subjects is clear when thinking of SRM's robust and almost maintenance free construction. In research done by (Cai, 2004), SRM had only moderate success, but SRM was analyzed based on out dated information.

3.2 Control theory for basic SRM operation

Different ways to design the mathematical model, power electronics and control algorithms of SRM are shown in the following sub sections. First, the mathematical models to calculate the most essential outputs and internal parameters are discussed. Second, some basic knowledge of power electronics used in SRMs is described. Third, commutation and how to control the rotation speed of SRM are explained. Usually, a type of mathematical model of SRM is required to design a controller. A basic

controller takes care of the commutation of SRM. More advanced controller algorithms include pulse shaping to optimize for instance the torque ripple or the noise and vibrations emitted. The control algorithms are usually realized in a digital electronics controlling the driving power electronics.

3.2.1 Mathematical model

From the system point of view, the primary output of a motor can be considered torque. Caused by the torque, a motor starts to rotate the shaft at specific acceleration dependent on the inertia of the system together with the motor torque and resistive torques. Hence, when these are known the acceleration can be calculated. This is why it is important to have an accurate model to estimate the motor torque. Due to the non-linear nature of SRM, the exact model is hard to define. Firstly, the torque has a strong fluctuation in relation to rotation angle. This means forgetting the peak value of the torque, because it would give optimistic performance. The peak value is held only a short period, although this depends on the motor type and control method. What really is relevant is the average torque. Usually the average is at the midpoint of the peak value and the base value, at least this is the case with the 8/6 type SRM. The torque fluctuation between the highest and the lowest value is actually called torque ripple. It would not be much of a problem if the lowest value would not be that much lower. However, when it is, the average value suffers. The lowered average is not the only problem, because when the torque suddenly drops, it affects directly to speed. This means fluctuation in torque that causes the rotation to be fluctuated also. With correct control strategy, the torque ripple can be reduced, which will be discussed later. When working with a motor that has varying output, it would be useful to obtain the whole waveform of the torque to get an understanding of its behavior. In practice, this means simulating the SRM for example in MATLAB Simulink environment. Moreover, getting the correct waveform may be difficult. An estimate close enough to the available performance can be achieved by simulating the average torque. An idea is to perform an analysis of the simulated acceleration or some other demanding situation where known resistive torques are also included.

There are different ways to calculate the average torque. Some of the methods are suggestive and simple, giving values that are larger than some others give. First, some of these will be presented in order of ascending complexity though leading to methods that are more accurate. After this, a short review of them will be given. As a reference is the simulation model that is presented in more detail way further in the work. Many of the mathematical models include unknown variables that are hard to acquire in other ways than experimentally or with simulations. This is why using a FEM software may come handy when discovering the variables. Methods may also include constant terms that are motor type dependent, so when using this kind of method one needs to find out the relation between the motor type and the constant term values.

In FEM analysis, the magnetic flux of SRM is simulated. Doing this is essential when designing a new rotor and stator geometry. A two-dimensional FEM-model gives rather accurate estimates of the flux behavior. When the analysis is done in three dimensions, even better quality can be achieved, but a magnetic flux simulation in 3D is not

common being more time consuming and laborious. Of course the density of the FEM mesh has influence on the computation time together with the level of non-linearity of the model. With FEM, it is also possible to do torque calculations. Good idea is to combine the FEM model with the Simulink model to get best out of both.

The simplest method to calculate the torque is an **energy conversion** from electrical energy to mechanical energy. This is used as primary technique in (Yeadon & Yeadon, 2001) to approximate the average torque. The value of the voltage is not self-explanatory because SRM is fed with PWM. It is not clear what value should be used in calculations, because the maximum available voltage is higher than the nominal voltage to enable fast raise in current. The voltage V needs to be estimated using current I and change of inductance L

$$V = I \frac{dL}{dt}. \quad (4)$$

If behavior of the change of inductance is assumed linear, the time derivative of the inductance can be expressed as difference between the aligned and unaligned inductances, L_a and L_u respectively, when the magnets are activated in relation to time passed during this. In 8/6 SRM the angle that is travelled during the activation is 30° . Therefore, with rotational speed ω , the voltage becomes

$$V = \frac{360}{30 \cdot 2\pi} \omega I (L_a - L_u). \quad (5)$$

The input energy is simply product of the supplied voltage, current and time t . The energy needed for changing the current when magnets are switched on and off has to be also included. With two opposite coils active at the same time the input energy is

$$E_{in} = 2 \left(VIt - \frac{1}{2} L_a I^2 + \frac{1}{2} L_u I^2 \right). \quad (6)$$

The output energy is

$$E_{out} = \omega t T, \quad (7)$$

which is a general equation of energy in the rotational movement, that consists of rotational speed ω , torque T and time. When ignoring the efficiency, the input and output are equal and torque is

$$T = \frac{2VIt - I^2(L_a - L_u)}{\omega t}. \quad (8)$$

When (8) is combined with (5), expression of torque becomes

$$T = \frac{360}{30 \cdot 2\pi} I^2 (L_a - L_u). \quad (9)$$

This method needed voltage value, which was estimated using aligned L_a and unaligned L_u inductance information. The method that is described next, is also using voltage value, hence it is estimated in the same manner. The built in Simulink model block that is the one used as a reference calculating method for torque together with the FEM model, uses L_a and L_u too. These values were obtained from the FEM model, which also uses them to calculate the torque. The FEM model and Simulink model give torque values that are close to each other.

The second method is also based on the energy balance. This method is referred as **SRM-type derived** method and it is introduced by (Miller, 1993). In addition, it takes into account the different periods during one energy-conversion loop. Typically thirty five percent of the energy is returned back to supply. Hence, Miller used the energy ratio E of 65% in calculations. This means the amount of energy transforming into mechanical energy is

$$W = EW_{motor} , \quad (10)$$

where W_{motor} is the energy supplied to the motor. This method is based on strokes during one revolution. The number of strokes per revolution means the number of energy-conversions during one revolution. When the number of strokes during one rotation is the product of rotor poles N_r and phases m , the average torque produced in one rotation can be written as

$$T_{avg} = \frac{mN_r}{2\pi} W . \quad (11)$$

The supply energy is

$$W_{motor} = Pt = 2VIt , \quad (12)$$

hence when thought of energy supplied during one revolution, the time t is

$$t = \frac{2\pi}{\omega} , \quad (13)$$

Now combining these with (5) and (10) the torque can be calculated. Because this method defines the strokes in a way that assumes magnetic activation to last only 15°, the expression of torque becomes

$$T_{avg} = \frac{360}{15 \cdot \pi} I^2 m N_r E (L_a - L_u) . \quad (14)$$

The **SRM-size derived** method introduced by (Miller, 1993) gives the peak value for torque. It represents situation where the rotor and the stator are encountering, which is usually the situation when the maximum torque is produced. It is assumed that the flux density B_s is 1.7 T, which is a typical value for electrical steels. The peak torque equal to

$$T_{peak} = B_s r_1 l_{stk} \cdot 2N_p I, \quad (15)$$

is composed of stator bore radius r_1 and length of it: l_{stk} . N_p is the number of winding turns per pole and i is the current. A peak value for torque is higher than an average value, which is used in other methods. According to torque performance tests done by (Cajander & Le-Huy, 2006), the average value can be expressed as

$$T_{avg} = 0.75 \cdot T_{peak}. \quad (16)$$

The first method introduced did not take into account any physical properties of SRM. The second one used stroke, pole and phase numbers in addition to the first method. The third one used also magnetic properties of SRM materials and some major dimensions of the motor. The fourth way to calculate the torque can be described as **inductance values with SRM-dimensions derived** method (Li, et al., 2009). The aligned and unaligned inductance values are included originally in the method, not as additional information by the author as it was with the first two. Compared to the previous method, this uses information of the air gap length l_{gap} and coupling of the poles by using the knowledge of number of coils connected in series N_{ser} together with the number of coils connected in parallel N_{par}

$$T_{avg} = -\frac{\mu_0 (N_p I)^2 r_{gap} l_{stk}}{2l_{gap}} \cdot \frac{N_{ser}}{N_{par}} \left(1 - \frac{L_u}{L_a}\right). \quad (17)$$

In (Li, et al., 2009), equation (17) was introduced in form that had l_{gap} in power of two. This must be an error, because compared to the torque value that is believed to be closest to the true value the method gave over 200-times larger values. In addition, the units did not match in that formula. When calculated using the equation (17), the value for torque is more sensible.

The fifth method is the **advanced angle** method (Takemoto, et al., 2001). It uses the same motor dimensions as the previous method. In addition, couple of motor type dependent constants is used together with universal coefficients. The inductance values are not included. Inside the formula, a control method for the rotational speed is included. This so-called advanced angle θ_m can be used to calculate average torque in different states of the speed control. With advanced angle, it is possible to control the torque production that affects to the acceleration and therefore to the speed. In full acceleration state, $\theta_m = 15^\circ$ (with 8/6 SRM) is kept constant. The original formula in (Takemoto, et al., 2001) was deduced for 12/8 SRM. This means changing some of the constants in proper way to get it working with other configurations. After modifications, the average torque becomes

$$T_{avg} = \frac{12N_p^2 I^2}{\pi} \left\{ \frac{\mu_0 l_{stk} r_{gap}}{l_{gap}} 2\theta_m + \frac{4\mu_0 l_{stk}}{\pi} \ln \left\{ \frac{\pi l_{gap} - 4cr_{gap} \left(-\frac{\pi}{12} + \theta_m\right)}{\pi l_{gap} - 4cr_{gap} \left(-\frac{\pi}{12} - \theta_m\right)} \right\} \right\}. \quad (18)$$

The c used in here is a constant of 1.49.

(Cao, et al., 2009) presented a similar method for 12/8 SRM with more detailed explanation steps. In this **adjustable angles** method, the steps and conclusions are actually almost identical with advanced angle method. A close relation to advance angle method (18) can be seen

$$T_{avg} = \frac{12N_p^2 I^2}{\pi} \int_{\theta_{on}}^{\theta_{off}} \mu_0 l_{stk} r_{gap} \left\{ \frac{1}{l_{gap}} - \frac{16(l_{gap} - r_{gap}\theta)}{(4l_{gap} - \pi r_{gap}\theta)^2} \right\} d\theta. \quad (19)$$

θ_{on} and θ_{off} are related to the advanced angle. Because advanced angle determines the maximum output torque, the values of θ_{on} and θ_{off} need to be chosen to represent the acceleration situation. The angle θ is zero at aligned position. The motor windings are normally turned off in aligned position to prevent negative torque, meaning $\theta_{off} = 0$. In 8/6 SRM the motor windings are turned on when $\theta = -15^\circ$ to get maximum torque. In addition, the coils can be used simultaneously. Then during every other stroke, there are two coil pairs in active at the same time. This is executed by choosing $\theta_{on} = -22.5^\circ$. In advanced angle method, the angle cannot be this high, but in adjustable angles it is possible. Optimal angles to operate 8/6 SRM are discussed in (Pires, et al., 2006).

To compare the methods described here, the same situation is calculated with all of them. The parameters are chosen to represent the machine that will be tested in the test setup (Table 3). The dimensions are same, but the motor type is 4/2 in the test setup. Figure 5 explains physical meanings behind these parameters. The calculated torque values are presented in Table 2.

Table 2. Comparison of different methods to calculate the output torque of SRM.

Method	Calculated torque
Energy conversion, T_{avg}	0.0070 Nm
SRM-type derived, T_{avg}	0.4383 Nm
SRM-size derived, T_{avg}	0.2984 Nm
Inductance values with SRM-dimensions derived, T_{avg}	0.0041 Nm
Advanced angle, T_{avg}	0.0099 Nm
Adjustable angles, T_{avg}	0.0086 Nm
Simulink model, T_{avg}	0.0108 Nm
FEM model, T_{avg}	0.0100 Nm

The second and third method seemed to produce largest torque values. The problem with the second method is the usage of the input voltage. The voltage cannot be defined in same manner as it was done in first method. This method may be incompatible for PWM fed voltage, because the method was introduced already in 1993, when SRMs were controlled without PWM. One reason for too large value of method three is too

large value of flux density $B_s = 1.7$ T, suggested by Miller. The flux density changes while the inductance changes and it is dependent of current, number of winding turns and area A that flux is piercing

$$B = \frac{\frac{L_u + L_a}{2} I}{N_p A} \approx 0.15 \quad (20)$$

Therefore, the torque value gets an error having magnitude of one decade. Still the value is larger than with most of the values.

The first three methods in Table 2 are lacking the air gap length. Usually the air gap is smaller than in the test setup. When the torque is calculated with the advanced angle method using common SRM air gap length of 0.25 mm, what is one fifth of the original, the torque increases 7 times. Therefore, the first three methods produce too high values partly because of abnormally long air gap.

It seems that the advanced angle and adjustable angles methods are the most accurate. With them, the results were close to both of the simulation methods. Although conclusions cannot be made before experiments with the test setup are performed. Both of these methods were originally derived to different type of SRM, which was compensated by changing certain values inside the formulae. The first method proved to be usable

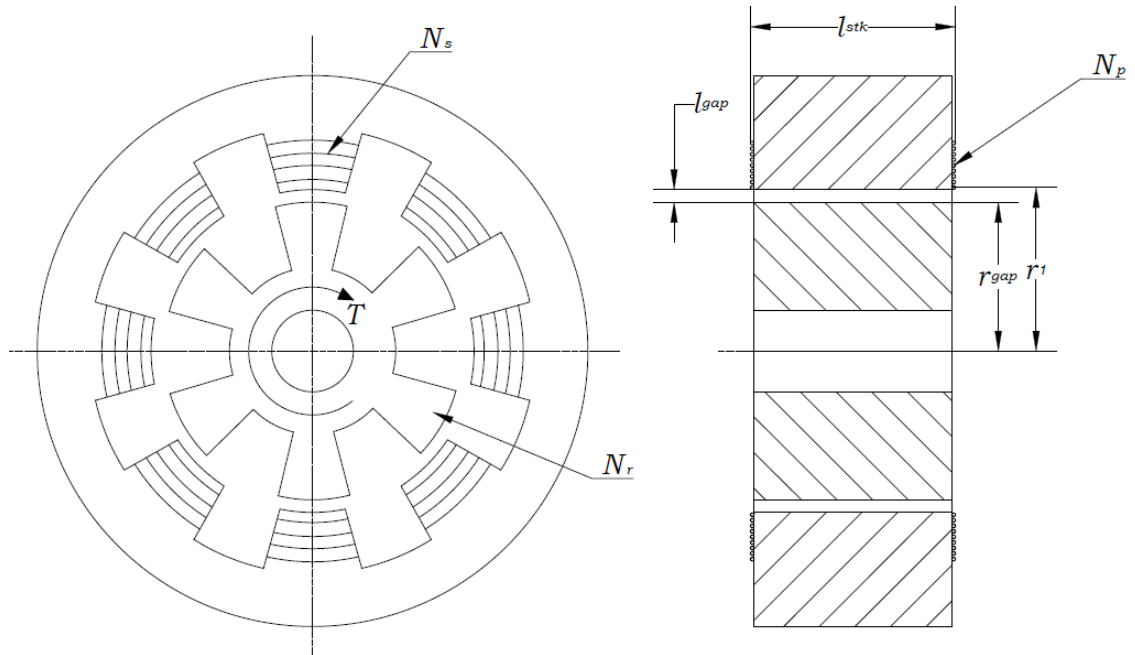


Figure 5. SRM dimensions and parameters appearing in calculations

Table 3. Parameters of the designed SRM to be used in the test setup.

Parameter	Value
Current, I	2.4 A
Radius of the stator bore, r_1	25 mm
Stack length, l_{stk}	65 mm
Number of winding turns per pole, N_p	30
Permeability constant, μ_0	$1.2566 \cdot 10^{-6} \frac{H}{m}$
Radius of the rotor, r_{gap}	23.75 mm
Length of the air gap, l_{gap}	1.25 mm
Coils in serial during one phase, N_{ser}	2
Coils in parallel during one phase, N_{par}	1
Aligned inductance, L_a	0.0012553 H
Unaligned inductance, L_u	0.0006168 H
Constant, c	1.49
Advanced angle during acceleration, θ_m	-15°
Switching on angle, θ_{on}	$-7.5^\circ + \theta_m$
Switching off angle, θ_{off}	0°
Number of rotor poles, N_r	6
Number of stator poles, N_s	8
Number of phases, m	4
Cross section area of stator pole, A	495 mm^2

3.2.2 Power electronics and controller

The power electronic controller is an extension for software part of the controller. The borderline between these two is vague when considering certain controlling tasks. It comes down to opinion of either doing it programmatically or by hardware. The control program can be designed and verified at the same time with simulations. Problem with the simulations is the ideal response of the motor to controller's signals. In real life, for example the current level is not constant; it has some kind of a waveform, it has delay from control signal and it cannot be measured ideally precise. The power electronics tries to provide as good current as possible by minimizing these tendencies. In general, the SRM controller is considered as more complex than other electric motor controllers are (Miller, 1993). This stands both from electronic and software point of view. In Figure 6 is a block diagram of the control system for SRM. The block "SRM & Power electronics" presents hardware part of the system, making rest of the blocks belong to the software part of the control system.

The main power electronic components are converter and current controller. Converter has a fundamental task of converting DC to AC of specific waveform. Current controller controls the converter. Commonly used converter configuration is the asymmetrical half-bridge. It has two switches per phase that is opened and closed with output signals of the current controller. The current controller can be hysteresis type or PWM type. The hysteresis controller is the preferred one although they both have their

benefits. Current controller is fed with signals from the software, and more precisely from the commutator. (De Doncker, et al. 2011)

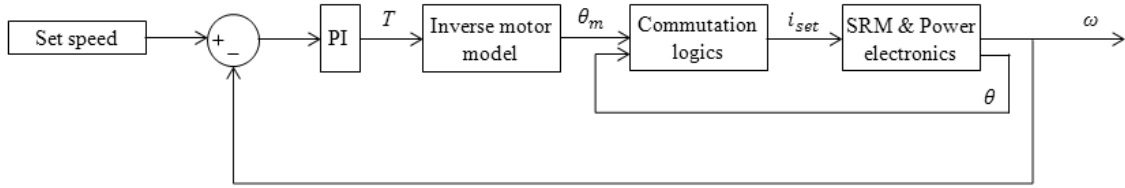


Figure 6. Block diagram of basic control system for SRM speed control. Everything else but the contents of the block “SRM & Power electronics” is implemented into the software part of the control system.

The commutator, or Commutation logics as it is presented in Figure 6, has an output signal that is a logic value of zero or one representing the magnetization state of a certain phase of the SRM. Therefore, the main task is to compare measured rotational angle to desired θ_{on} and θ_{off} values, and to supply the activation information to current controller. On and off values are calculated by the software part of the SRM controller. As said earlier, their value depends on the value of advanced angle θ_m of Figure 7, which is calculated from the mathematical model of the SRM (18). This kind of speed control method is more efficient than those which use constant values for θ_{on} and θ_{off} . The measured speed is compared to set speed and the error value is supplied to PI controller in every method. The main difference is the output of the PI. In this method, the output is used as an estimate of the torque needed to reach the desired speed. This signal is an input for the mathematical model. Hence, the speed is controlled by changing the average torque produced. The torque is also controlled by the same rotational speed feedback loop. There is no need for separate torque measurement. If loading torques tend to slow down the motor, the speed control raises the output torque to prevent the decrease in speed. In practice, to decrease the rotation speed the momentary winding current is set to zero. At this situation, the torque is also zero and the loading torques decelerates the speed. Of course it is possible to use the negative torque for braking, but the speed tends to slow down fast enough just by itself. With properly tuned PI controller, the overshoot of speed in the situation of acceleration to target speed is almost unnoticeable.

The magnitude of the torque is determined by the timing of the on/off switching of the coils. Figure 7 presents how torque is formed from inductance and current. This applies to an ideal case. In real motor, the waveforms have more rounded shapes and they are fluctuated. Torque is formed as it was described earlier in equation (3). The waveform of inductance depends on the physical properties of stator and rotor. If current is switched on before slope of inductance starts to rise, the torque is still zero. The horizontal line between the strokes represents the passive state of the phase in question. In the case of Figure 7 the motor is 4/2 type, so there are two phases. When phase one is in passive state, the phase two is active. If waveform of torque is examined, it can be seen that the average value for torque during on rotation is only one third of the

maximum value. When the other phase is also taken into account, the average torque is of course doubled. With real motor, the waveform of torque is not this ideal. The maximum value is held shorter time, it being only spike usually on the either end of the square wave.

When speed control method that relies on θ_m is used, the value of θ_{on} changes according to θ_m that is controlled by PI-controller. The minimum value of θ_{on} depends on the type of SRM. In theory, it could be -90 with 4/2, but negative torque may occur. This is why -67.5 is preferred value. θ_{off} can be kept constant at zero, but it is possible to couple it to θ_m also. Sometimes the switching off cannot be delayed into total aligned position, because negative torque may appear. In this case, θ_{off} needs to be smaller, for instance -10°.

In addition, the boundary values for θ_{on} and θ_{off} are affected by the number of rotor and stator poles. The accuracy of switching on and off compared to optimal values should be 0.25° – 0.5° (Miller, 1993). Therefore, the calculated values in relation to measured instantaneous angle should be correct together with the measured value to get exact timing. To maximize the torque, simultaneous coil pair activation can be used in some motor types, but not with 4/2. In (Pires, et al., 2006) were deduced optimal angles to do this. With 8/6 SRM, the phase should be turned on 22.5° before aligned position, which results in two active phases at the same time. This is true only in every 7.5° intervals. At the rotation angle where the advance of 22.5° has changed to 15° (coil No. 2), the previous coil (coil No. 1) has reached an aligned position. Therefore, it takes another 7.5° to rotate to position where the next one (coil No. 3) can be activated. If it is done before this, there may occur negative torque.

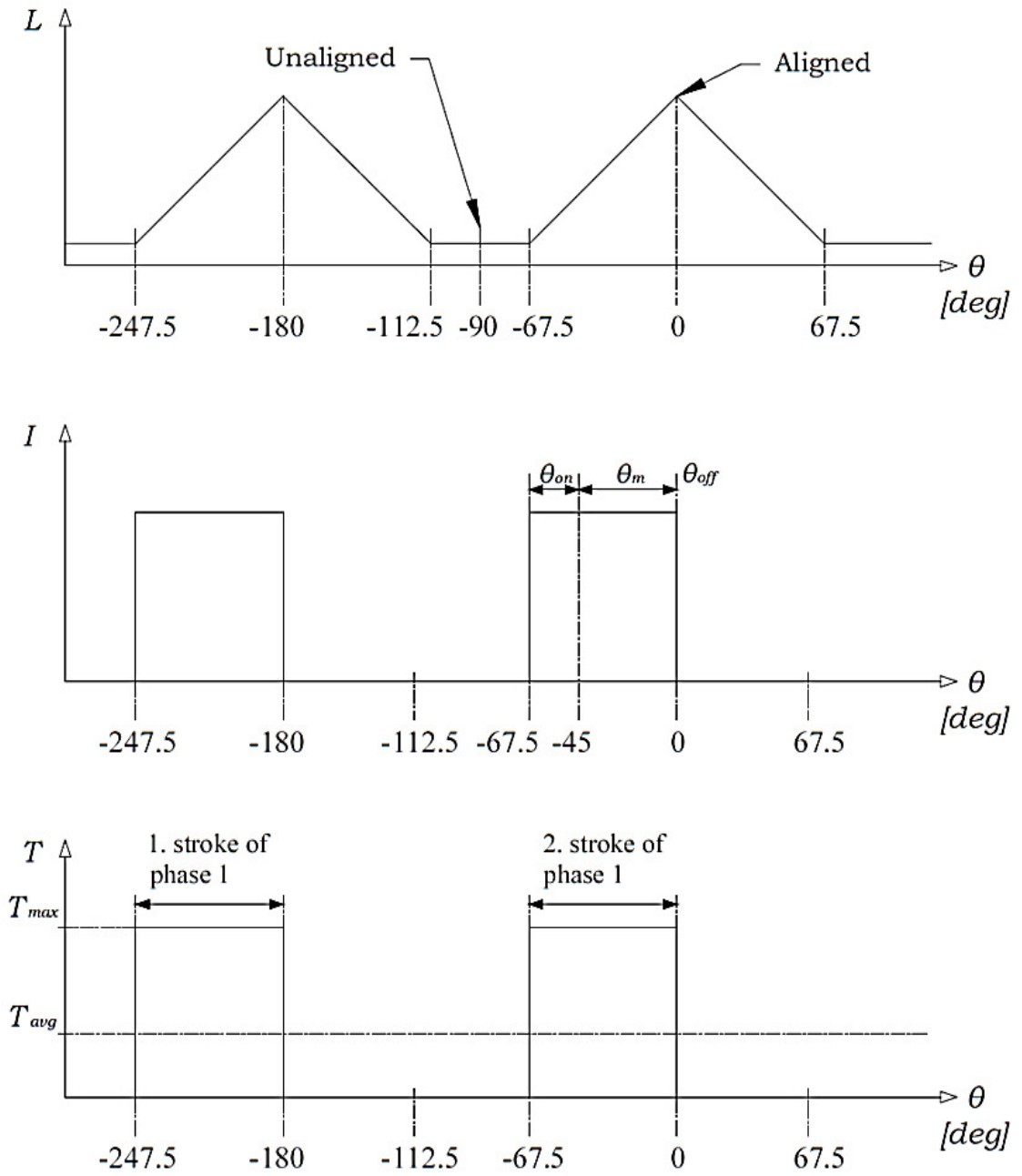


Figure 7. Inductance L , current I and instantaneous torque T of one phase of 4/2 SRM in idealized form.

3.3 Solutions for problems with SRM

In this section, ways to manage with rest of the major SRM's problems are investigated. The basic challenges were already discussed in the previous chapter. Now the aim is at the problems that can be seen as secondary when compared to previous ones such as difficulties in commutation, which is a primary concern of motor usage. Although the problems now on a table are secondary, they are more demanding to solve and cannot be neglected when commercialization of SRM is on mind.

3.3.1 Torque ripple

The most effective and therefore most popular way to affect to torque ripple is to use control-engineering tools. Studied by (Russa, et al., 1998), a commutation strategy that can be used with SRMs was proposed. The strategy of Russa, et al. works for motor types that have at least two phases producing positive torque at the same time at any given rotor angle. Hence, the most simple construction that could benefit from this is the 8/6 SRM. The method is using non-linear SRM model, it is speed dependent and the motor is controlled based on real-time calculations instead of precalculated data. Russa, et al. (1998) minimized the torque ripple by forcing a zero voltage to the coil near aligned position and switching the following coil on; even better performance was achieved by supplying the coil with negative voltage before forcing zero voltage. The key idea in studies of Russa, et al. (1998) was to produce smooth transition of output torque between the phases decreasing the torque ripple by increasing current drop rate; the speed dependency in the demagnetization periods was utilized. In slow speeds, the negative voltage is not needed, but when the speed is increasing the zero and negative voltage durations need to be adjusted. The drawback from switching the first coil to zero voltage is the lower maximum torque. The average torque may not be negatively affected from this control method because the maximum torque is usually only a narrow peak. According to (Russa, et al., 1998) this algorithm maximizes the motor's capability to produce torque.

The research of (Cajander & Le-Huy, 2006) had a goal on finding a way to reduce torque ripple, using simulations of a certain motor to discover the precalculated commutation on and off angles. In this study the motor type was 8/6 SRM as well. Unlike in the previous research, this one was targeting on an optimized controller for only one specific motor. Thus, the results cannot be generalized but the method can be used to any given motor if enough precise motor parameters can be obtained for the simulations. The main idea is to simulate different θ_{on} and θ_{off} values in ranging speed from starting the motor to presumable maximum speed. The average torque is highly affected by θ_{on} especially. It seems that the proposed method has a good influence on the average torque, but the ripple seems to remain the same. However, the relative torque ripple becomes lower when the average torque gets higher.

As the ripple seems to be a function of the state of the motor, a controller that can adapt to current state of the system seem to be needed. The preceding studies introduced methods that were adapting into the speed of the motor, which has been empirically shown to affect to the torque ripple. However, they did not adapt in to the ripple itself or

something that describes the ripple, such as acceleration, torque or speed ripple. A neuro-fuzzy compensating mechanism to reduce the torque ripple was investigated in studies of (Henriques, et al., 2000). The research concentrated on how to train the controller to work on optimal way in simulations. According to the simulation results, the ripple went down significantly.

The use of control engineering is not the only way to affect the torque ripple. In (Lee, et al., 2004), rotor geometry for low torque ripple was researched and a notched tooth was proposed. The research method was based on FEM, as it usually is when torque ripple is studied using control engineering tools as well. The use of control methods are more broadly researched although it seems that with geometry changes the ripple can be reduced at least as much. Many of the control engineering methods actually did not reduce the ripple but they increased average torque reducing relative ripple. It would clearly make sense to combine these two approaches to exploit both of these good results. Lee, et al. (2004) managed to reduce the ripple almost 50 % and it affected especially on the deepness of the canyons and height of the spikes in torque waveform. The rotor notch was discovered by analyzing shapes that would reduce flux leakage just before overlap of the stator and the rotor teeth. According to Lee, et al. (2004) this flux leakage is the main reason for torque variations. When the leakage is reduced, the inductance in relation to rotational angle -profile is more linear. If the inductance profile were perfectly linear, the torque ripple would be zero.

3.3.2 Radial vibration

The radial vibration is divided into vibration of stator and into vibration of rotor. The rotor in here includes also the shaft; the key in here being the mass concentration that rotor produces for the shaft. Different stator and rotor deformation shapes and modes are presented in Figure 8. The tendency for deformation comes from the flexibility in the stator, in the rotor and in the bearings. The modes of Figure 8 should be considered as property of the system that is awoken if the system is excited in a right way. The excitation source is a force either due commutation or due rotation. The latter can be specified even more dividing it into centrifugal forces and into mechanical forces. The commutation force is the radial electromagnetic force acting between the rotor and the stator poles. The centrifugal forces are dependent of the rotation speed and unbalance distribution in the rotor. The mechanical force is developed mainly from journal bearings and possible touchdowns between the rotor and the stator during rotation.

When the origin for the radial vibration is the radial force acting between the rotor and the stator, the force is affecting as a pulling force towards the stator. The rotor does not experience deformation with ease, because it is stiffer than the stator (Ellison & Moore, 1968). The stator has a tendency to deform into an oval shape, which is the lowest normal mode of the stator (in Figure 8, lowest deformation mode of stator). The vibration is born when the force is switched off and the contracted oval shape stator elongates in a way that is analogous to a mechanical spring (Li, et al., 2009). Methods described in here to cope with this phenomenon are minor modifications here and there to patch certain characteristics. The most researched solution, bearingless switched reluctance motor, will be discussed in its own part. As it was in the case of torque

ripple, with radial vibrations the means for solving the problems can be divided into mechanical and control engineering. In practice, the mechanical stands for designing a stator that does not resonate with an excitation the radial force is producing. The power control of the commutation phases to operate the SRM is in the favor of control engineering research. When simplified, the problem is how to switch on and off the transistors of the H-bridges that control the voltage that affects to current passed to the motor coils.

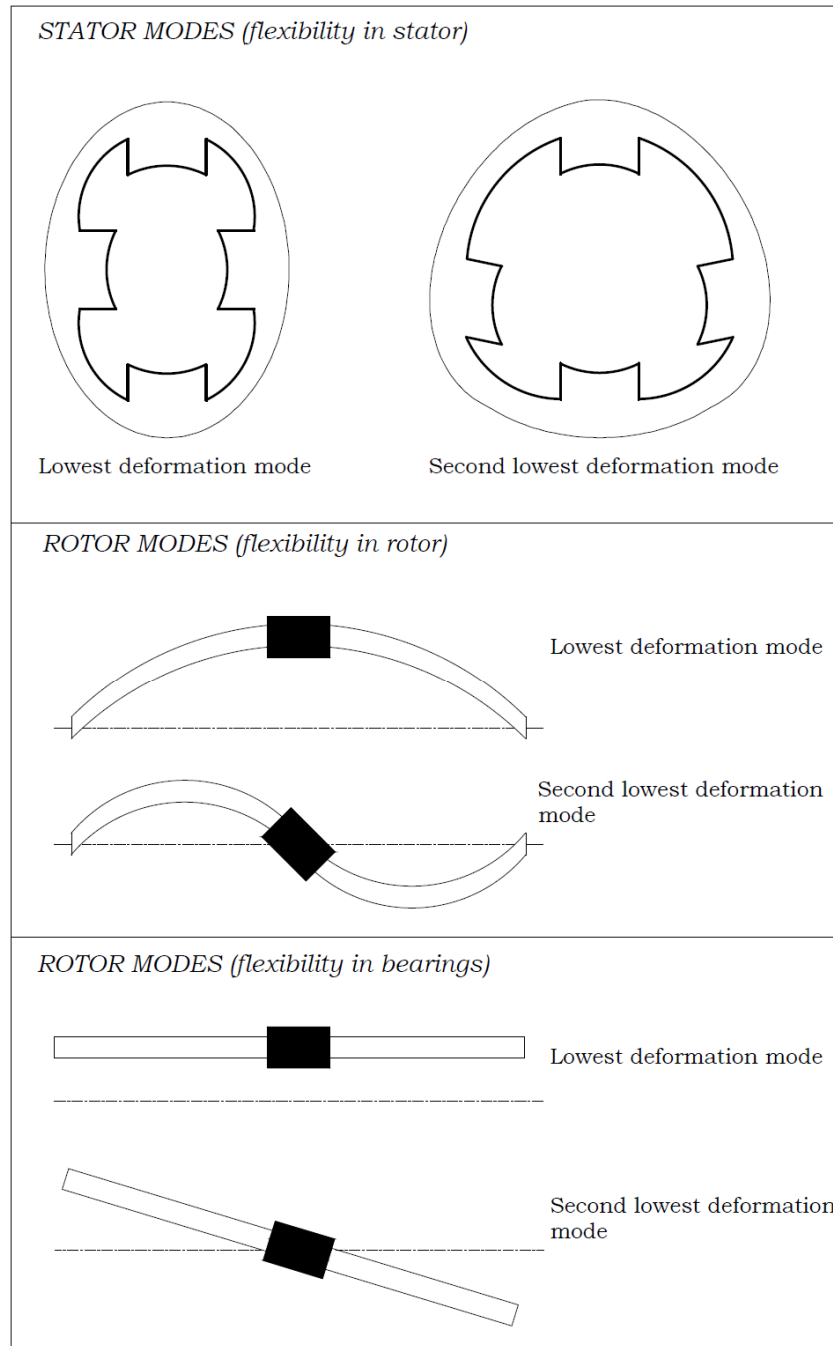


Figure 8. Two lowest deformation modes for stator and rotor.

The active vibration control (AVC) by controlling the power electric transistors has been widely recognized to be the best supply manipulation-based way to reduce radial vibrations. This method was first proposed by (Wu & Pollock, 1995) and even fifteen years later, it has still been analyzed in studies of (Liu, et al., 2010). The method has negative effect on the output torque performance; however been still less than the other methods. The dominant stator deformation, at lowest mode, happens when the switches of an H-bridge are turned off to end the commutation of the phase. Normally, the two switches of one H-bridge are switched off at the same time. The basic idea of the method is not to do the switching simultaneously, but first switching other one and the last one after half of a resonant cycle later. This will result in suppressed vibration. In (Liu, et al., 2010) the topic was on finding an analytical model for predicting the level of the vibration reduction when AVC method is used. In addition, Liu, et al. (2010) analyzed factors that can influence the vibration and reduction of the vibration.

In some cases AVC has not been applied, but mechanical design means to control vibrations passively has been developed. Surprisingly, the mechanical design means are more recent than the other methods. The reason can be found from the suitable method to study vibrations of deforming bodies: FEM. As it has been with many other problems of SRM, the research towards them has been arisen more after advances in computer science. This case makes no difference, since relatively much computation power in FEM is needed to include non-linear formulas using small step size with dense meshing. The study by (Li, et al., 2009) concentrated on investigating the reduction of vibration caused by two aspects, namely radial force excitation and the structure born transfer function. The latter is determined by the geometrical design of the machine, and to be exact, by resonant frequencies of the stator. To examine this, a modal analysis was carried out. An ideal stator construction was found for the motor matching the specifications. In addition to FE analysis, vibrations of different stator frames were measured using an experimental setup. The research included a rule of thumb for eliminating the source of the radial vibration as well. Li, et al. suggested using low current and instead to use high number of turns in the stator pole when designing the stator coils. This practice is conducted to achieve delay in the decay time of radial force when the phase excitation is switched off. The delay comes from the increased inductance and thus the electrical time constant. This means decreased slope of the radial force, which affects positively to the deformation properties of the stator. This study is rather recent and it describes well the trend in research of SRM: the approach to problems is done both mechanically and electromagnetically. The solutions are actually simple, but to understand the problem, one needs to know well both mechanical and electrical fields of research.

3.3.3 Noise

The noise is usually a symptom of the radial vibration. The portion that arises from the radial magnetization force can be easily verified performing a test where commutation is switched off and movement of the stator is being measured. Thus, if the noise is still audible after switching the commutation off, the noise is not coming from radial force but from aerodynamic interface (Fiedler, et al., 2005). The remedies for radial force born noise are the same ones discussed in previous sections. In the case of aerodynamic

noise, the decay is not easy to measure, therefore Fiedler, et al. suggested that the best way is by ear. Sources for aerodynamic noise can be divided into several categories: escape noise, inflow noise, cavitation and rotating pressure fields (Fiedler, et al., 2005). Excluding the last one, these noises are born especially when cooling air is conducted through the rotor slots, according to Fiedler, et al. Pressure fields start to rotate and emit noise when rotational speed is high enough and therefore pressure difference between in front of the rotor pole and trailing side of the pole is high. In this same research, methods for aerodynamic noise such as filling the rotor slots with nonmagnetic material, keeping pole number low as possible and having a long air gap were proposed. The whirling rotor can increase the pressure fields especially when rotation speed approaches the natural frequency of the rotor. The lowest deformation mode of flexible rotor (Figure 8) is the one where the middle point of the shaft rotates with eccentricity, having larger rotational radius than the radius of the shaft itself. This means smaller air gap, which increases the pressure of the rotating pressure fields. In the worst case, the rotor can touch the stator that will most likely emit noise.

3.3.4 Bearingless SRM

BSRM itself can be seen as a reasonable objective but in addition, it makes possible to affect positively to radial vibration problems. The fundamental idea is to replace the mechanical bearing with an AMB function of a BSRM. Besides producing just a supporting force, it is possible to form a desired resultant force composed of different force components. With intelligent control system, motor that performs multiple compensation tasks by quickly alternating between tasks can be achieved. Hence, in theory it would be possible to combine supporting of the shaft, radial movement compensation of the rotor with compensation of the deflecting radial magnetization force. The first and second one can be combined together because they both are producing force to keep the radial movement of the shaft at minimum. The radial force compensation has a different goal. The idea is to produce a force that compensates the oval shape tendency of the stator frame.

Adding the AMB function to an SRM brings out many new problems, such as decreased performance because of negative torque that is produced when auxiliary radial force components are added to gain desired resultant force. There are three different topologies to design the BSRM. Inside one topology can be added different construction variations and different SRM types (number of rotor and stator poles). The simplest topology in controller's point of view is the one that combines a separate AMB stator with a separate SRM stator. In Figure 9, the variation 1.1 represents this kind of construction that has decent distance between AMB and SRM. They both have rotor constructions of their own. The next one, 1.2, is the same thing with minimal distance between the stators in addition with a rotor that consists of two partitions. This construction is more compact then the previous one although the 1.1 had an advance of being capable of operating without AMB and SRM disturbing each other's magnetic fields. Simpler version would be the 1.3, which has a uniform rotor cross section. Problem with this one is the SRM rotor cross section, which would have to work out for AMB also. The number 2 in Figure 9 has one stator that needs to have double number of windings compared to previous topologies to get the same amount of torque. This is

because there are two successive layers of windings to enable the force function that combines AMB with SRM. The rotor cross section needs to be uniform. Even though the separate force and torque windings are affecting each other, it is possible to control them independently (Cao, et al., 2009). When using only one set of windings in one coil, BSRM operation can be still achieved (3.1 and 3.2 in Figure 9). The control system is the most complicated, but the construction is simpler. Both uniform rotors and separate cross sections are used.

Not all of the topologies mentioned are researched at all or at least they are hard to confront. This subject is so novel that review of different methods cannot be found yet, therefore it is not clear which topology is the best. It may even be so that the best one is still to be discovered. The research of BSRM has been concentrating mostly on topology 2 of Figure 9. The construction is more compact than in the first three that have consecutive windings for AMB and SRM. Conventionally the motor type is 12/8 that has double winding layers on every pole (Takemoto, et al., 2001). Takemoto, et al. published one of the very first studies of BSRM, proposing control methods that cross use the radial force and torque but now the state in research has moved on to control these both independently (Cao, et al., 2009). A special variation of topology 2 is introduced by (Guan, et al., 2011). Guan, et al. used motor type of 8/10, hence the rotor unusually having more poles than the stator. In addition, the motor has separated torque and radial force poles. This said there are four dedicated coils for both functions. The suspension of the rotor seemed to work well with this topology, but the motoring function was not analyzed in the same detail. The output torque and especially the ripple in it may be a problem.

Topologies 3.1 and 3.2 are more fresh than the others. Hofman has studied recently the variation 3.2 of Figure 9, using an 8/6 type motor (Chen & Hofmann, 2006), (Chen & Hofmann, 2007), (Chen & Hofmann, 2010) and (Li & Hofmann, 2012). The novelty can be seen from the progress of the mentioned publications that all handle the same research. The control method is developed further in every research. In the most recent (Li & Hofmann, 2012), the stator has always six of eight coils excited at any given moment, which calls for well-engineered controller. The motor type was 8/6, but the same kind of one layer winding arrangement with 12/8 type has been under investigation by (Lin & Yang, 2007) also. On the other hand, the control method is entirely different. With 12/8 motor, sinusoidal current signal is fed to separately control the force and the torque. The results showed some attenuation in vibration but the torque performance was not good with sinusoidal exciting. The variation 3.1 that has two different sections in a rotor was used by (Morrison, et al., 2008). The circular part was included to help with the radial forces. When comparing variations 3.1 and 3.2, not much advance was gained when non-uniform rotor (3.1) was used.

The study on topologies 1.1-1.3 is not found interesting enough amongst researchers at least to inspire them to publish research involving these topologies. It would be easy to combine for example the AMB studied by (Tammi, 2007) to any given working SRM, for instance to the one used in this particular Master's thesis. In Tammi's (2007) research, the actuator controller was designed to keep the eccentricity at minimum. Therefore, the aim of the combined system would be the same as it is in every BSRM.

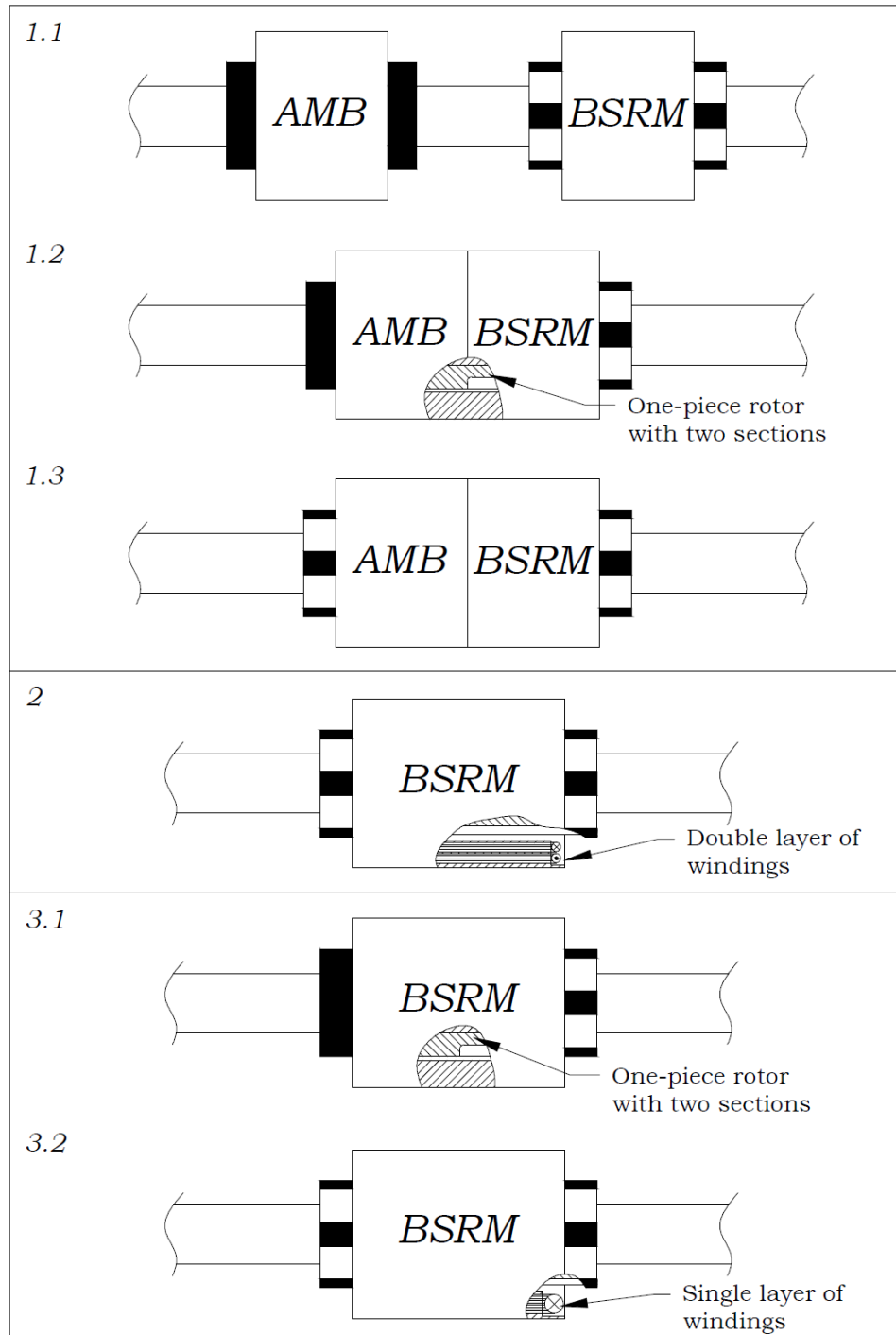


Figure 9. Three different topologies to implement bearingless switched reluctance motor. Topology one has three variations, topology two one and topology three two variations.

4 Materials & methods

4.1 Test environment

Description of simulation models and the test setup is presented in this chapter. The initial idea was to use the original AMB testing environment without any significant structural changes. Only the rotor of the setup was to be changed. The original test setup was used in studies of (Tammi, 2009). Fortunately, the designing of the first version of the rotor (Figure 10) was started in early meters so it arrived from the manufacturing in good time. This gave a chance to perform a quick test of the system. The system had a graphical user interface for rapid testing. With this, it was possible to feed the desired signal to the stator without making any changes to the source code of the system. It did not take long to realize that not everything was correct with the setup. The AMB's performance was coarsely verified earlier to work as it used to. Therefore, the problem was not in the original system. After analyzing the situation with my colleagues, it was turned out that the stator was not the type it was believed to be. Externally it seemed to be an eight-pole stator, but in practice, the windings were coupled in a way that it worked as a four-pole stator. The problem was with the adjacent coil coupling that formed a horseshoe magnet. It was known that the stator of the AMB device was built by coupling two coils together forming four horseshoe magnets. However, the impression was that the coupled poles where the opposite ones not the adjacent ones. The difference between these two constructions is that in SRM the opposite coils are always excited at the same time. Opposite coils are activated to produce more torque and to prevent the rotor to move towards the stator by producing force components pointing to opposite directions to cancel each other's effect. This is the fundamental working principle and it is generally used as a base of a design.

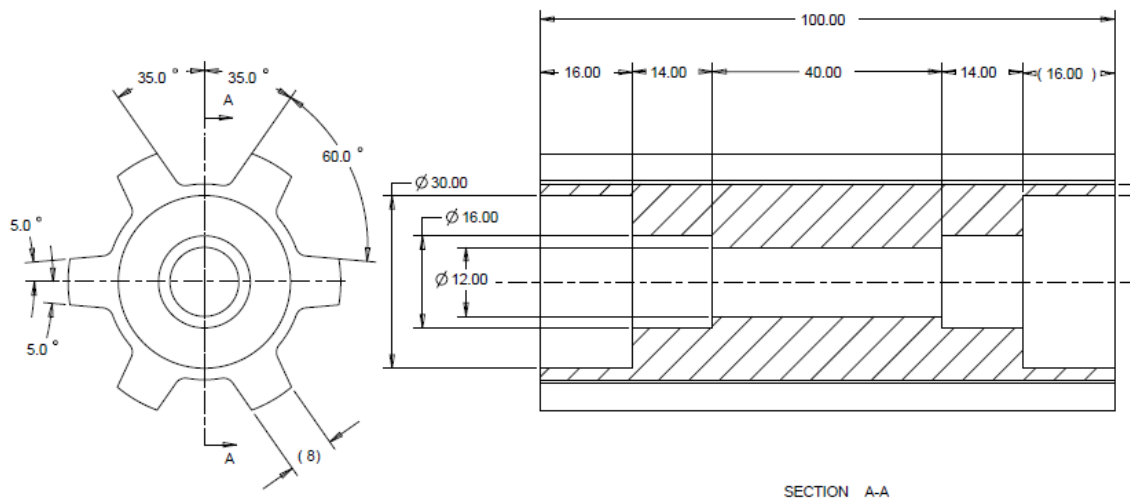


Figure 10. The first version of the 6-pole rotor.

For the construction that works with the four-pole stator, another version of the rotor (Figure 11) was designed. A more specific description of the rotor is given in the later section that covers all the other rotor designs too. The type of the motor is 4/2 2-phase. In contrast, the eight-pole version is an 8/6 4-phase motor.

The test rig that is used in both of the test setups, included a stator that has a topology such is presented in the left most view of Figure 12. The type of the motor is 4/2, which means there are four poles in the stator and two poles in the rotor. The actual number of poles in the stator of the test rig is eight, but as said before, the adjacent poles are connected to each other. This is why the stator works in a same manner as the four-pole stator in the right most view of Figure 12.

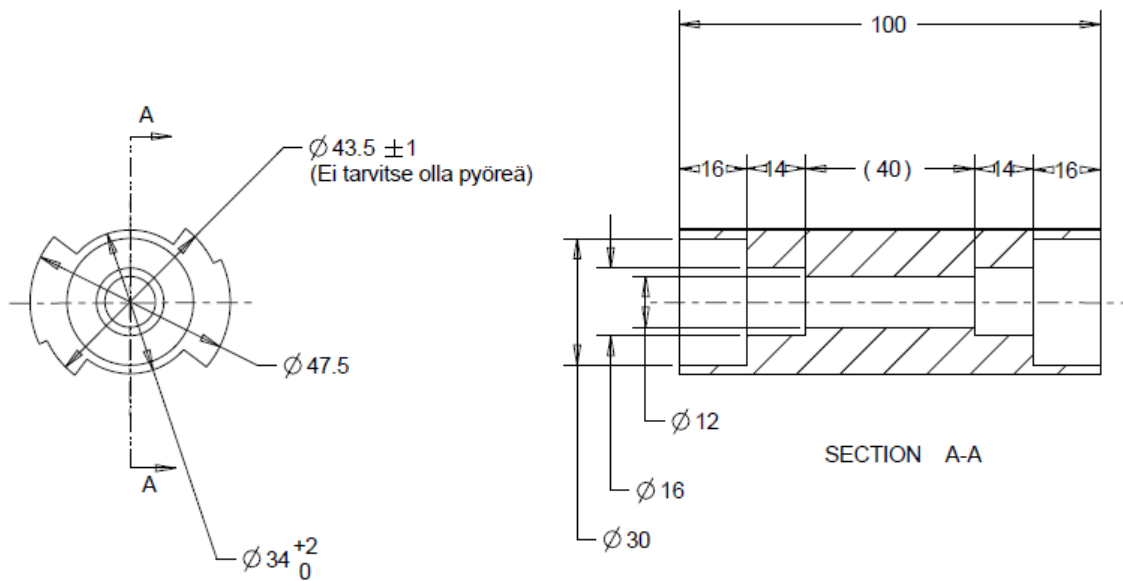


Figure 11. The 2-pole rotor for the 4/2 2-phase SRM that has adjacent main flux. The rotor is designed to be a self-starting type to start rotating on every starting position.

Problem with the conversion from AMB to SRM is that the optimal AMB stator is not the optimal SRM stator. The reason for this is the difference in the flux paths. The flux should go through the rotors center to the opposite side of the stator rather than from the adjacent stator pole to other (see Figure 12). The horseshoe configuration was used in the AMB setup to maximize the flux density and therefore to produce the maximum force. Better controllability of the force production was achieved by utilizing an opposite horseshoe magnet pair excitation meaning that in all there was four coils active simultaneously to produce force into horizontal or vertical direction. This is a common construction for AMBs. Opposite magnetic flux -constructions are also researched, and especially the one with three poles seems to be potential (Chen & Hsu, 2002). In this, the configuration does not use the horseshoe magnets, but it uses method that is more close to the one that is used in SRMs. This is the reason why it is possible to be misled between the different coil coupling methods. A minor change had to be done to the

Assembly source code of the original AMB control system. With this change, the opposite horseshoe magnets were forced to be active at the same time. According to FEM simulations, the flux does not pierce through the rotor in test setup's case at all but it is high between the adjacent poles of the horseshoe magnet (Haarnoja, 2012). Still, the output torque is low because of the large air gap at the situation where the previous coil pair is switched off and the next one is switched on. This is actually something that is inevitable with two phase SRMs, and the large air gap just decreases torque even more.

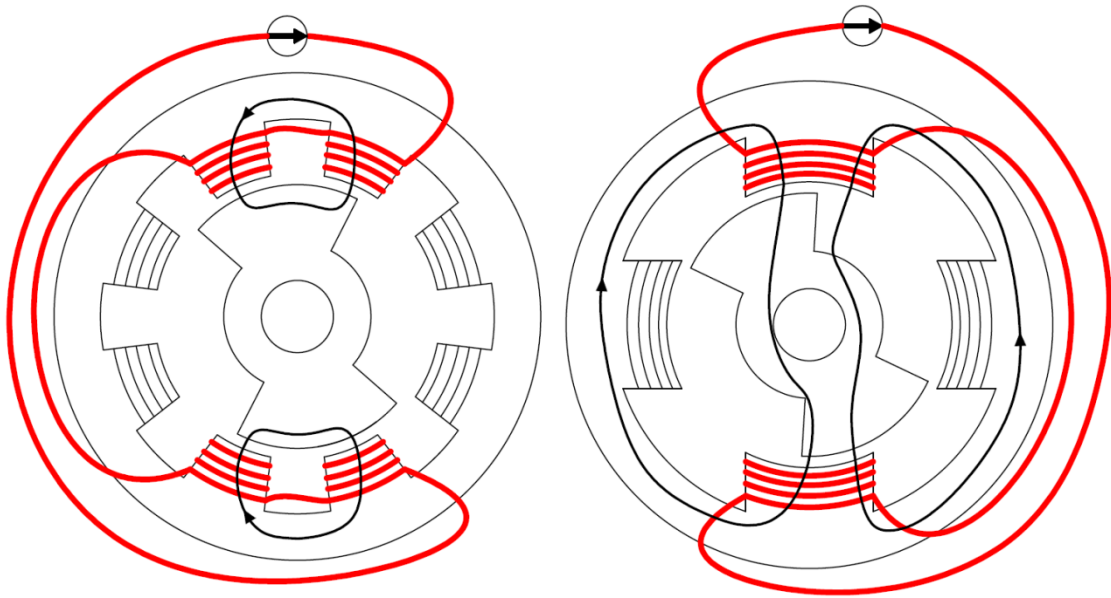


Figure 12. 4/2 type SRM modified from an AMB (left) and normal 4/2 type SRM.

The software part of the test setup was done using National Instrument's LabVIEW that has its own VI block diagram programming language that reminds of Simulink model building. With LabVIEW, it is also easy to do the required measurements from the system using the CompactRIO data acquisition platform. In addition to the two test devices the test environment included also the simulation models of the 8/6 4-phase and 4/2 2-phase motors.

4.1.1 Simulations of the model

The initial usage for the simulation model was to get an understanding of the non-linear nature of the SRM. The model was built to give an estimate of the achievable performance level of the test setup's motor. MATLAB Simulink includes a simple example model to demonstrate the built-in SRM block. This model was used as a starting point. The demonstration model is for 6/4 3-phase motor. The model does not contain any other control from the feedbacks than the mandatory current commutation control. There was not much to use as such, but at least some idea for the simulation logic was found useful. Still the model for the electronics behind the commutation logic was used as it is. The SRM block needed the motor specific parameter values to

simulate its behavior. FEM model of the motor's magnetic fluxes during commutation was needed to obtain some of the parameters.

The first thing to add to the demo-model was the feedback for the desired rotation speed. In this, the PI-controller sets the target torque to minimize the error between the set value of the speed and the measured speed. The torque value is used for defining the advanced angle. The mathematical model between these variables forms an inverse motor model. Regular form of the mathematical model is the one discussed in (18) in the section 3.2. This control method that uses θ_m is adapted from (Takemoto, et al., 2001). When SRM was simulated, the fed current was kept constant. To change the motor torque, the current is chopped to phase currents according to advanced angle, which controls the commutation by affecting to the turn-on angle of the motor phases. The chopped current vector is compared to actual current and the error value is discretized on every simulation step. From this on, the electronics feed the current to the motor. In real control system, this is implemented in different way. A block diagram of the simulation model is shown in Figure 6, which is valid for the real control system too. In Appendix A, this model is presented in more detail as a Simulink block diagram. From this model, a simplified version was built to be converted into LabVIEW simulation model. The detailed Simulink block diagram is presented in Appendix B. This model has same functional contents as the one shown in Figure 6, but the SRM block is replaced with self-made function that describes SRM properties. This so-called ideal model lacks the simulations of the power electronics that are included in previously introduced specific model. The specific model was not available for 4/2 SRM, this motor type was simulated only with the ideal model. The 8/6 type was simulated with both models even though the test setup uses 4/2 type motor. The results of simulations of specific 8/6 model can be used for comparison when the ideal model of this motor type is also simulated. Detailed description of Figure 6, which includes most important parts of both ideal and specific simulation models, is given further of this work when the test setup is described. Test setup's main control logic is based on these simulation models.

As said, the ideal model was converted into LabVIEW simulation model. Detailed block diagram of this model can be found in the Appendix C. The model is created by importing the MATLAB Simulink model into LabVIEW, which converts Simulink's blocks into equivalent LabVIEW blocks. The conversion does not work for all the blocks at all, and for some blocks, the conversion produces something that has completely different function. In practice, the conversion still helps when building a new LabVIEW simulation model by creating at least a placeholder for every block.

4.1.2 Test setups

Two test setups were used for testing SRM. Both of these use the same test rig that includes stator, rotor, shaft and mechanical bearings (Figure 13). The first tests were performed using a control system that is originally designed to control active magnetic bearing. This system had a user interface that could be used for performing quick tests and diagnosing the system. First, it was confirmed that the original AMB system was working properly. Discovering the correct values for necessary parameters was the most

difficult part. After this was done, the cylindrical rotor was replaced with 2-pole rotor and the control system was modified to match the SRM requirements. First the AMB's basic nature of applying only positive or negative force in certain direction was changed to excite opposite forces, which is the fundamental working principle of SRM. Because AMB tries to pull rotor into given direction, the counter force to opposite direction would cause smaller resultant force. This logic was originally implemented with Assembly source code into software part of the controller. The change itself was only minor, but finding this from numerous source code files required effort. With this change done, it was possible to excite rotation by feeding periodical signal to stator coils. It was possible to use either sinusoidal signal or square wave signal. When the signal has positive values, the phase one is active and with negative values, the phase two is active. This way the rotation happens without any feedback from the rotational angle. The rotational speed can be calculated from the frequency of the signal by dividing it by two. By changing the supply frequency, it was possible to adjust the rotational speed, but the change had to be done carefully because without the feedback the rotor can easily drop out of the pace. When this happens, the rotation stops immediately. When sine wave was used, the frequency could be raised by sweeping it, so the smooth sweep partly prevented getting out of pace. With square wave, the frequency had to be raised manually by changing the value itself. To start the motor, the magnetic field needed to be first set to rotate in at least 240 rpm. Then an initial speed for the rotor was given by hands to catch the magnetic field.

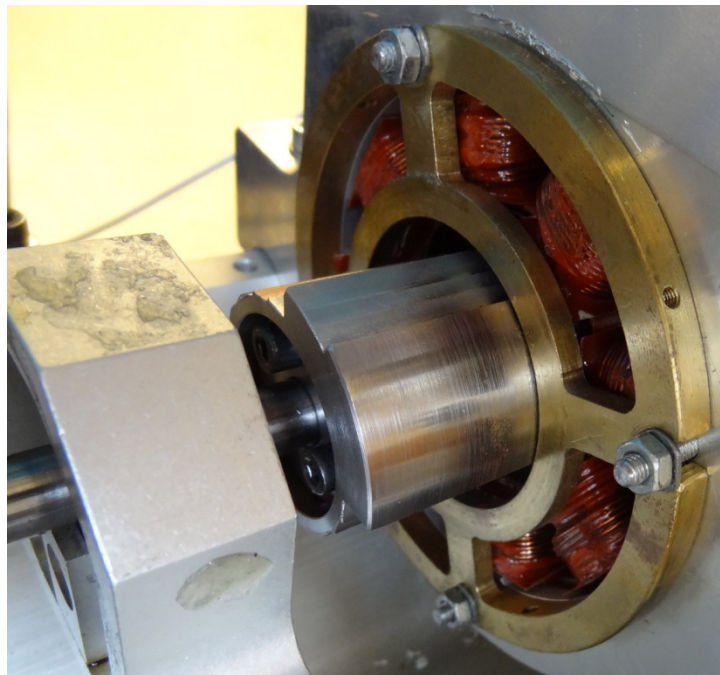


Figure 13. Most essential parts of the test rig: stator, rotor, shaft and mechanical bearing.

and other time-critical tasks. The real time part can read the values of the variables being handled in the FPGA. This way the real time feature is capable of handling the commutation, speed control and some other subtasks that are needed. The FPGA part has many restrictions in available blocks to be used. In addition, the compilation and building to final executable takes about 30 minutes. This means waiting the 30 minutes before program can be started, if any changes have been done to source code since last run. In real-time part, the wait time is under half a minute. This drives the division between these two towards real-time biased, which makes the overall control system slower.

The encoders are the same ones that were used in the original AMB test setup to measure deflections of the shaft. In SRM use, they are harnessed into rotation encoding. The encoder system consists of two eddy current sensors that are measuring holes of the encoder disks (Figure 16). These disks work also as flywheels: additional masses to smooth the dynamics of the test rig. There are only two opposite holes in one disk. With two sensors and two disks it makes four in total, which means 90° , still being not much as a resolution for angular position measurements. For measuring the speed, this is enough. To go around the resolution problem, the encoder disks are adjusted on the shaft such a way that the holes are aligned with sensors when corresponding SRM's phase is in alignment. Therefore, when phase one should be activated the sensor one sees a hole, which can be seen as a high pulse in signal waveform produced by the sensor.

The signals coming from the sensors are low-pass filtered to eliminate high frequency noise. A block "Pulse counter" is located in upper left corner of Figure 14. In here, the waveform of the sensors is analyzed and speed is calculated. The information of the sensors' waveform is passed to a block called "Rotational angle" transducer. This block transforms the pulse train into square wave that represents states of phases. For both of the phases, there are own square waves. These waveforms are in opposite phase. They are high 90 degrees at a time alternately. With these signals the motor can be already operated. The external H-bridge can be fed with these signals because it has its own integrated current control. For DC-Servo, these signals are used as a reference signal for target current. In Figure 14, under the label FPGA is area called "Current loop". Here the reference current is compared to measured current and the PI controller tries to set the duty-cycle rate for PWM generator to produce a voltage PWM signal that corresponds to the reference current.

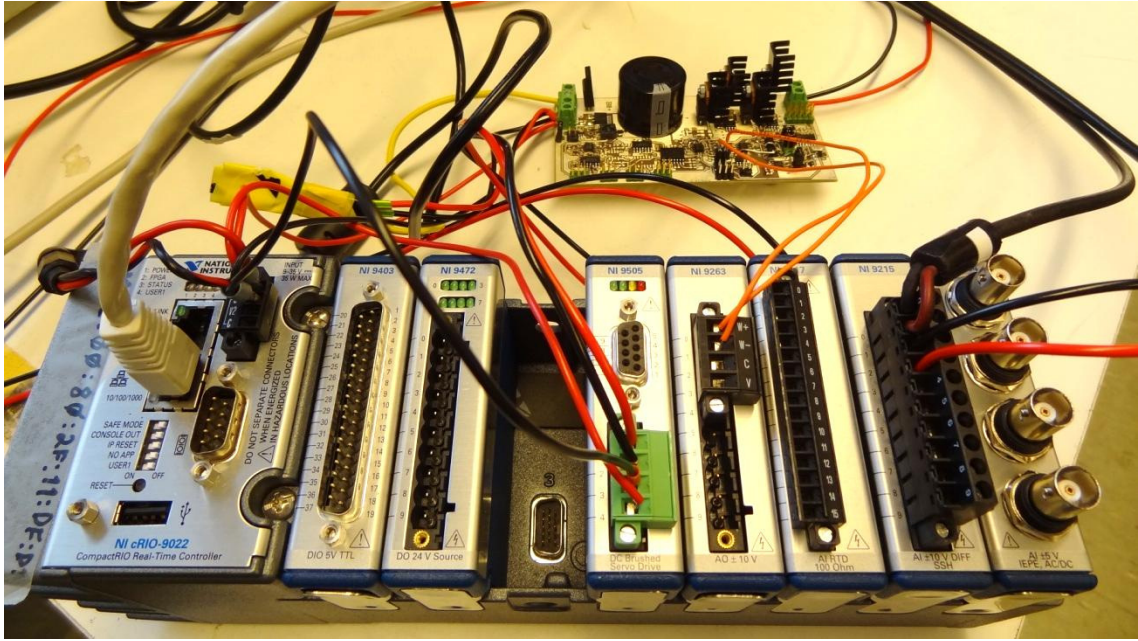


Figure 15. CompactRIO with the external H-bridge on the background.

When the reference current is the previously described square wave that is always high for a period of 90 degrees, the rotational speed needs to be controlled by limiting the level of the reference current. This speed control method may not be the best one for SRM, but it should perform well enough. A bigger problem is the constant 90-degree commutation period. As it was discussed in the end of chapter 3.2, this 90-degree commutation may produce negative torque. The commutation should be started little after the un-aligned position and it should be stopped little before the aligned position. To implement this, the resolution for angular position measurement should be more than the 90 degrees that is available with the previously described encoders. This is why the angular position is calculated from the speed by integrating it. This produces delayed information of the position and it is not even accurate. However, it does have quite high resolution. When this high-resolution delayed signal is combined with information of the original low-resolution real-time signal, we get high-resolution real-time signal that has unfortunately rather low accuracy. In here, the low accuracy means that the value of the measured angular position is lagging behind the real rotational angle. There is also weighted averaging filter that restricts capability to sense acceleration. Therefore, the acceleration is limited to certain level, although this level is most probably quite high. This does not cause any problems when the motor is running steadily, because the limits for θ_{on} and θ_{off} can be adjusted to cancel out the delay by advancing them. Nevertheless, high acceleration or deceleration may cause some problems. For example, torque ripple causes fluctuation into the rotational speed, which consists of momentary accelerations and decelerations.



Figure 16. Eddy current sensor that is used for detecting holes on the encoder disk to work out the angular position and speed.

Another method than limiting the reference current to control the speed is labeled as “Advanced angle speed control” in Figure 14. This method uses the possibility to control the starting and ending of the commutation. In addition, it exploits the inverse model of the motor. This kind of control method should be more efficient than the other one. In the “Output current generation” block of Figure 14 is done the conversion of control signals to reference current signals.

4.2 Test planning

4.2.1 Rotor designs

All the rotors described here were designed by first finding an example form to get started with. This was reshaped to produce the performance needed and to match the boundary conditions of the rest of the setup. The most important thing when considering the performance of the SRM rotor is the cross-section of the rotor. The geometrical shape of the cross-section was analyzed briefly with FEM to get an idea of the efficiency (Haarnoja, 2012). The tolerances were not included in the manufacturing drawings to give some freedom for the machining. Dimensions that had functional tolerances were the outside diameter of the rotor and the inside dimensions concerning the shaft mounting. These dimensions were machined precise as possible. Addition to the drawing, the mounting parts fitting inside the rotor were given to the machinist to ensure their matching to internal dimensions of the rotor. These mounting parts were initially designed and used with the AMB rotor.

The first rotor designed was meant to work in 8/6 motor. The initial shape was found from illustrational pictures of 8/6 SRMs. Their geometrical cross-section shapes seemed roughly the same in every source. The dimensions for the designed rotor were mainly determined by the stator. Some relations between the certain dimensions were found to be repetitive from source to source, but their utilization was restricted by the boundary conditions against them, mainly arising from stator dimensions. A part of manufacturing drawing of rotor's first version can be found from Figure 10.

As explained earlier, the first version of the rotor did not work with the original stator. Therefore, to get the original setup working, another rotor was designed. From the literature was not found anything exactly matching to the motor type in hand. The suggestive form for 4/2 2-phase SRM was used as it was found to be the closest to adjacent flux path machine. The design found was an example of self-starting 4/2 2-phase rotor, suggested by (Miller, 1993). Some optimization was done to get the maximum torque and to ensure the motor starts rotating on every rotor angle when stationary. The length of the rotors is twice as much as the length of the stator, as it can be seen in Figure 13, which shows the extra part of the other end of the rotor. This is because an option for using the same rotor together with two separate stators wanted to be left open for the future. With two stators, it would be possible to implement the motor that attenuates radial vibrations. A part of manufacturing drawing of 4/2 SRM's rotor can be seen in Figure 11. Four other versions were shaped from the original 2-pole rotor, but they were not found to be useful when analyzed with FEM.

4.2.2 Steps of the tests

The main goal for this research was set on implementing a control system for speed control of the SRM. In addition, observing behavior of SRM was also mentioned. These frames were guiding the test process. The tests were done using both the old AMB and the new SRM control systems. The idea was to compare different commutation methods, since with the AMB controller the commutation was done in open loop using sinusoidal or square wave signal. The new SRM controller used closed loop commutation with two alternative strategies. The tests were divided into maximum performance tests and into precision tests. Maximum performance was measured using angular acceleration tests and maximum speed tests. All of the maximum performance tests were done using both of the control systems. The precision tests were done only with the new control system, because closed loop was needed for this kind of usage. The precision was measured with capability to follow set target speed. These tests could be classified as speed control tests. Radial movement of the shaft with stator vibration was measured during all the tests.

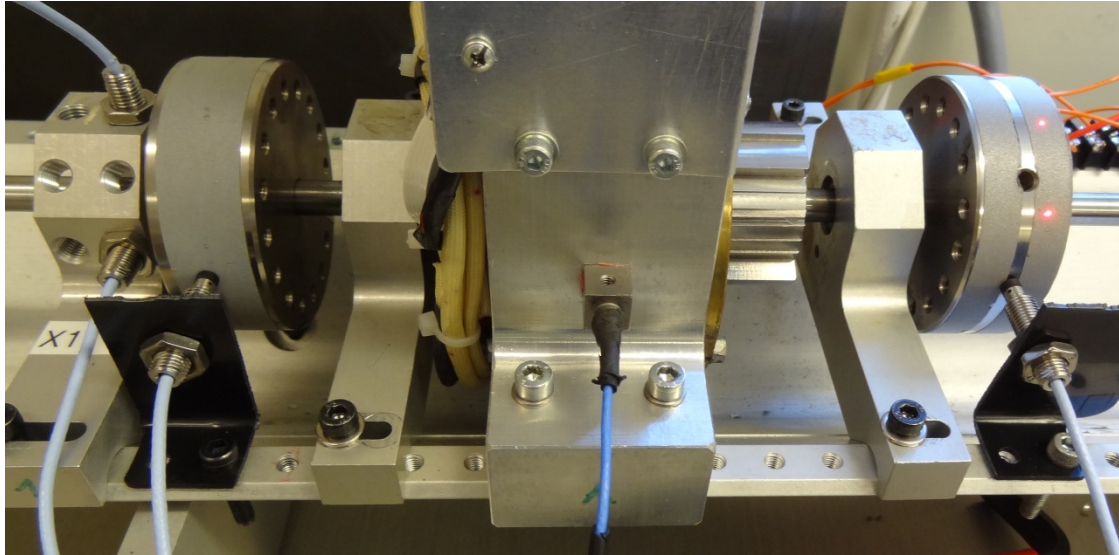


Figure 17. Measuring the SRM behavior. All the measuring devices can be seen in the picture from left to right: two eddy current sensors to measure radial movement of the shaft, eddy current sensor for encoding and commutation of phase one, 3d acceleration transducer for obtaining the radial vibrations of the stator, eddy current sensor for encoding and commutation of phase two and two laser dots from the laser vibrometer that is measuring speed.

The tests were done using multiple measuring devices. Figure 17 shows all the test probes used. Only the laser itself is out of the view, because it had to be 600 mm away from the measured target. Still, the dots from the laser beams can be seen. All sensors were gathering measurement data during every test, thus it was possible to observe relations between the measured events. The sensors were connected to cRIO, which handled the sensor reading at the same program that was used for controlling the motor. Measurement results were transferred into text file that were analyzed using MATLAB. Only one file that includes multiple quantity columns was created for one measurement. The columns were time, laser -measured speed, non-filtered eddy current -measured speed, filtered eddy current -measured speed, x-axis of the acceleration transducer, y-axis of the acceleration transducer, z-axis of the acceleration transducer, x-axis of shaft radial displacement and y-axis of shaft radial displacement. The right hand coordinate system had z-axis parallel with the shaft, x-axis parallel with the floor and y-axis perpendicular to the floor.

The basic test procedure was to repeat the same test three times. In addition, with the AMB controller the tests were done using both 4 A and 6 A currents. This was done to examine the influence on performance when the current was raised, especially in the case of acceleration and maximum speed. Added to this the raised current should have a negative impact on the torque ripple and vibration of the stator. The torque ripple should be visible from the speed ripple. With the cRIO controller only 4 A current was used, because raising the current affects to current controller settings and even though the new settings could have been found, it would have been impossible to distinguish the

electromagnetic phenomenon from the other impacts of raised current arising from new current controller settings. However, the AMB controller does not suffer much from the raised current when compared to the cRIO system. This makes the AMB controller more suitable for testing what is the effect on torque and torque ripple.

Angular acceleration tests were done to determine the average torque the machine could produce in an actual operating situation. With the AMB controller, the rotational speed of the magnetic field needed to be swept using predetermined maximum acceleration value that does not stall the motor. The sweeping was available only with sinusoidal signal making possible to use only the sinusoidal signal, not the square wave signal. The cRIO system produces square wave signal, thus it would have been fair to use square wave signal with AMB instead of sinusoidal.

With AMB, the initial speed was set to be 240 rpm, because the rotor was having a hard time catching the pre activated rotating magnetic field in speeds lower than this. This meant that comparative cRIO tests had to be also done using the same initial speed and doing the acceleration from zero speed only with cRIO. In addition to comparison between the AMB and the cRIO system, four different methods to control the motor using the cRIO were compared using the same test procedure. These methods were namely advanced angle controller using the linearized motor model (AALZ), advanced angle controller assuming linear behavior of the motor (AAAL), current controller using adjustable angles (CCAA) and current controller using constant angles (CCCA). The abbreviations are used in later chapters when referred to these methods. Even though called adjustable angles, the CCAA method is using constant values for the commutation angles: $\theta_{on} = -45^\circ$ and $\theta_{off} = -22.5^\circ$, that were found to be optimal values experimentally. The difference to CCCA is a possibility to set desired values for the angles, but in CCCA they are defined by the test arrangement to be $\theta_{on} = -90^\circ$ and $\theta_{off} = 0^\circ$. With AALZ and AAAL the commutation start angle θ_{on} experiences changes from -90° to -45° by the controller but the commutation stop angle remains untouched at $\theta_{off} = -22.5^\circ$.

Maximum speed tests were done using sinusoidal signal of the AMB, square wave signal of the AMB, constant angles of the cRIO and variable angles of the cRIO. Capability to follow the set target speed had three speed levels that had to be reached. Each level was kept as a constant speed target for 6 seconds as soon as the level was reached. These tests were done using the same four control methods of the cRIO that were used in acceleration tests as well.

When angular acceleration α and moment of inertia I are known, sum of torques T_i can be calculated from the equation of motion

$$\sum_{i=1}^n T_i = \alpha I . \quad (21)$$

The sum of torques can be divided into output torque of the motor T_m and into resistance torque T_r deduced from all the resistive forces and loads. Hence if resistance torque is known, the output torque can be calculated when (21) is written as

$$T_m = T_r + \alpha I . \quad (22)$$

The T_r can be defined using the test setup by obtaining the deceleration when the motor has been switched off. The moment of inertia is also needed. The rotor was designed with 3D drawing software, therefore the moment of inertia was calculated in the software. In addition to the rotor, the shaft and flywheels were modeled also to obtain accurate inertia values.

4.3 Estimations for error

4.3.1 Error in mathematical methods

The error in simulations comes from accuracy of the mathematical model describing the physical system. Therefore, to estimate the error in simulations, an error budget for the mathematical model of motor's capability to produce torque is needed. This budget was done using software that automatically calculates the budget when equation with values for variables and their errors are given. The error values of the variables mean the uncertainty when compared to actual physical magnitude. This said the errors originate from measurement accuracy. Because the simulation itself is assumed not to produce any error into result, it was not included in the budget. In addition, some variables are treated as perfectly accurate because they are not measureable quantities. For example, the input current is set for certain value and the simulation is able to feed perfectly the desired current. When compared to test setup, the current has difference, but the error is in test setup and therefore it should not be included in mathematical error budget of the simulation. On the other hand the idea in simulation is to model the real system, thus it would be justified to include all known uncertainty in the error values. Consequently, two error budgets were built. First one (Appendix F) describes the error of the mathematical model and the second one (Appendix G) error or more precisely difference between the simulation and the test setup. First budget suggested air gap length to have the biggest contribution to uncertainty (52.6 %) of torque. The total error was ± 15 percentage. The second one stated advanced angle (47.1 %) and current (41.5 %) for the most significant sources for total error of ± 45 percentage.

4.3.2 Error in test setup

The method for determining the torque by obtaining acceleration from speed curve has an error from the method that is used for finding the angular coefficient that represents the acceleration. The method for acquiring the slope was a visual linear curve fitting into waveform. The problem with this method is choosing correct begin and end points for the fitted curve. Especially if the original curve has a strong fluctuation that is not wanted to be included in the fitted curve, thus the curve should be low-pass filtered or at least measured from peak-to-peak. Hence, in this study the peak-to-peak method was used together with taking three identical measurements and calculating an average of

three. In addition, the amount of samples was chosen to contain period of 0.1 s in order to decrease the error of ripples in the waveform. The resistance torque has same kind of problem. It rises with speed because of aerodynamic resistance and possibly from other factors too. The method for determining the average resistance torque was the same angular acceleration as with motor torque, but from the deceleration.

Other source for error in test setup is the limitations of the measuring system. The measured results may suffer from low and uneven sampling frequency. The measurement functions were included in the motor control loop. The execution of the loop was occasionally slowed down, lowering the sampling frequency of the measurements. Hence, some phenomena may not be noticed. The speed measurement should not suffer from this problem, but for the ripple in high speeds, the sampling frequency may be too low. The accelerometer and radial movement sensors are also suffering from this same thing. Because the measurements and the motor control were executed in common system, the motor control is interfering the measurements electrically as well. This may appear as high frequency noise in the test results of cRIO-controlled system that is not visible in AMB controlled system.

5 Results

5.1 Deceleration measurements to obtain resistance torque

The value of resistance torque is not constant over the rotation speed. Because the output torque of the motor is deduced from acceleration tests using equation of motion, the inertia and resistance torque need to be known. Hence, the resistance torque behavior need to be clarified before output torque can be calculated. When the motor was switched off at speed of 420 rpm and rotation speed was measured until zero rpm was reached, it produced speed curve of Figure 18. Because of non-linear behavior, resistance torque was calculated in three regions: T_{avg} , T_{rmax} and T_{rmin} . Full length of the curve was used for calculating the average resistance torque, the steepest range for the maximum resistance torque and the lowest grade range for the minimum resistance torque. Both the min and max ranges were chosen to cover at least period of 0.1 seconds. The corresponding resistance torque values calculated from Figure 18 as an average of three repetitions were $T_{\text{avg}} = 0.0021 \text{ Nm}$, $T_{\text{rmax}} = 0.0048 \text{ Nm}$ and $T_{\text{rmin}} = 0.0006 \text{ Nm}$.

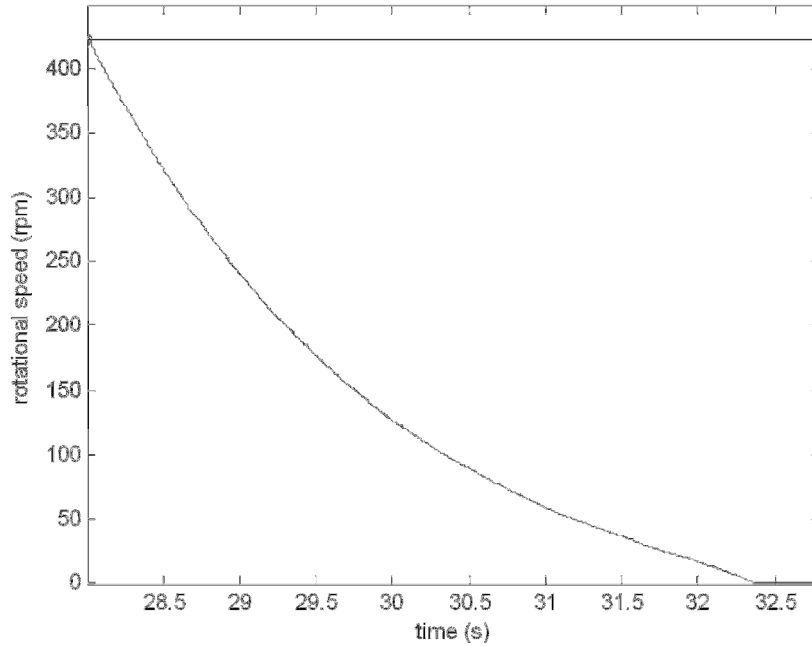


Figure 18. Measured deceleration from 420 rpm to 0 rpm after switching off the motor. The data is from the first run of three repetitions.

5.2 Acceleration measurements to obtain torque values

The test results of accelerations tests are shown in this section. Phenomenon worth noticing are emphasized, but analysis that is more detailed is performed in the discussion chapter. All the other tests results follow this principle too. Acceleration was

measured to discover the output torque of the motor using different control methods. The actual measured magnitude was speed as a function of time. The acceleration can be solved by calculating the angular coefficient of speed curve. The torque values can be calculated from the equation of motion when acceleration and moment of inertia together with resistance torque are known. As a resistance torque, corresponding value discovered in previous test according to speed range of the test was used. There were two speed ranges: 0-250 rpm and 240-420 rpm. The first one used average of T_{avg} and T_{min} . The second range used T_{max} . The resistance values describe well the actual resistance of the corresponding speed ranges. Three different intervals were used for obtaining average torque T_{avg} , maximum torque T_{max} , and minimum torque T_{min} . The average torque was calculated by using full length of the curve, the maximum by using the steepest range and the minimum by using the lowest grade range. Both the min and max ranges were chosen to cover at least period of 0.1 seconds. When AMB controller is used, the acceleration needs to be decided beforehand to use the sweeping sinusoidal signal. The maximum acceleration was discovered by experimentally iterating acceleration values that did not stall the motor. With 4 A current the value was discovered to be 0.25 Hz/s and with 6 A current it was 3.75 Hz/s. With cRIO, the acceleration is performed using different control methods that try to give the motor a maximum acceleration possible when 4 A current is used.

5.2.1 Acceleration from 240 rpm to 420 rpm using the AMB controller

The corresponding torque values with 4 A, calculated from Figure 19 as an average of three repetitions were $T_{avg} = 0.0053$ Nm, $T_{max} = 0.0057$ Nm and $T_{min} = 0.0050$ Nm. The average angular acceleration was measured to be 0.36 Hz/s, which is more than the 0.25 Hz/s that was used as a magnetic field sweep speed. When the current level is 6 A, the acceleration test will produce speed curve having a form that is something between Figure 20 and Figure 21. These two are repetitions of the same test, and they were supposed to produce identical results. The main difference is in torque variance and in overshoot: overshoot of 9 rpm, variance in torque $9 \cdot 10^{-6}$ Nm² and overshoot of 38 rpm, variance in torque $0.3 \cdot 10^{-6}$ Nm² respectively. The average values of the three runs were $T_{avg} = 0.0132$ Nm, $T_{max} = 0.0150$ Nm and $T_{min} = 0.0118$ Nm. The average angular acceleration was measured to be 5.87 Hz/s. The difference to set sweep speed was remarkable.

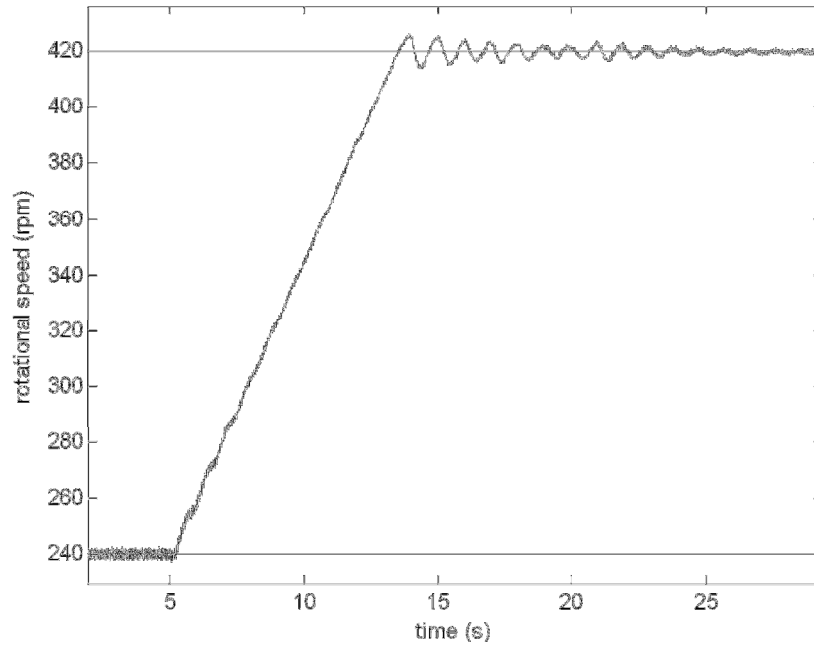


Figure 19. Measured speed in acceleration from 240 rpm to 420 rpm with AMB controller and 4 A current. The data is from the first run of three repetitions. The fed magnetic field angular acceleration was 0.25 Hz/s.

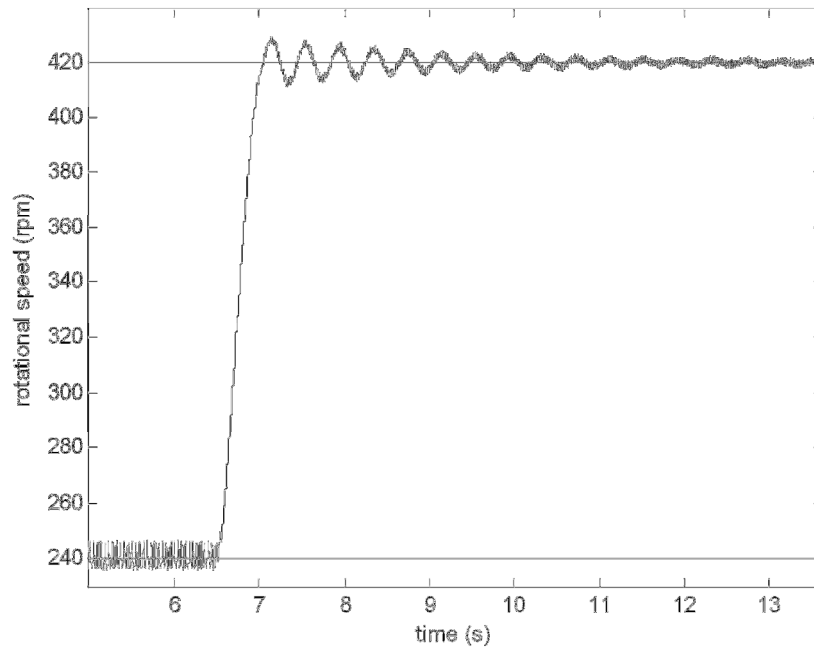


Figure 20. Measured speed showing small overshoot in acceleration from 240 rpm to 420 rpm with AMB controller and 6 A current. The data is from the first run of three repetitions. The fed magnetic field angular acceleration was 3.75 Hz/s.

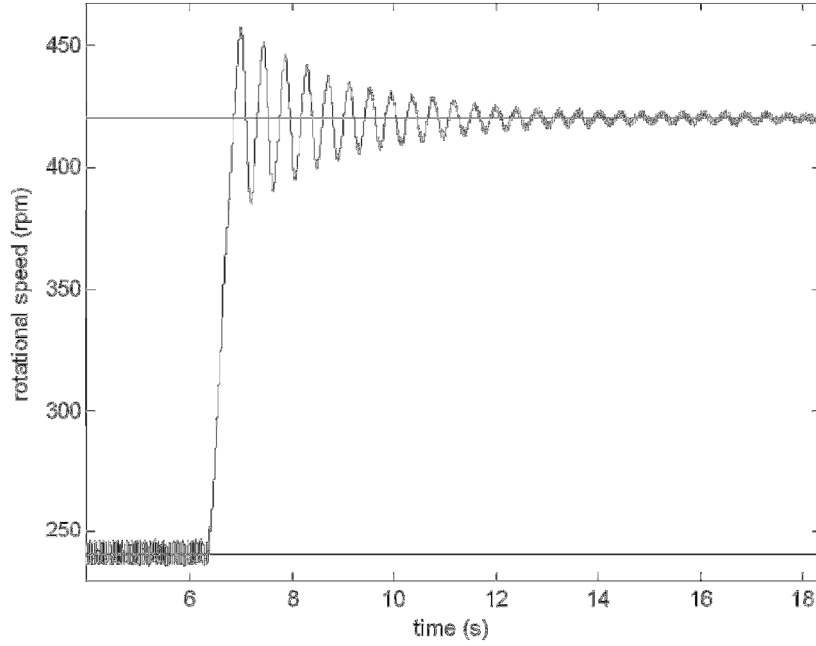


Figure 21. Measured speed showing large overshoot in acceleration from 240 rpm to 420 rpm with AMB controller and 6 A current. The data is from the third run of three repetitions. The fed magnetic field angular acceleration was 3.75 Hz/s.

5.2.2 Acceleration from 0 rpm to 250 rpm using different control methods in the cRIO

Calculated torque values with **AALZ** control method (Figure 22) as an average of three runs were $T_{avg} = 0.0097$ Nm, $T_{max} = 0.0139$ Nm and $T_{min} = 0.0078$ Nm. Figure 23 represents speed curve that was obtained when **AAAL** control method was used. The calculated torque values as an average of three runs were $T_{avg} = 0.0094$ Nm, $T_{max} = 0.0127$ Nm and $T_{min} = 0.0058$ Nm. A waveform of the speed when the motor was accelerated from 0 rpm to 250 rpm with the **CCCA** control method is presented in Figure 24. The calculated average torque values of three runs were $T_{avg} = 0.0088$ Nm, $T_{max} = 0.0129$ Nm and $T_{min} = 0.0056$ Nm. The **CCAA** control method produced a speed curve of Figure 25. The corresponding torque values from three runs were $T_{avg} = 0.0081$ Nm, $T_{max} = 0.0109$ Nm and $T_{min} = 0.0050$ Nm.

The AALZ and AAAL methods show slight overshoot, while the CCAA stays under the target speed most of the time. The CCCA has the smallest steady state error in average rotational speed. In ripple, significant differences cannot be found.

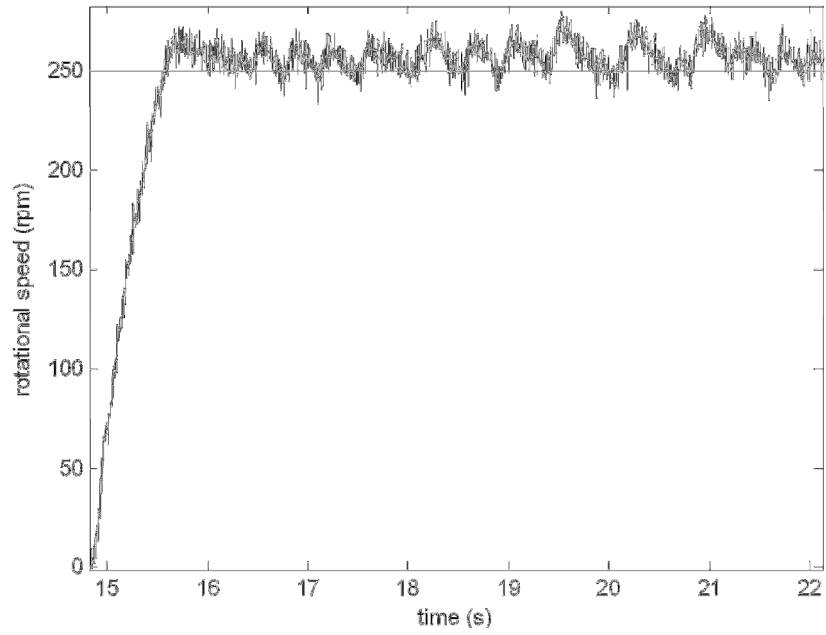


Figure 22. Measured speed in acceleration from 0 rpm to 250 rpm with Advanced angle controller using adjustable angles and linearized motor model with 4 A current. The data is from the first run of three repetitions.

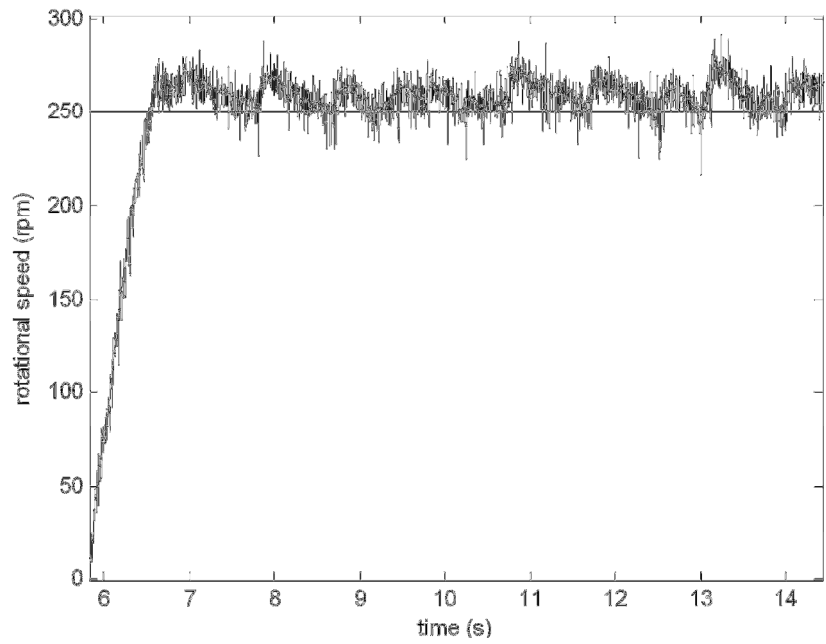


Figure 23. Measured speed in acceleration from 0 rpm to 250 rpm with Advanced angle controller using adjustable angles and 4 A current. The data is from the first run of three repetitions.

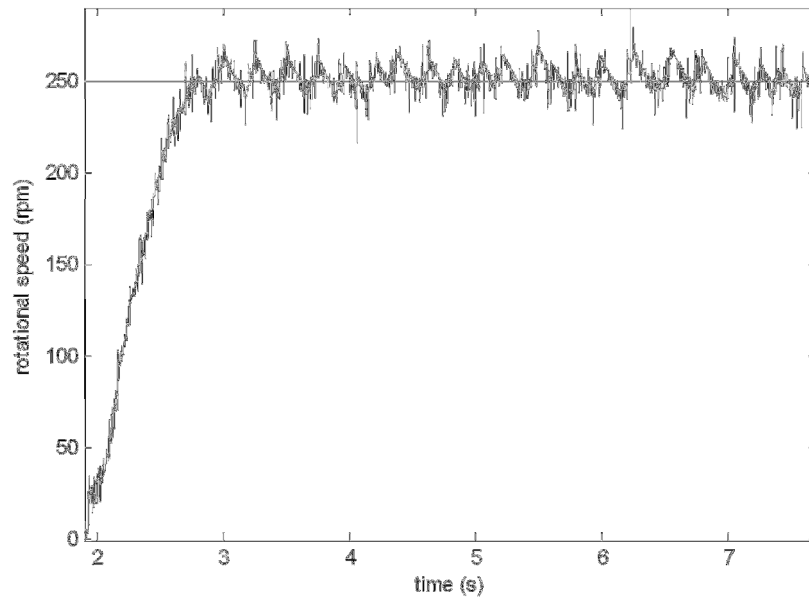


Figure 24. Measured speed in acceleration from 0 rpm to 250 rpm with current controller using constant angles and 4 A maximum current. The data is from the second run of three repetitions.

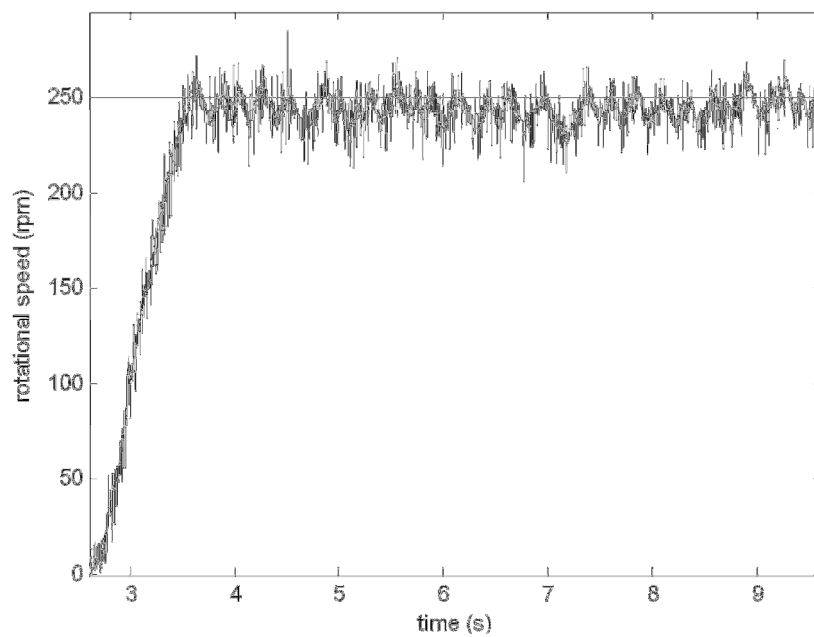


Figure 25. Measured speed in acceleration from 0 rpm to 250 rpm with current controller using adjustable angles and 4 A maximum current. The data is from the first run of three repetitions.

5.2.3 Acceleration from 240 rpm to 420 rpm using different control methods in the cRIO

This test was performed to obtain comparable cRIO results with AMB results. With cRIO, the motor can be started from stationary, but with AMB controller, this is not possible. The initial speed of AMB was 240 rpm, because AMB was not capable of running in lower speeds. The speed range of tests in previous sub-section suited better for cRIO, as it can be seen from the figures of this sub-section. The commutation method that uses constant commutation angles is not capable of running the motor in high speeds (Figure 28). The current controlled speed control method is also having problems (Figure 29). In the speed range of the previous test, the CCAA had high steady state error, and in this test, the error is even higher.

Calculated torque values for **AALZ** controlled test (Figure 26) in average of three runs were $T_{avg} = 0.0077$ Nm, $T_{max} = 0.0090$ Nm and $T_{min} = 0.0059$. Figure 27 represents speed curve that was obtained when **AAAL** control method was used. The calculated torque values as an average of three runs were $T_{avg} = 0.0079$ Nm, $T_{max} = 0.008$ Nm and $T_{min} = 0.0064$ Nm. With the **CCCA** method, the motor did not reach the desired speed (Figure 28). Therefore, the minimum torque was not calculated. Other torque values for this control method were $T_{avg} = 0.0059$ Nm, $T_{max} = 0.0073$ Nm. In Figure 29 is presented the speed curve for the **CCAA** control method. The torque values for this method were as an average of three runs $T_{avg} = 0.0074$ Nm, $T_{max} = 0.0089$ Nm and $T_{min} = 0.0060$ Nm.

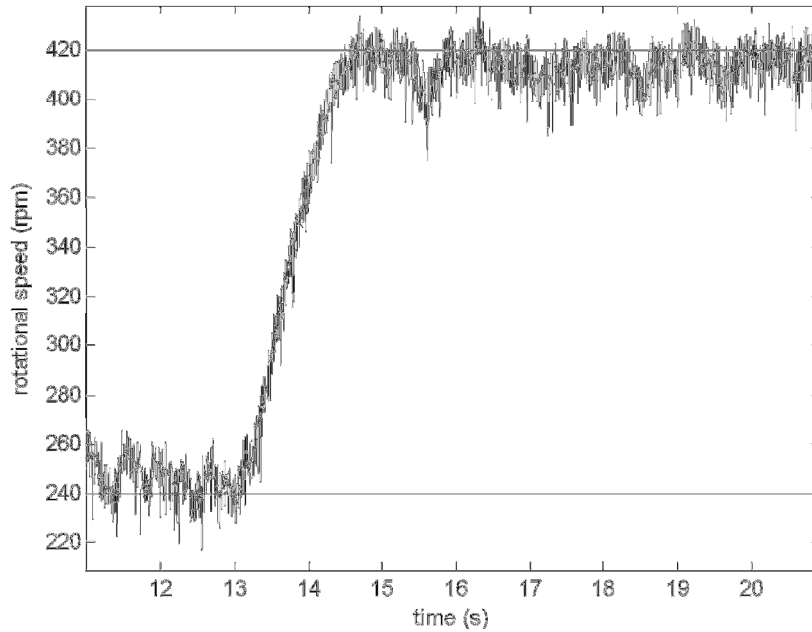


Figure 26. Measured speed in acceleration from 240 rpm to 420 rpm with Advanced angle controller using adjustable angles together with a linearized motor model and 4 A current. The data is from the first run of three repetitions.

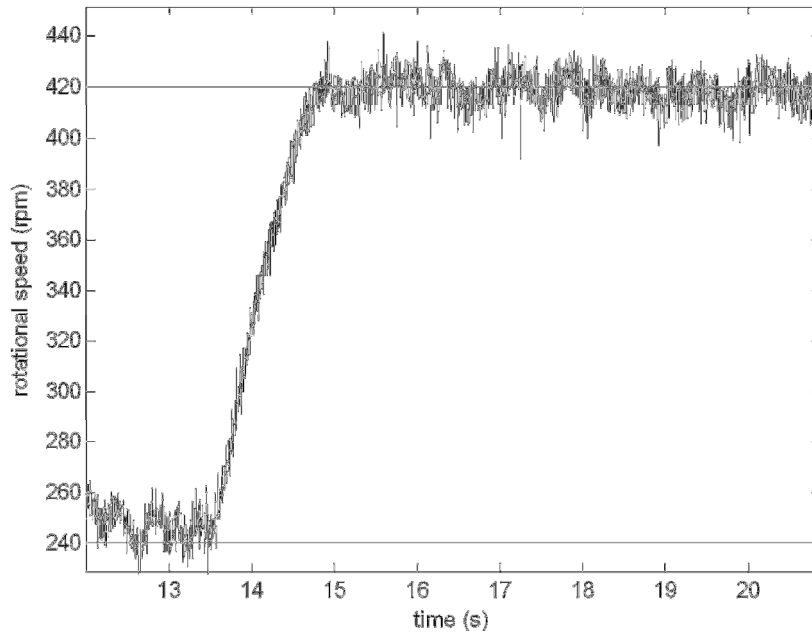


Figure 27. Measured speed in acceleration from 240 rpm to 420 rpm with Advanced angle controller using adjustable angles and 4 A current. The data is from the second run of three repetitions.

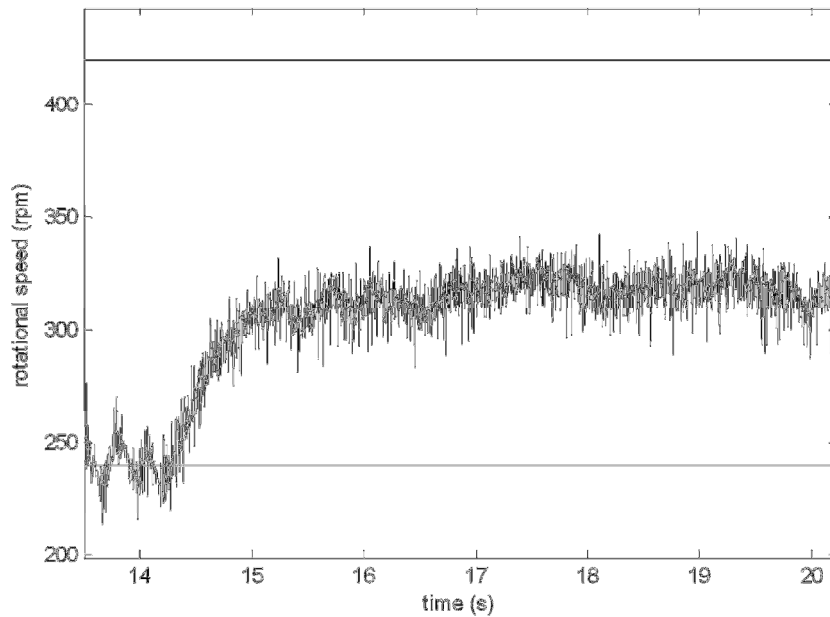


Figure 28. Measured speed in acceleration from 240 rpm to 420 rpm with current controller using constant angles and 4 A maximum current. The data is from the second run of three repetitions. The maximum speed with this control method limited the speed to 316 rpm.

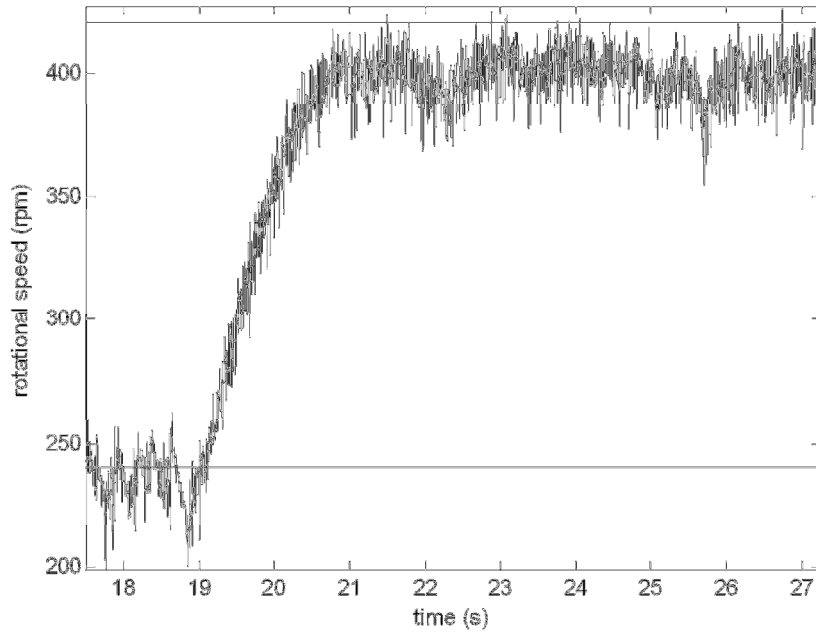


Figure 29. Measured speed in acceleration from 240 rpm to 420 rpm with current controller using adjustable angles and 4 A current. The data is from the second run of three repetitions.

5.2.4 Acceleration in simulations

This sub-section contains results of three simulation models. Speed curve and torque curve is provided from each of the models. From the torque curves, a difference between simplified and specific model should be noticed. In addition, the effect of different torque curves on the speed curves is important. The simulated tests correspond to physical tests of the test setup.

Simulations with **4/2 type SRM in simplified model** produced speed curve of Figure 30. When torque values were calculated in a same manner as it was done with the test setup, it results in $T_{avg} = 0.0166$ Nm, $T_{max} = 0.0175$ Nm and $T_{min} = 0.0160$ Nm. In simulations, it was possible to monitor the torque also directly as it is shown in Figure 31. Simulations with **8/6 type SRM in simplified model** resulted in torque values of $T_{avg} = 0.0401$ Nm, $T_{max} = 0.0419$ Nm and $T_{min} = 0.0382$ Nm. The speed curve is presented in Figure 32 and torque waveform in Figure 33. Simulations with **8/6 type SRM in specific model** produced speed and torque of Figure 34 and Figure 35 respectively. The calculated torque values were $T_{avg} = 0.0172$ Nm, $T_{max} = 0.0203$ Nm and $T_{min} = 0.0158$ Nm. A summary of all the measured and simulated torque values is in Table 4.

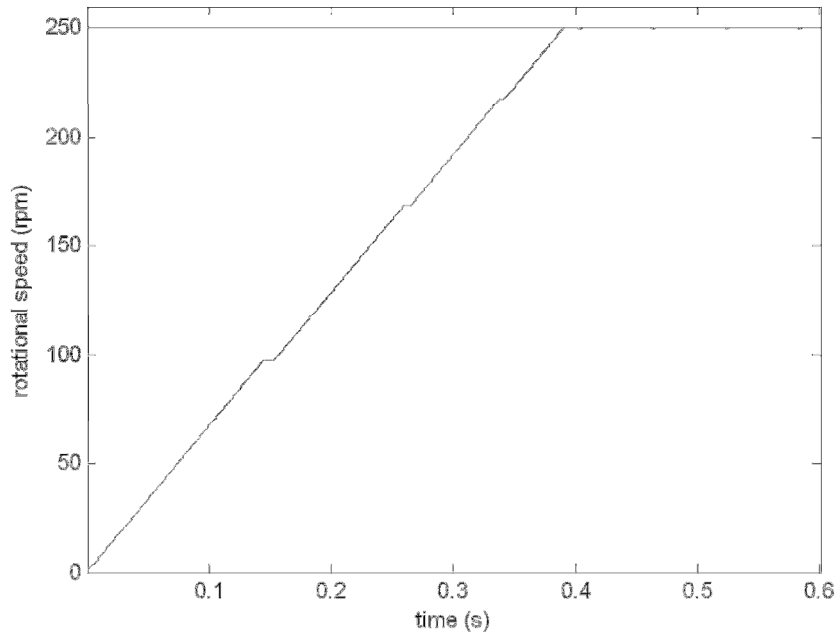


Figure 30. Simulated acceleration from 0 rpm to 250 rpm using simplified 4/2 type SRM model. Simulation used Advanced angle controller together with adjustable angles and linearized motor model with 4 A current.

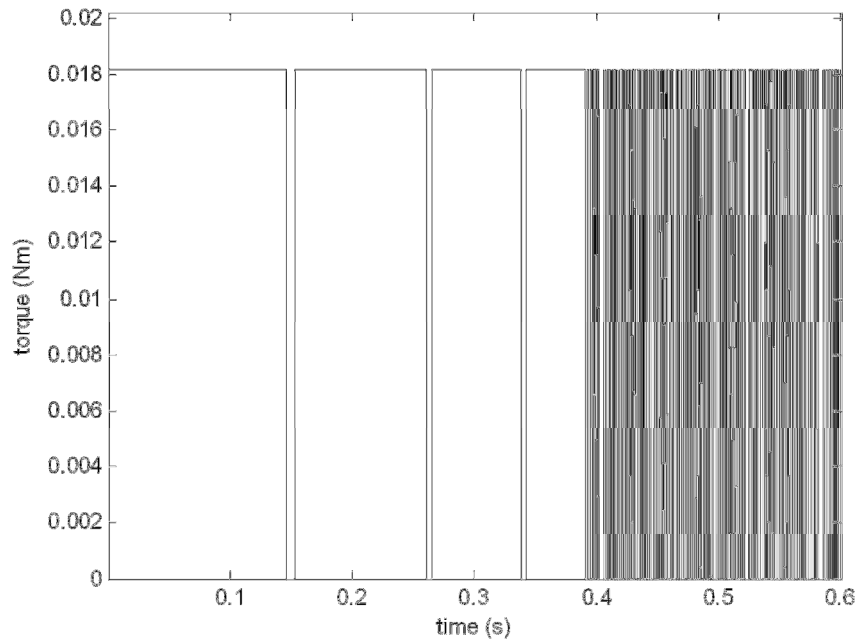


Figure 31. Simulated torque when the motor was accelerated from 0 rpm to 250 rpm using simplified 4/2 type SRM model. Simulation used Advanced angle controller together with adjustable angles and linearized motor model with 4 A current.

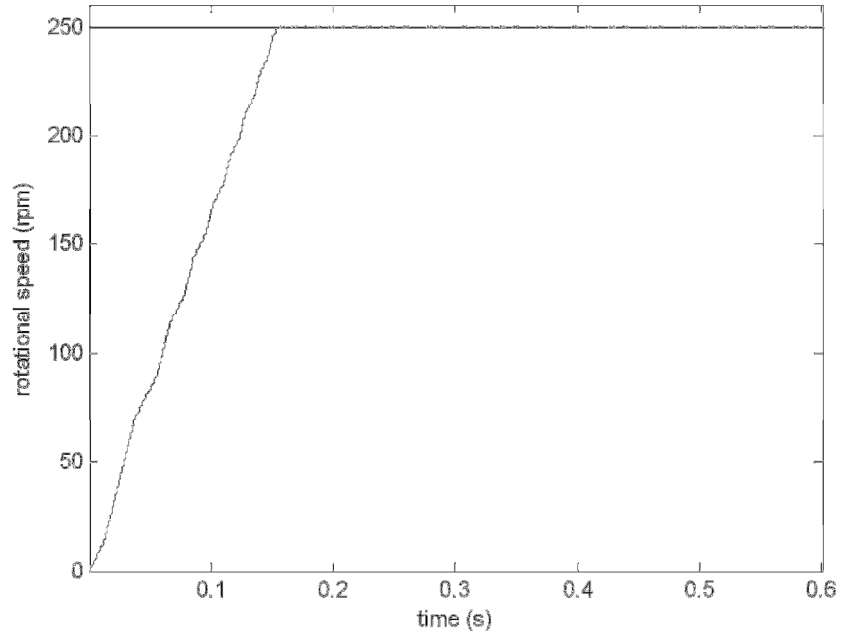


Figure 32. Simulated acceleration from 0 rpm to 250 rpm using simplified 8/6 type SRM model. Simulation used Advanced angle controller together with adjustable angles and linearized motor model with 4 A current.

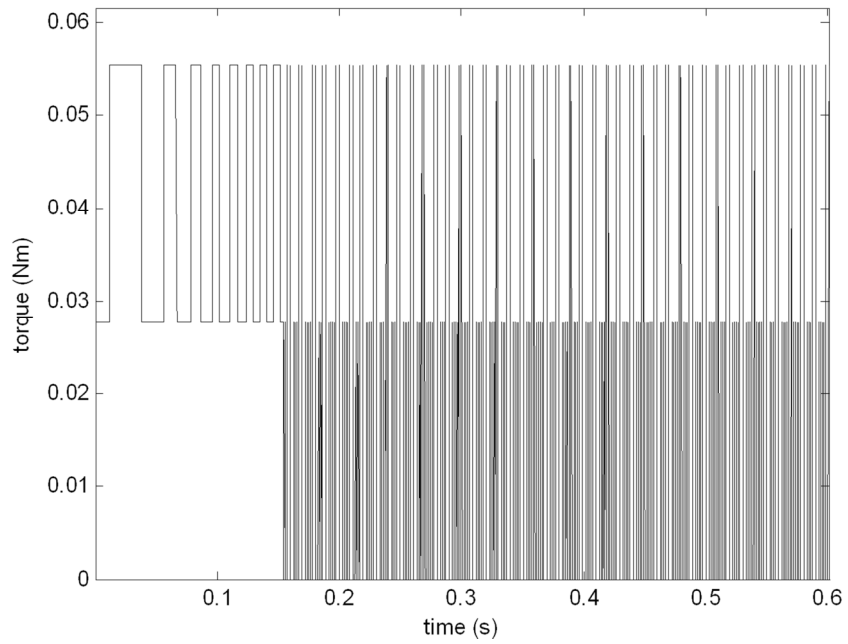


Figure 33. Simulated torque when the motor was accelerated from 0 rpm to 250 rpm using simplified 8/6 type SRM model. Simulation used Advanced angle controller together with adjustable angles and linearized motor model with 4 A current.

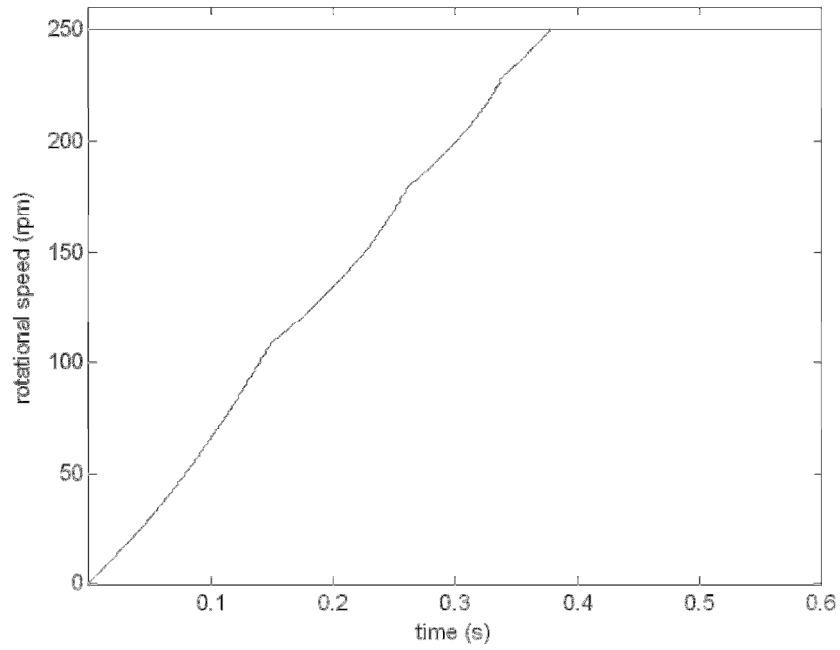


Figure 34. . Simulated acceleration from 0 rpm to 250 rpm using specific 8/6 type SRM model. Simulation used Advanced angle controller together with adjustable angles and linearized motor model with 4 A current.

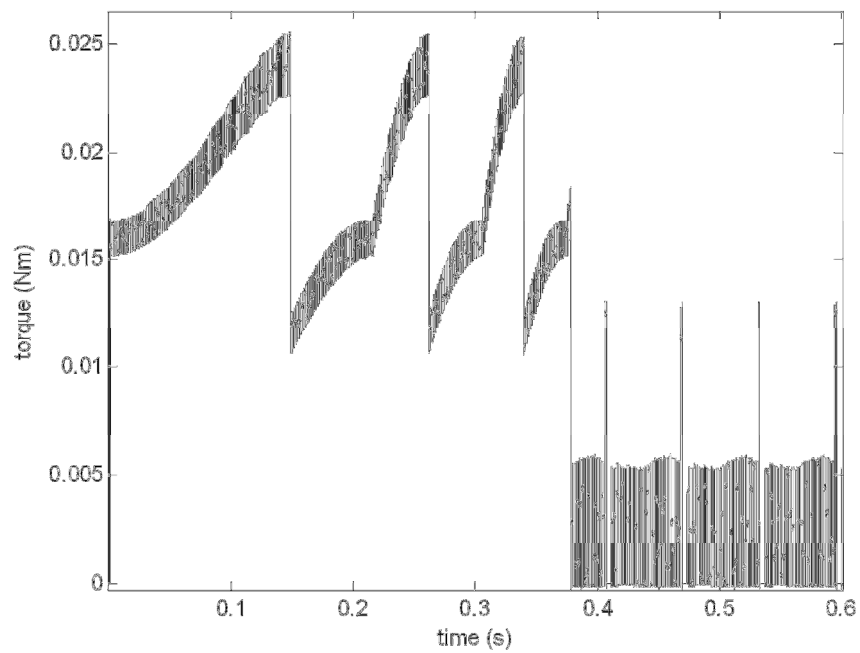


Figure 35. Simulated torque when the motor was accelerated from 0 rpm to 250 rpm using specific 8/6 type SRM model. Simulation used Advanced angle controller together with adjustable angles and linearized motor model with 4 A current.

Table 4. Comparison of different control methods and simulations to produce torque.

Method	T_{avg}	T_{max}	T_{min}
AMB 4 A, 240-420 rpm	0.0053 Nm	0.0057 Nm	0.0050 Nm
AMB 6 A, 240-420 rpm	0.0132 Nm	0.0150 Nm	0.0118 Nm
AALZ-method, 240-420 rpm	0.0077 Nm	0.0090 Nm	0.0059 Nm
AAAL-method, 240-420 rpm	0.0079 Nm	0.0088 Nm	0.0064 Nm
CCCA-method, 240-420 rpm	0.0059 Nm	0.0073 Nm	-
CCAA-method, 240-420 rpm	0.0074 Nm	0.0089 Nm	0.0060 Nm
AALZ-method, 0-250 rpm	0.0097 Nm	0.0139 Nm	0.0078 Nm
AAAL-method, 0-250 rpm	0.0094 Nm	0.0127 Nm	0.0058 Nm
CCCA-method, 0-250 rpm	0.0088 Nm	0.0129 Nm	0.0056 Nm
CCAA-method, 0-250 rpm	0.0081 Nm	0.0109 Nm	0.0050 Nm
Simplified simulation 4/2 0-250 rpm	0.0166 Nm	0.0175 Nm	0.0160 Nm
Simplified simulation 8/6 0-250 rpm	0.0401 Nm	0.0419 Nm	0.0382 Nm
Specific simulation 8/6 0-250 rpm	0.0172 Nm	0.0203 Nm	0.0158 Nm

5.3 Step and sweep response measurements

The accuracy to follow the set speed in AMB usage was measured by sweeping the rotation speed of the magnetic field. The used acceleration was low because the idea was to measure the ability to keep the rotation of the rotor steady. With cRIO, step response was used for testing the motors capability to reach the target speed as fast as possible. In addition, steady rotation of the rotor can be analyzed from the step response. Tests were performed using four control methods in comparison. With AMB, four target speeds after initial speed of 240 rpm were 540 rpm, 840 rpm, 1140 and 1440 rpm. With cRIO, the start speed was 0 rpm, the targets being: 250 rpm, 150 rpm and 400 rpm. Different methods to measure the rotational speed were also tested in beginning of both AMB and cRIO tests, because the motor itself does not use the same speed measuring method that was used for recording the tests to be displayed in the results.

5.3.1 Sweep response with AMB

Figures from Figure 36 to Figure 38 are from the same test run. Figure 36 is obtained with laser showing smaller fluctuation compared to Figure 37, which represents speed that is measured with eddy current sensors. In Figure 38 is the same signal after filtering. From these figures, it is clear that using the non-filtered eddy current signal in speeds above 540 rpm is not recommended.

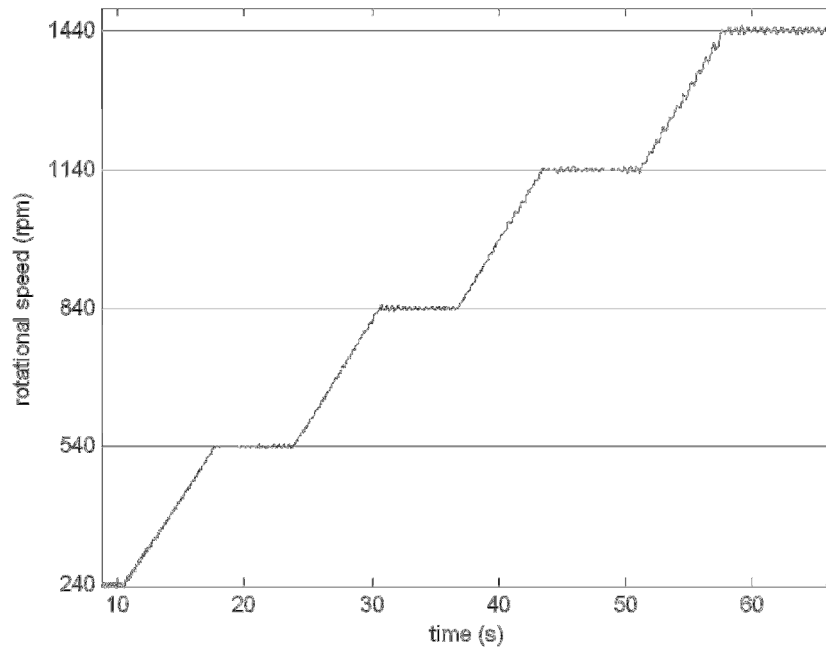


Figure 36. 1 Hz/s sweep response with AMB controller having four target speeds using increments of 300 rpm.

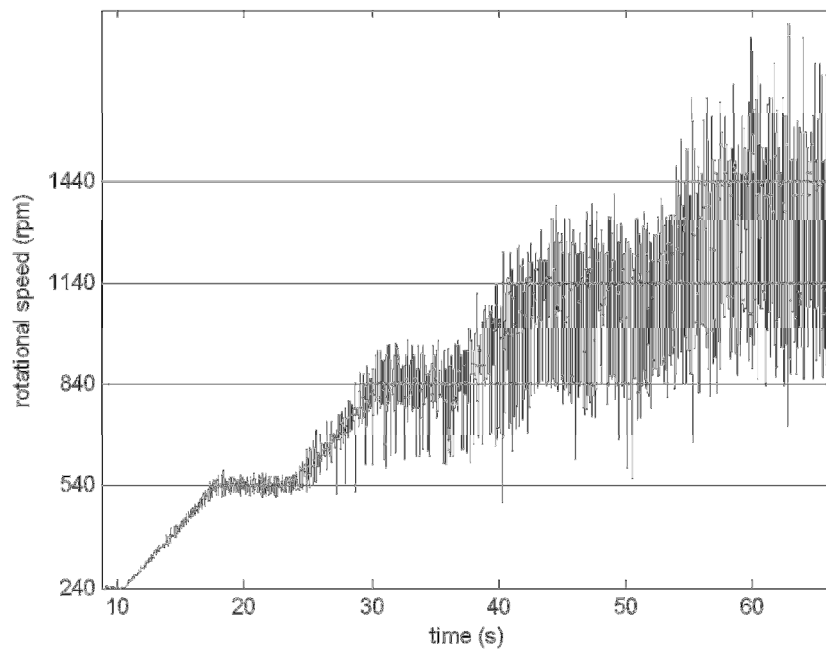


Figure 37. Speed curve of 1 Hz/s sweep response with AMB controller measured with eddy current sensors.

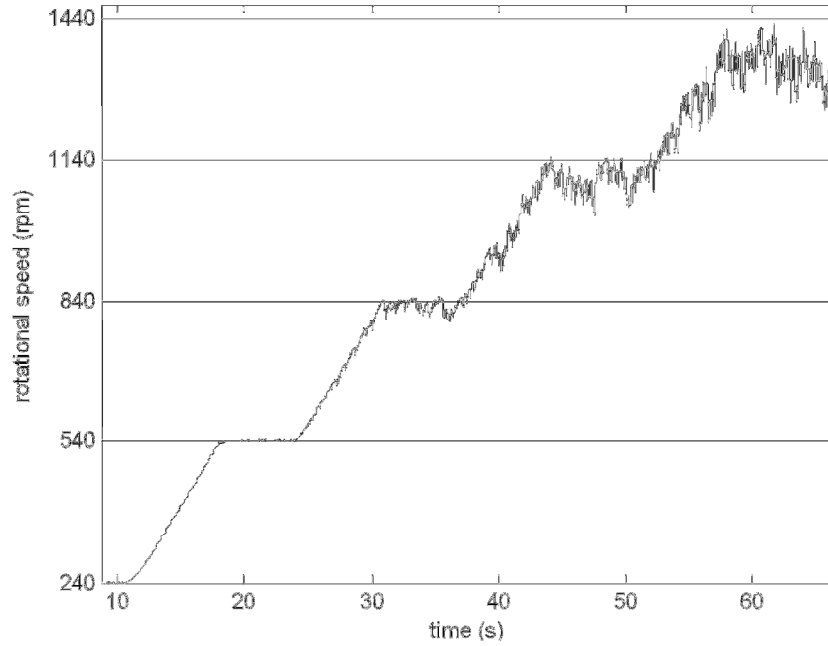


Figure 38. Filtered speed curve of 1 Hz/s sweep response with AMB controller measured with eddy current sensors.

5.3.2 Step response with cRIO

The same test run measured with different methods, is presented in figures from Figure 39 to Figure 41. The test results in Figure 39 and Figure 40 address that in lower speed, the problem with eddy current sensors is not severe. However, another problem is visible. The Figure 41 is the speed using filtering in measurements. The filtering results in round off in the speed curve. Hence, when the speed has already reached the target speed, the filtered speed has reached only 40 % of the speed. This delay was discussed earlier in the work. The delay causes error to the angular position measurement that is used for timing the commutation, thus making the commutation to work in asynchronous with the actual rotational angle. The problem is not critical if it is taken into account when designing the controller.

The AALZ control method in Figure 39 has higher amplitude fluctuation in speed than using the AAAL control method of Figure 42. The CCCA control method in Figure 43 limited maximum speed of the motor to be less than required final target speed. In addition, the fluctuation had the highest amplitude of the four methods. With CCAA method (Figure 44), the fluctuation was reduced but it was still larger than with AALZ or AAAL.

Using **AALZ** control method:

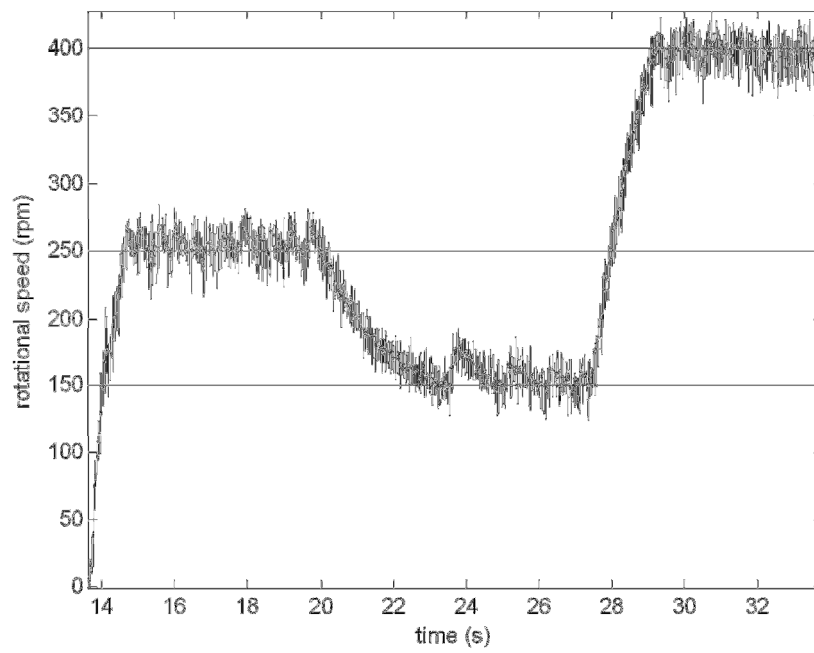


Figure 39. Step response of three steps when motor was controlled with AALZ method.

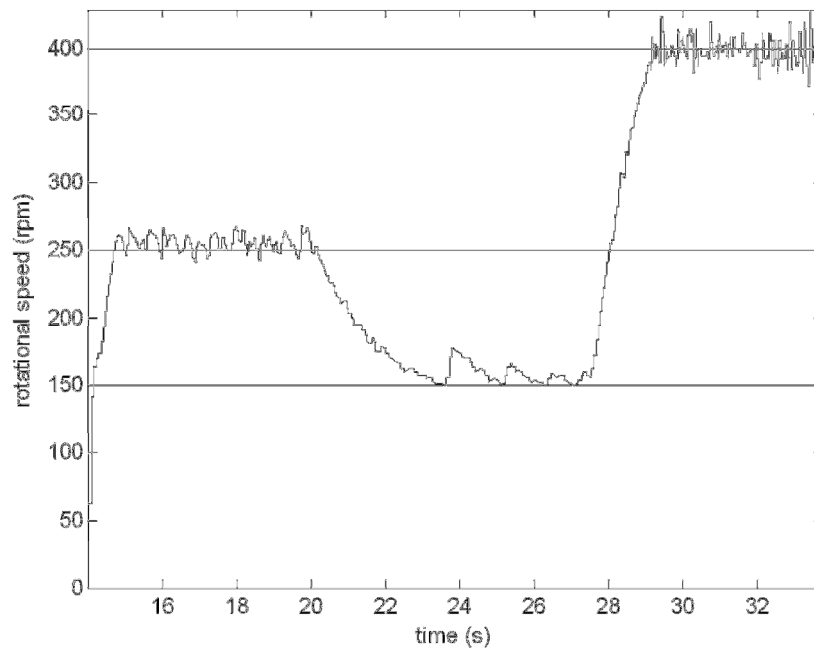


Figure 40. Step response of three steps when motor was controlled with AALZ method. Measured with eddy current sensors.

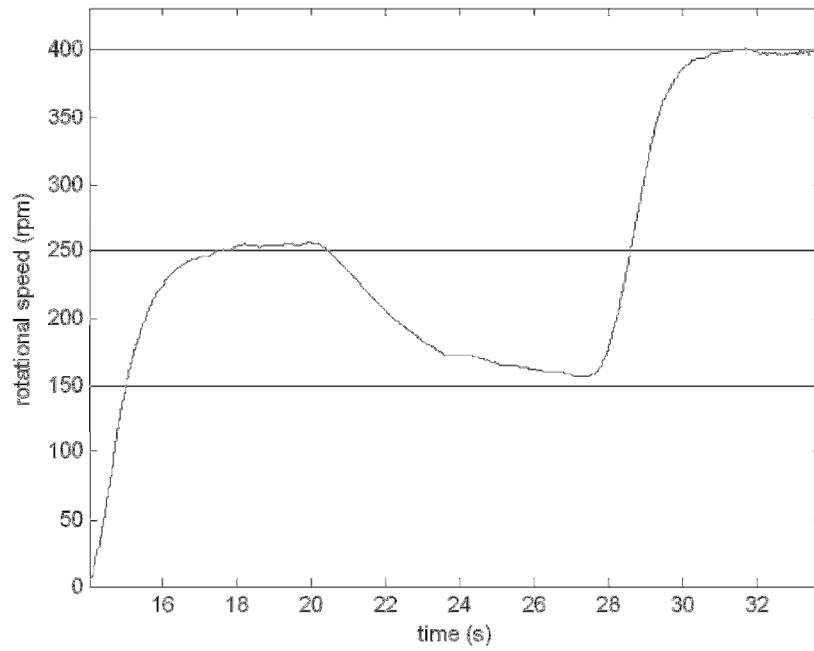


Figure 41. Step response of three steps when motor was controlled with AALZ method. Measured with eddy current sensors using filtration.

Using **AAAL** control method:

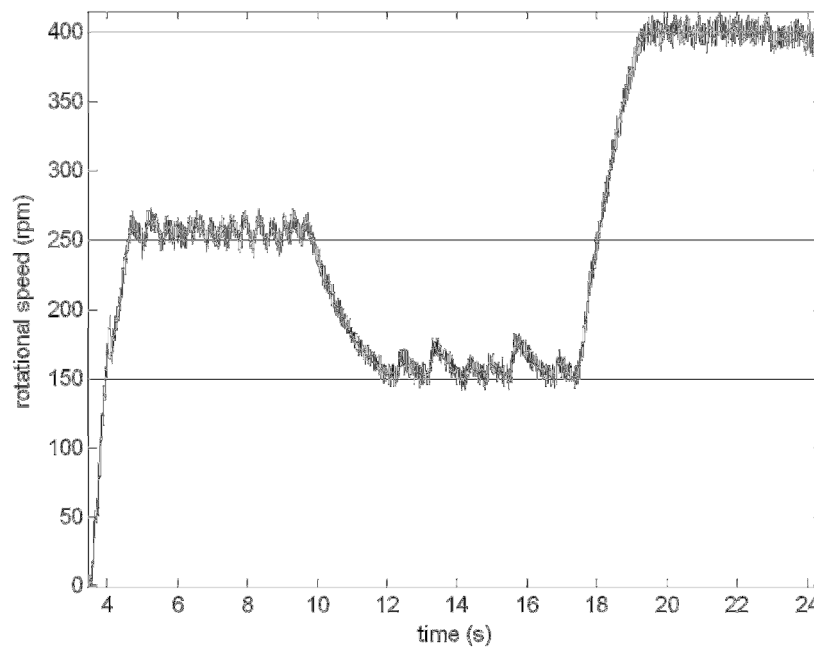


Figure 42. Step response of three steps when motor was controlled with AAAL method.

Using **CCCA** control method:

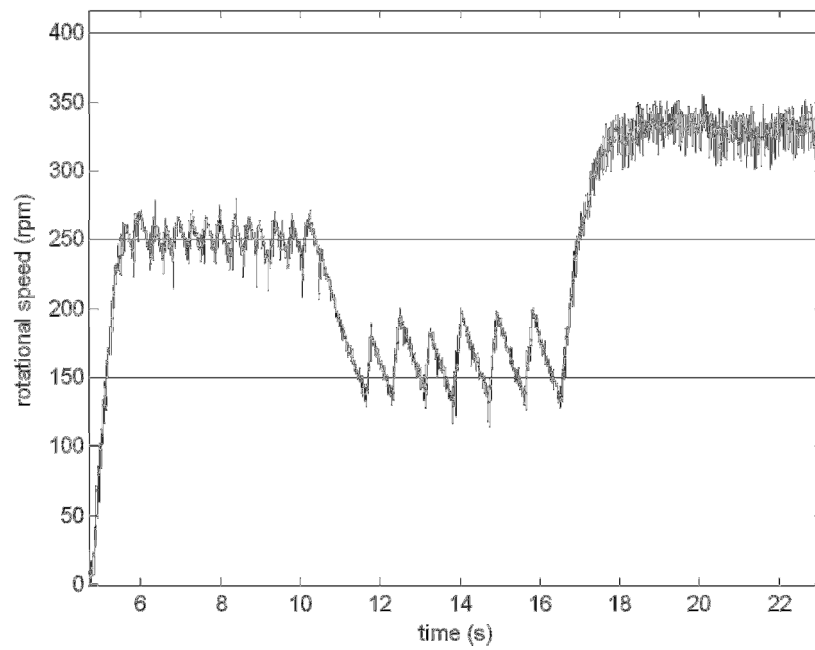


Figure 43. Step response of three steps when motor was controlled with CCCA method.

Using **CCAA** control method:

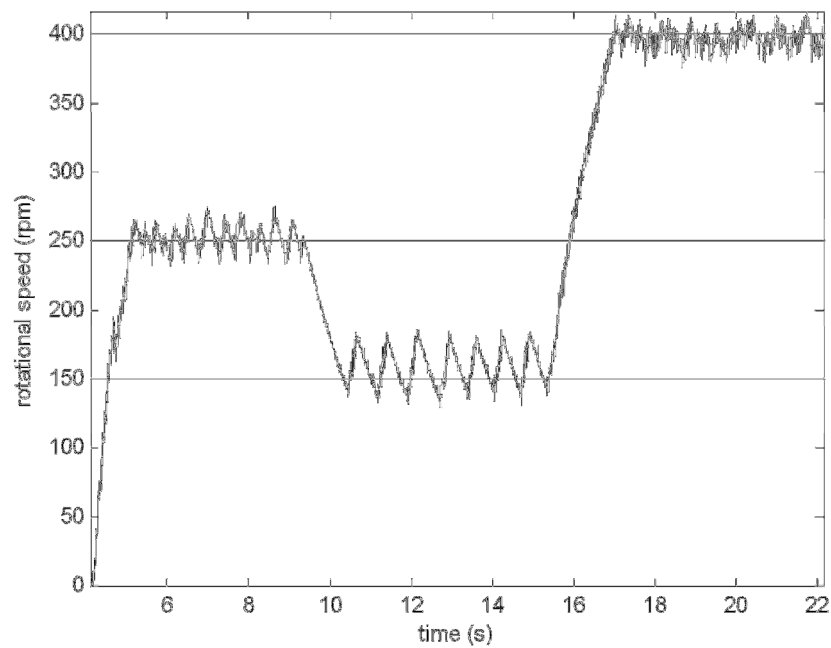


Figure 44. Step response of three steps when motor was controlled with CCAA method.

5.4 Maximum speeds

5.4.1 Using AMB

With sinusoidal sweeping input using 4 A, the reached maximum speed was 648 rpm (Figure 45). The sweeping was done using half the maximum sweep speed to reach as high maximum speed as possible. With square wave stepping input using 4 A, the reached speed was 510 rpm. The reason for the lower maximum speed can be seen in the waveform of the square wave fed speed curve in Figure 47. The increase is done using steps of 30 rpm, because it was the smallest possible step size with this method. The rotor drops out of the phase easily, because the overshoot is almost 30 rpm when the increase is applied. The stepping was tested also with sinusoidal signal using the same 30-rpm step size. The result was 480 rpm, showing the effect of the sweeping compared to stepping. When the current was increased to 6 A, the sinusoidal sweeping reached speed of 2010 rpm (Figure 46). With square wave stepping input using 6 A, the reached speed was also 2010 rpm. It seems that the square wave stepping input control method gained more from the raised current. From Figure 48 can be seen the overshoot remaining the same, even though the maximum speed was quadrupled.

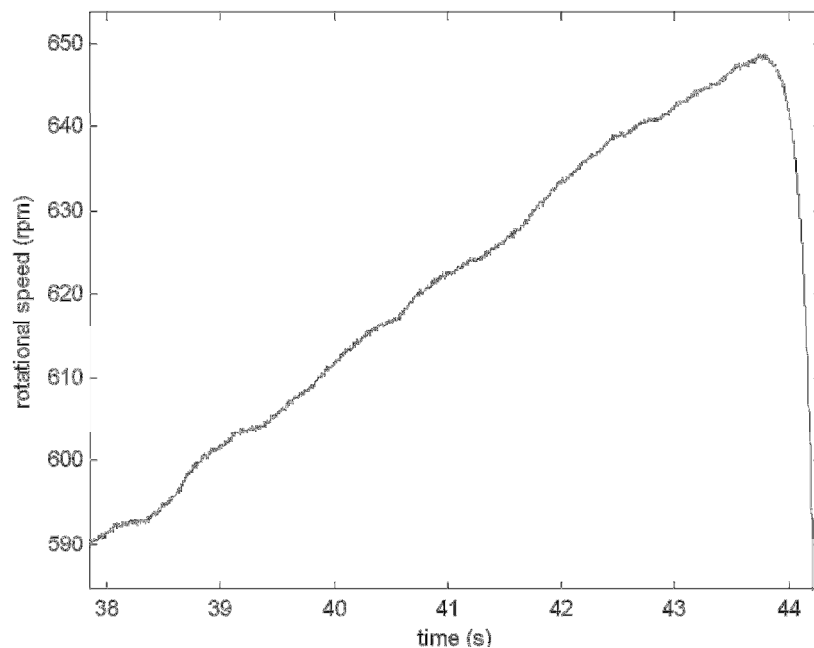


Figure 45. Sinusoidal sweeping input using 4 A.

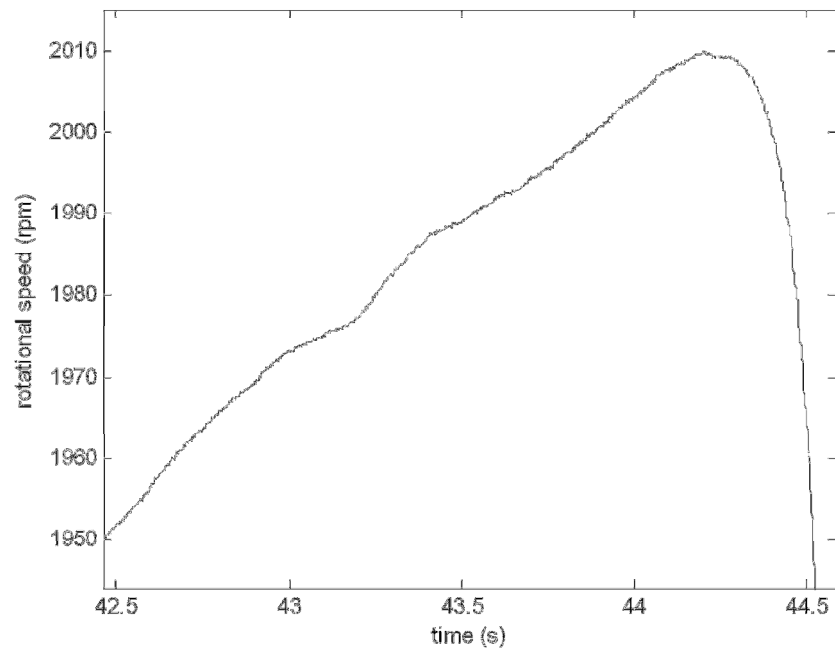


Figure 46. Sinusoidal sweeping input using 6 A.

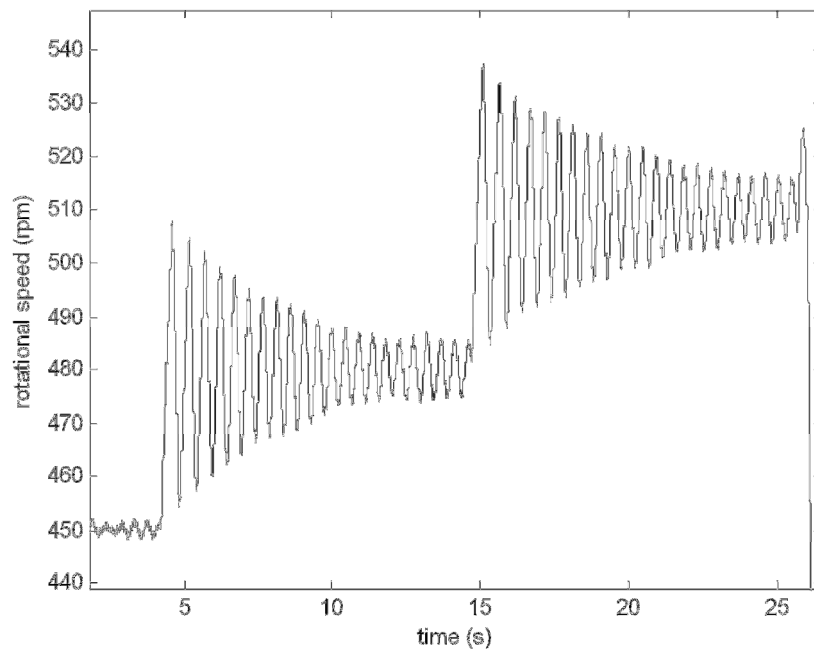


Figure 47. Square wave stepping input using 4 A.

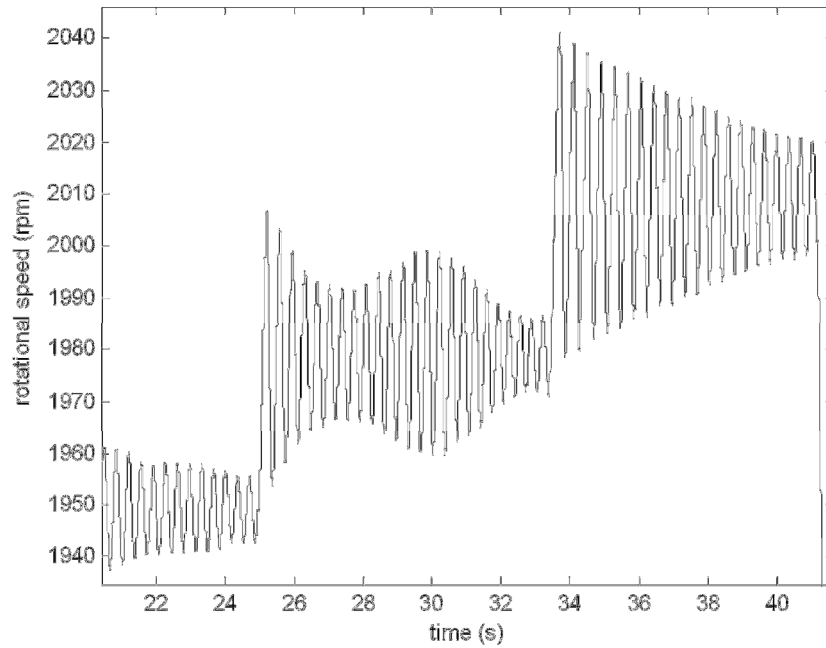


Figure 48. Square wave stepping input using 6 A.

5.4.2 Using cRIO

The maximum speed was measured with two different commutation principles: constant angles and adjustable angles. With constant angles using 4 A current, the reached speed was 320 rpm (Figure 49). With adjustable angles and 4 A, the reached speed was 485 rpm (Figure 50). The difference comes from the negative torque, which has bigger role when the angles are constant. The magnet is still excited when the aligned position has already passed. With adjustable angles, the controller is pre-programmed to stop commutation just before the aligned position.

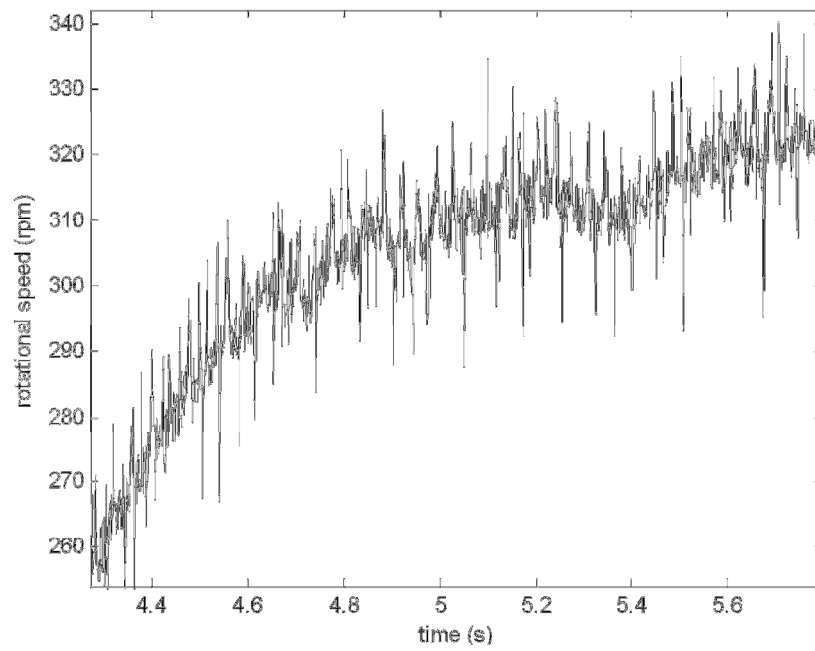


Figure 49. Constant angles commutation using 4 A.

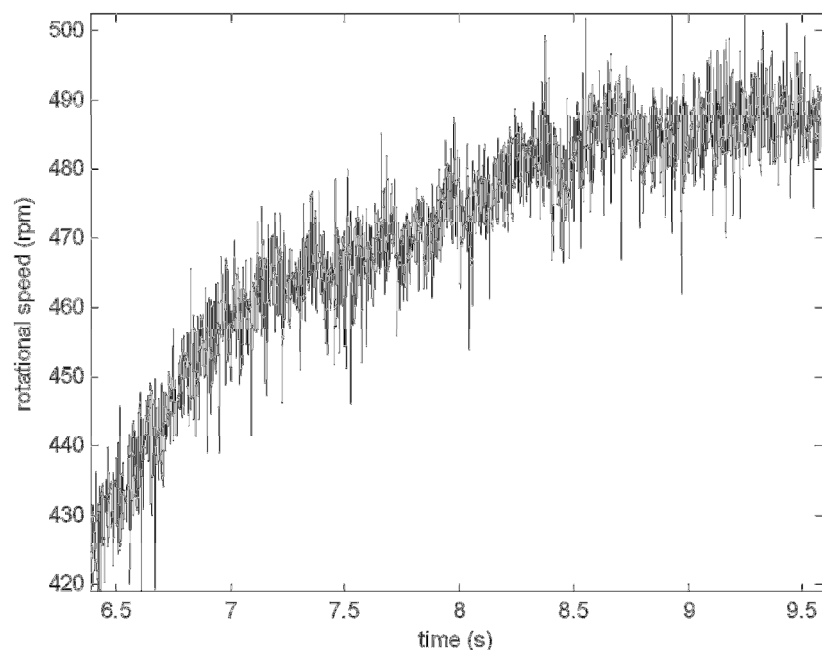


Figure 50. Adjustable angles commutation using 4 A.

6 Discussion

6.1 Conclusions from test results

The tests were divided into three categories to examine torque production, accuracy and maximum speed. Before the motor torque T_m could be calculated, the resistive torque T_r needed to be determined. The measurements for T_r showed parabolic behavior in speed above 40 rpm. One source for this can be an aerodynamic resistance, but the behavior starts from slow speeds, thus there must be some other phenomenon leading into combined effect. Alternatives for the other phenomenon are limited into viscose nature of the mechanical journal bearings. The most important usage for the resistive torque in this study was to determine output torque of the motor. The torque tests were done using speed range of 0 rpm to 420 rpm. On this range, the maximum value for resistive torque is double the average resistance value T_{avg} . Thus, when the resistive torque values were used for T_m calculations, an error occurred if the speed range that was used for determining T_m was far from the speed range of the resistive torque.

Another non-ideality that was discovered from the results was the sweep function of the AMB controller. There was a significant difference in between the measured angular acceleration and the fed magnetic field sweep speed when the AMB controller was used in acceleration tests 5.2.1. The reason for the difference possibly comes from the AMB controller having uneven sweep speed, that affect also into the speed and torques as low frequency fluctuation.

The acceleration tests of 5.2.1 with 6 A current produced speed curves showing different kind of behaviors. The first run produced a curve that showed large variance in torque but low overshoot. The results of the last run were vice versa: small variance in torque and high overshoot. This behavior has something to do with the timing of the beginning of acceleration. In the case of large torque variance, the rotor is having a hard time keeping up with the rotating magnetic field. This will produce acceleration that changes as a function of time, also known as second time derivative of speed: jerk. Therefore, the run that had small variance in torque did not suffer from jerk, but it ran into another problem being the sudden stop of the magnetic field's acceleration. The first run did not experience this problem as seriously because it was running out of magnetic field's phase. Hence, the acceleration was already decreasing just before the target speed. In the last run, the rotor was experiencing the full acceleration when the target speed was reached thus this caused the high overshoot. The run between these two runs showed behavior being something between these two extreme cases. Only difference in the tests between the runs was the timing of the acceleration startup compared to instantaneous torque the motor is producing. The instantaneous torque is alternating from positive to negative because of on-off switching of the magnets during one revolution, also known as torque ripple. When the waveforms were closely examined, there was found a clear difference between the instantaneous torques at the moment acceleration was started. The run that produced small variance in torque (2nd run) was started at a moment when the instantaneous torque was positive, and in the other run, the torque was negative when acceleration begun.

Three torque values were given: minimum, maximum and average. Even though named as minimum and maximum values, these two are also average values of periods lasting at least 0.1 second to minimize the amount of error when choosing the start and end points for curve fitting.

The sampling rate of the measurement software was running at maximum of 1 kHz, which should be enough for noticing the torque ripple. There can be seen fluctuation in measurement results when plotted in time domain, but to analyze it more, the plotting should be done in frequency domain. The magnetization born torque ripple should occur in frequency that is four times as much the rotational speed, but the frequency domain does not show anything special. The problem may be in the uneven sampling rate. The sampling frequency was working in 750 ± 250 Hz, hence the constructed waveform was changing all the time, which confuses the frequency domain algorithm. However, the measured minimum and maximum values reveal something else about the motor's nature, but if they are compared to simulated extreme values, there is a smaller variation around the average torque in measured values than in the simulated instantaneous values. When the simulated torque values were calculated in the same manner as it was done with test setup, the variance in extreme values of torque is smaller than in test setup. The high frequency variance, or ripple, comes probably from the commutation that is experiencing change in current level because of non-ideal power controller. When the power controller is not capable of producing smooth current, it affects to the output torque. The power controller was mainly implemented into the FPGA part of cRIO and partly into the Real-Time part. The FPGA part uses electrical components of H-bridge. All these three affect into the quality of the commutation, which was suffering from high frequency ripple. The real-time software part could have had severe effect on the ripple, when the execution frequency changes. In addition, when the measurements are done by the same system that is taking care of the power control, there can occur serious disturbance in the measured signals. Both the low sampling frequency and the disturbances in measurement signals were affecting into the acceleration and radial movement of the shaft measurements as well. The results of these measurements were not presented in the previous chapter, because there was nothing to see. Both of these signals had high frequency noise and the increasing rotation speed did not bring out phenomenon not seen already in lower speeds. Especially the acceleration signal was reminding almost white noise having a frequency spectrum of amplitude one at almost every frequency from zero to 700 Hz at frequency domain. The radial movement signal had a form of sinusoidal signal whose frequency was increasing with the rotational speed, without any change in maximum and minimum amplitude.

The accuracy to follow target speed was tested using step and sweep response in cRIO and AMB respectively. This test was used also for analyzing the smoothness of rotation in constant speed. With AMB, the speed range used was wider because the test itself was also different. AMB test results matching the cRIO speed range can be used when analyzing the smoothness of rotation, because in theory the only source for ripple seen in AMB results is the electromagnetic effect on torque ripple. When controlled with cRIO, there can be seen high level of fluctuation when compared to AMB's results. The AAAL control method showed best accuracy and smoothness of the cRIO control

methods. The CCCA method had the worst results. The AMB results cannot be compared directly into cRIO results, because the AMB test concentrated on smoothness of the rotation. The fluctuation of speed with AMB controller was found smaller, even while running in speed that was 3.6 times as high.

The accuracy tests in step response with AALZ method were measured using also the eddy current sensor measurements that are used for commutation and control of the motor. From the results can be seen the problems that occur when low-resolution encoder is used for providing the speed feedback information. The non-filtered signal is rough and digitized and the filtered signal has delay.

The maximum speed tests of AMB controller showed that rising the current from 4 A to 6 A has positive effect on maximum speed. The maximum speed is raised because the torque also rises. With 4 A the maximum sinusoidal sweeping acceleration corresponded to 0.0026 Nm torque. The actual maximum torque in constant speed should be higher, because the acceleration using the AMB controller is more demanding than the steady speed. The maximum speed was measured to be 648 rpm, where the resistive torque should be about the same as the maximum output torque with AMB using 4 A current ($T_m = T_r$). With 6 A the torque in maximum acceleration was 0.0105 Nm. This is about four times the 4 A value, hence the maximum speed should be less than four times the 4 A maximum speed, if the resistive torque is limiting the maximum speed. This is because the resistive torque raises quadratic over the speed, hence when still accelerating near the maximum speed using the torque of 0.0105 Nm, the actual combined torque is higher. The maximum speed was 2010 rpm, which is 3.1 times the 4 A value. This behavior matches the assumption that at maximum speed, the resistive torque is limiting the speed, being

$$T_m \approx T_r . \quad (23)$$

With cRIO, the maximum speed was less than with AMB control. The problem might be with the commutation after certain speed is reached. The controller is not able to match the θ_{on} and θ_{off} with the actual rotation angle, because the eddy current measured speed signal is starting to have more error in it.

The overall review between different control methods to manage the tests of torque, accuracy and maximum speed, highlight the success of some of the methods. When the overall is looked, the AMB controller has the biggest issue being open loop controlled. When compared to cRIO control methods, only the results of 4 A tests can be used. Hence, the high-speed test was the only one it had good success. From the cRIO control methods, the AAAL seemed to do well in every test. The AALZ, which used the linearized motor model had higher torque, but the accuracy and the smoothness was worse. If the PI controller for current control and the PI controller controlling the speed itself had been re-tuned to match this control method, not the AAAL, the performance should have been better. The worst performer was the CCCA, having rough steady speed behavior and lower maximum speed compared to other methods. When the utilization of constant angles were replaced with adjustable angles, the current

controlled speed controller method started working better. The advanced angle controller showed clear potential, especially the step response test that describes real usage of electric motor, was well performed.

The simulations were done using three models: with 4/2 SRM simplified model and with 8/6 SRM using both simplified and specific model. The value of T_{avg} in 4/2 SRM simulation was 1.77 times the value of the AAAL method. When the same simplified model was built for 8/6 SRM, it resulted in T_{avg} , that was 2.33 times the torque calculated using the specific 8/6 SRM model. Hence, if the specific model produces torque values being about 0.44 times the simplified model, the specific 4/2 SRM model should give $T_{avg} = 0.0077$ Nm. Now the simulation result is 0.0017 Nm less than the measured value. The error budget that was done to describe the error between the simulation model and the test setup stated the error in simulation to be 45%. Therefore the average simulated torque with error limits is $T_{avg} = 0.0077 \pm 0.0035$ Nm. Hence, the value of the test setup is inside the limits. If the specific model could be built also for 4/2 SRM, the result would probably be even closer and the error limit range would have been smaller. Based on these results, it can be concluded that the use of Simulink simulations seems to be useful tool for predicting achievable performance of SRM.

6.2 Applications for SRM

To think of an optimal application for SRM, the pros and cons of the motor type need to be defined. Positive and negative properties are gathered in here. An inverse specification list of an optimal application for SRM can be deduced from these. Therefore, the specifications in Table 5 would be mentioned in specification list of some certain application when power source is under discussion. British SRM related company namely Switched Reluctance Drives Ltd. has sketched SRM for wide range of applications. They are manufacturing motors mainly for specific customer needs, but they are also engineering prototypes for various applications in collaboration with other companies and institutes. Applications they have researched are combined starter and generator, electric vehicles, hybrid vehicles, pumps, compressors, blowers, washing machines, belt conveyors in bulk handling and many others. (SRDrives Ltd., 2010)

The variation of possible applications is extremely high. If a complete analysis for any industry was performed using the specifications list in Table 5, it would produce multiple suitable applications. For example in paper machine rolls SRM could be used for ensuring roll nip load while the motor is controlling the rotation. Some other application could make use of the contactless operation between rotor and stator. The rotor could be insulated from the stator by capsuling the rotor together with drive shaft to be apart from conductors. Now the rotor can be in contact with possible pressurized medium without disturbing electrical properties of the stator. Especially if compact structure is needed, leading into placing motor close to the medium, using this kind of arrangement would be beneficial. From the Table 5, some idea for optimal applications can be found. Finding an application that would fulfill all the specifications is probably not possible, but to find combination of several points is still possible.

Table 5. An imaginary requirements list that would match to properties of SRM.

Deduced from positive properties	Deduced from negative properties
+ Motor needs to be almost maintenance free	– Torque ripple is not a problem
+ Radial vibration control of the shaft is needed to attenuate sudden radial loads	– Slight noise is desired
+ Construction needs to be robust	– Single supplier for motor and controller: a system contract
+ Heat conduction through stator is a must: rotor is not allowed to heat up too much	– Accurate measurements for angular position are needed for other functions also: using motor's measurements instead of external ones would be beneficial
+ High acceleration without load (low inertia of rotor)	– Novelty amongst conservative electric motors would bring attention towards products
+ High efficiency needed over a wide range of speed and torque	
+ Motor has to work in a high temperature environment	
+ Possibility for electrical braking and to work as a generator	
+ High rotational speed	
+ Between rotor and stator has to be an air gap in all times during operation	

6.3 Future work

The test results provided an insight into the main issues hampering SRM performance. The research started by this Master's Thesis will be continued amongst the same team the author was working in while doing this work. A faster measuring test setup needs to be put up to verify rest of the performance issues and to study the coupling process of vibrations more thoroughly. This information can be used when solutions for vibration problems will be studied. The main focus will be on BSRM and using it to attenuate the radial vibration of the rotor. The detailed project description is not yet available, and it remains to be decided what other tasks will be included. The motor type will be 8/6 with eight individual power control channels custom designed for this application. The alternatives for the tasks in estimated ascending complexity order are:

- Reducing the aerodynamic noise
- Using certain design parameters to reduce coupling of radial vibration of the stator
- Reducing torque ripple by re-shaping the rotor poles
- Utilizing a smart control method for transistor control of the converters to minimize the excitation of stator radial vibrations
- Mechanical design of the stator to prevent its radial vibration
- Optimization of θ_{on} and θ_{off} angles to minimize torque ripple
- Speed dependent and adaptive controller to reduce torque ripple
- Sensorless SRM to increase reliability

When the new system is designed, the problems with the original system will be taken into account. With the new test setup, the excessive air gap between the rotor and the stator can be reduced. The coil wiring in the stator can be implemented to be independent from the other coils. This non-horseshoe magnet construction makes it easier to implement the algorithm for the radial vibration attenuation. In theory, it is not impossible to make the newly built stator to work at the same time even as a rotating machine, as a stator vibration attenuator and as a shaft vibration attenuator. Besides implementing a BSRM consisting of only one stator that does both, the AMB and the SRM function, the original AMB stator can be used for performing preliminary tests of the attenuation when the motoring is done with the new stator.

The simulation part of this Master's Thesis included a simulation of commutation to produce torque that starts the rotation motion. In the future, also dynamics in the other directions of movement need to be taken into account. These include the radial vibration modes of the stator, radial vibration modes of the shaft + rotor system, rigid body modes of the shaft + rotor system, eccentric rotation of the shaft + rotor system and whirl motion of the shaft + rotor system. The simulation methods will be mainly MATLAB Simulink together with FEM analysis. Multi Body Simulations (MBS) may also be needed.

7 Summary

The primary purpose for this study was to research the similarities between AMB and SRM and particularly research the chances for converting AMB to SRM. The research began by resurrecting an AMB test setup that used to be a test environment in AMB study carried out by the member of the same team the author was working in while doing the thesis. The aim was also to look for ways to cope with the widely reported SRM problems.

The background of the topic was clarified extensively to give reader the required amount of information for understanding the actions done in later parts of the work. Especially understanding the source for non-linear behavior of SRM was clarified by presenting mathematical models to describe output torque the motor produces. Consequently, the non-linear nature has affected to how well known the SRM is, because the non-linearity puts extra challenge for designing a controller for SRM. Especially at the time the electric motors were making their breakthrough, even the simplest tasks of controller were harder to implement when compared to competing electric motors. In addition, SRM has problems that are not found from the other electric motors.

A literature review was performed and it showed that comprehensive studies on SRM have been done recently. Every problem of SRM has received attention by multiple studies and solutions for solving the problems have been proposed. Yet, there is work to be done for optimizing SRM, especially when BSRM is concerned.

A prototype for SRM was built by converting an AMB test setup into SRM test environment. Multiple control methods were implemented to find out the most optimal. Simulation models of the SRM were also used for designing the control methods and for obtaining an estimate of the available performance.

It is evident that to design a good SRM, an engineer needs to have good knowhow on mechanical engineering in addition to electrical and control engineering. It is rare to run into an electrical engineer that has studied mechanical engineering. This said it is not strange that SRM has not been in favor of people working with electric motors. Especially the radial vibration problem could be described as an electro-magneto-mechanical problem. Many people say that SRM is just a bad motor because it has the radial vibration problem that can easily lead into severe malfunction. It is true that radial vibration should be avoided, but approaching the problem both mechanically and electromagnetically, the radial vibration can be solved.

The test results of the test setup and simulations were close, hence using simulations as a support when designing an SRM is recommended. The tests showed that using the advanced angle controller that affects into the start angle of commutation produces better performance than using traditional controller that limits the current level of the windings. The controller that used a linearized motor model decreased performance in test setup but in simulations, it showed improvement. Therefore, more accurate motor

model of the prototype motor should be built. The motor model in test setup was the same one that was used in simulations.

According to this study, applications where SRM would perform well are not hard to find. The biggest advance SRM has to offer over the other electric motors is the potential to work in extreme conditions. Customized to work in special applications is still the most sensible target. The chances for succeeding in these applications will be even better if research on SRM is still continued. When sort out how to combine all the solutions for the problems, it will be easier to introduce the motor type into industries using electric motors produced in means of mass production.

References

- Barnes, M. & Pollock, C., 1998. Power Electronic Converters for Switch Reluctance Drives. *IEEE Trans. Power Electron.*, 13(6), pp. 1100-1111.
- Bass, J. T., Ehsani, M. & Miller, T. J. E., 1987. Simplified Electronics for Torque Control of Sensorless Switched-Reluctance Motor. *IEEE Trans. Ind. Electron.*, IE-34(2), pp. 234-239.
- Bose, B. K., Miller, T. J. E., Szczesny, P. M. & Bicknell, W. H., 1986. Microcomputer Control of Switched Reluctance Motor. *IEEE Trans. Ind. Appl.*, IA-22(4), pp. 708-715.
- Byrne, J. V., et al. 1985. *A High Performance Variable Reluctance Motor Drive: A New Brushless Servo*. Motorcon Proc. 1985, pp. 147-160.
- Cai, W., 2004. *Comparison and Review of Electric Machines for Integrated Starter Alternator Applications*. in Proc. IEEE Industry Applications Soc. Annu. Meeting, Oct. 2004, pp. 386-393.
- Cai, W., Pillay, P., Tang, Z. & Omekanda, A., 2003. Low-Vibration Design of Switched Reluctance Motors for Automotive Applications Using Modal Analysis. *IEEE Trans. Ind. Appl.*, 39(4), pp. 971-977.
- Cajander, D. & Le-Huy, H., 2006. Design and Optimization of a Torque Controller for a Switched Reluctance Motor Drive for Electric Vehicle by Simulation. *Mathematics and Computers in Simulation*, Volume 71, pp. 333-344.
- Cameron, D. E., Lang, J. H. & Umans, S. D., 1992. The Origin and Reduction of Acoustic Noise in Doubly Salient Variable-Reluctance Motors. *IEEE Trans. Ind. Appl.*, 26(6), pp. 1250-1255.
- Cao, X., Deng, Z., Yang, G. & Wang, X., 2009. Independent Control of Average Torque and Radial Force in Bearingless Switched-Reluctance Motors with Hybrid Excitations. *IEEE Trans. Power Electron.*, 24(5), pp. 1376-1385.
- Chan, C. C., 2007. The State of the Art of Electric, Hybrid, and Fuel Cell Vehicles. *Proc. IEEE*, 94(4), pp. 704-718.
- Chancharoensook, P. & Rahman, M. F., 2000. *Machine' s Characteristics Identification: A Preliminary Study on Direct Torque Control for Switched Reluctance Motor Drives*. presented at AUPEC' 2000 Conference, Brisbane, September 2000, pp. 132-137.
- Chancharoensook, P. & Rahman, M. F., 2002. *Dynamic Modeling of a Four-phase 8/6 Switched Reluctance Motor Using Current and Torque Look-up Tables*. in Proc. 28th Annual Conference of the Industrial Electronics Society, vol. 1, 2002, pp. 491-496.

- Chen, L. & Hofmann, W., 2006. *Analytically Computing Winding Currents to Generate Torque and Levitation Force of a New Bearingless Reluctance Motor*. in Proc. EPE-PEMC, Portoroz, Slovenia, Sep./Oct. 2006, pp. 1058-1063.
- Chen, L. & Hofmann, W., 2007. *Performance Characteristics of One Novel Switched Reluctance Bearingless Motor Drive*. in Proc. Power Convers. Conf., Nagoya, Japan, Apr. 2007, pp. 608-613.
- Chen, L. & Hofmann, W., 2010. *Design Procedure of Bearingless High-speed Switched Reluctance Motors*. in Proc. SPEEDAM, Pisa, Italy, Jun. 2010, 1442-1447.
- Chen, S.-L. & Hsu, C.-T., 2002. Optimal Design of a Three-Pole Active Magnetic Bearing System. *IEEE Trans. Magn.*, 36(5), pp. 3458-3466.
- Cheok, A. D. & Ertugrul, N., 2000. High Robustness and Reliability of Fuzzy Logic Based Position Estimation for Sensorless Switched Reluctance Motor Drives. *IEEE Trans. Power Electron.*, 15(2), pp. 319-334.
- Chiba, A. et al., 2005. *Magnetic bearings and bearingless drives*. : Elsevier's Science & Technology.
- De Doncker, R., et al. 2011. Advanced Electrical Drives, Power Systems. In: *Switched Reluctance Drive Systems*. : Springer Science+Business Media B.V., pp. 361-437.
- Earnshaw, S., 1842. On the nature of the molecular forces which regulate the constitution of the luminiferous ether. *Trans. Cambridge Phil. SOC.*, Volume 7, p. 79.
- Ehsani, M. & Fahimi, B., 2002. Elimination of Position Sensors in Switched Reluctance Motor Drives: State of the Art and Future Trends. *IEEE Trans. Ind. Electron.*, 49(1), pp. 40-47.
- Ellison, A. J. & Moore, C. J., 1968. Acoustic Noise and Vibration of Rotating Electric Machines. in *IEE Proc.*, 115(11), pp. 1633-1640.
- Fiedler, J. O., Kasper, K. A. & De Doncker, R. W., 2005. *Acoustic Noise in Switched Reluctance Drives: An Aerodynamic Problem?*. In Proc. IEEE Int. Electr. Mach. Drives Conf., May 2005, pp. 1275-1280.
- Gallegos-Lopez, G., Kjaer, P. C. & Miller, T. J. E., 1998. A New Sensorless Method for Switched Reluctance Motor Drives. *IEEE Trans. Ind. Appl.*, 34(4), pp. 832-840.
- Guan, Z., Lee, D.-H., Ahn, J.-W. & Zhang, F., 2011. *A Compensation Strategy of Suspending Force in Hybrid Type Stator Pole Bearingless Switched Reluctance Motor*. Electrical Machines and Systems (ICEMS), International Conference on, Aug 2011, pp. 1-6.
- Haarnoja, T., 2012. *Private discussion*. VTT, Espoo: 2012.

- Hannoun, H., Hilaiet, M. & Marchand, C., 2011. High performance current control of a switched reluctance machine based on a gain-scheduling PI controller. *Control Engineering Practice*, 19(11), pp. 1377-1386.
- Henriques, L. et al., 2000. Torque Ripple Minimization in a Switched Reluctance Drive by Neuro-Fuzzy compensation. *IEEE Trans. Magn.*, 36(5), pp. 3592-3594.
- Hongwei, G., Salmasi, F. R. & Ehsani, M., 2004. Inductance Model-Based Sensorless Control of the Switched Reluctance Motor Drive at Low Speed. *IEEE Trans. Power Electron.*, 19(6), pp. 1568-1573.
- Ho, W. K., Panda, S. K., Lim, K. W. & Huang, F. S., 1998. Gain-scheduling control of the Switched Reluctance Motor. *Control Eng. Pract.*, 6(2), pp. 181-189.
- Hudson, C. A., Lobo, N. S. & Krishnan, R., 2008. Sensorless Control of Single Switch-Based Switched Reluctance Motor Drive Using Neural Network. *IEEE Trans. Ind. Electron.*, 55(1), pp. 321-329.
- Jessi Sahaya Shanthi, L., Arumugam, R. & Taly, Y., 2012. A novel rotor position estimation approach for an 8/6 solid rotor switched reluctance motor. *Neural Computing & Applications*, 21(3), pp. 461-468.
- Laiho, A., Kalita, K., Tammi, K. & Garvey, S. D., 2011. *Dynamics of Bridge-Configured Built-in Force Actuator for Vibration Control in Four-pole Cage Induction Machine*. 18th International Congress on Sound & Vibration, Rio De Janeiro, Brazil July 2011, pp. 1-8.
- Laiho, A. et al., 2009. Electromechanical Interaction in Eccentric-Rotor Cage Induction Machine Equipped with a Self-Bearing Force Actuator. *Journal of System Design and Dynamics*, 3(4), pp. 519-529.
- Larminie, J. & Lowry, J., 2003. *Electric Vehicle Technology Explained*. : Wiley.
- Lee, J. W., Kim, H. S., Kwon, B. I. & Kim, B. T., 2004. New Rotor Shape Design for Minimum Torque Ripple of SRM Using FEM. *IEEE Trans. Magn.*, 40(2), pp. 754-757.
- Li, C. & Hofmann, W., 2012. Speed Regulation Technique of One Bearingless 8/6 Switched Reluctance Motor with Simpler Single Winding Structure. *IEEE Trans. Ind. Electron.*, 59(6), pp. 2592-2600.
- Li, J., Song, X. G., Choi, D. & Cho, Y. H., 2009. *Research on Reduction of Vibration and Acoustic Noise in Switched Reluctance Motors*. Advanced Electromechanical Motion Systems & Electric Drives Joint Symposium, 8th International Symposium on , pp.1-6, 1-3 July 2009.

- Lin, F. & Yang, S., 2007. Instantaneous Shaft Radial Force Control with Sinusoidal Excitations for Switched Reluctance Motors. *IEEE Trans. Energy Convers.*, 22(3), pp. 629-636.
- Liu, X., Pan, Z.-P. & Zhu, Z., 2010. Analysis of vibration reduction level in an 8/6 switched reluctance machine by active vibration cancellation. *Journal of Zhejiang University - Science C*, 11(10), pp. 808-816.
- Materu, P. & Krishnan, R., 1990. *Analytic Prediction of SRM Inductance Profile and Steady State-Average Torque*. in Proc. Conf. Rec., Ind. Applicat. Soc. Annu. Meeting, 1990, pp. 214-223.
- Matsumura, F., Okada, Y., Fujita, M. & Namerikawa, T., 1997. State of the Art of Magnetic Bearings. *JSME Int. J.*, 40(4), p. 553-560.
- Mese, E. & Torry, D. A., 2002. An Approach for Sensorless Position Estimation for Switched Reluctance Motors Using Artificial Neural Networks. *IEEE Trans. Power Electron.*, 17(1), pp. 66-75.
- Miller, T. J. E., 1993. *Switched Reluctance Motors and Their Control*. New York: Clarendon.
- Miller, T. J. E., 2001. *Electronic Control of Switched Reluctance Machines*. Oxford, U.K.: Newnes.
- Miller, T. J. E., 2002. Optimal Design of Switched Reluctance Motors. *IEEE Trans. Ind. Electron.*, 49(1), pp. 15-27.
- Miller, T. J. E. & McGlip, M., 1990. Nonlinear Theory of Switched Reluctance Motor for Rapid Computer-Aided Design. *Proc. Inst. Elect. Eng., pt B*, 137(6), pp. 337-347.
- Mir, S., Elbuluk, M. E. & Husain, I., 1999. Torque Ripple Minimization in Switched Reluctance Motors Using Adaptive Fuzzy Control. *IEEE Trans. Ind. Appl.*, 35(2), pp. 461-468.
- Morrison, C. R., Siebert, M. W. & Ho, E. J., 2008. Electromagnetic Forces in a Hybrid Magnetic-Bearing Switched-Reluctance Motor. *IEEE Trans. Magn.*, 44(12), pp. 4626-4638.
- Nordmann, R. & Aenis, M., 2004. Fault Diagnosis in a Centrifugal Pump Using Active Magnetic Bearings. *International Journal of Rotating Machinery*, 10(3), pp. 183-191.
- Petrus, V. et al., 2011. Comparative Study of Different Current Control Techniques for a 4-Phase 8/6 Switched Reluctance Machine. *Journal of Electrical and Electronics Engineering*, 4(1), pp. 173-178.

- Pires, A. J., Martins, J. F., Branco, P. J. & Dente, J. A., 2006. An Average Values Global Model for The Switched Reluctance Machine. *Mathematics and Computers in Simulation*, Volume 71, pp. 466-475.
- Pop, A.-C. et al., 2011. On the Firing Angles Control of a 8/6 Switched Reluctance Machine. *Journal of Electrical and Electronics Engineering*, 4(1), pp. 189-194.
- Rahman, K. M. et al., 2000. Advantages of Switched Reluctance Motor Applications to EV and HEV: Design and Control Issues. *IEEE Trans. Ind. Appl.*, 36(1), pp. 111-121.
- Ray, W. F. & Al-Bahadly, I. H., 1993. *Sensorless Methods for Determining the Rotor Position of Switched Reluctance Motors*. in Proc. EPE, Brighton 1993, vol 6, pp. 7-13.
- Rfajdus, P., Zrak, I. & Hrabovova, V., 2004. Analysis of the Switched Reluctance Motor (SRM) Parameters. *J. Elect. Eng.*, 55(7-8), pp. 195-200.
- Russa, K., Husain, I. & Elbuluk, M. E., 1998. Torque-Ripple Minimization in Switched Reluctance Machines Over a Wide Speed Range. *IEEE Trans. Ind. Appl.*, 34(5), pp. 1105-1112.
- Schweitzer, G., 2002. *Active magnetic bearings—chances and limitations*. Sydney, Australia, in Proc. IFTOMM 6th Int. Conf. Rotor Dyn., vol. 1.
- Schweitzer, G. & Maslen, E., 2009. *Magnetic Bearings -Theory, Design, and Application to Rotating Machinery*. Berlin, Germany: Springer Verlag.
- Soares, F. & Costa Branco, P. J., 2001. Simulation of a 6/4 Switched Reluctance Motor Based on Matlab/Simulink Environment. *IEEE Trans. Aerosp. Electron. Syst.*, 37(3), pp. 989-1009.
- SRDrives Ltd., 2010. *Switched Reluctance Drives by Nidec Corp.*. [Online] Available at: www.srdrives.com [Accessed 23 April 2012].
- Stefanovic, V. R. & Vukosavic, S., 1991. SRM Inverter Topologies: A Comparative Evaluation. *IEEE Trans. Ind. Appl.*, 27(6), pp. 1034-1047.
- Takemoto, M., Chiba, A. & Fukao, T., 2001. A Method of Determining the Advanced Angle of Square-Wave Currents in a Bearingless Switched Reluctance Motor. *IEEE Trans. Ind. Appl.*, 37(6), pp. 1702-1709.
- Takemoto, M. et al., 2001. Improved Analysis of a Bearingless Switched Reluctance Motor. *IEEE Trans. Ind. Appl.*, 37(1), pp. 26-34.
- Tammi, K., 2007. *Active control of radial rotor vibrations: Identification, feedback, feedforward, and repetitive control methods*, Helsinki University of Technology, Department of Automation: Doctoral Dissertation, pp. 1-165.

Tammi, K., 2009. Active Control of Rotor Vibrations by Two Feedforward Control Algorithms. *Journal of Dynamic Systems, Measurement, and Control*, Volume 131, pp. 1-10.

Toliyat, H. A. & Kliman, G. B., 2004. *Handbook of Electric Motors*. New York: Marcel Dekker.

Wu, C. Y. & Pollock, C., 1995. Analysis and Reduction of Acoustic Noise in the Switched Reluctance Drive. *IEEE Trans. Ind. Appl.*, 31(6), pp. 91-98.

Xue, X. D., Cheng, K. W. E. & Cheung, N., 2008. *Selection of Electric Motor Drives for Electric Vehicles*. in Proc. AUPEC, Sidney, Australia 2008, pp. 1-6.

Yeadon, W. H. & Yeadon, A. W., 2001. *Handbook of Small Electric Motors*. New York: McGraw-Hill.

Appendix A: Specific Simulink model

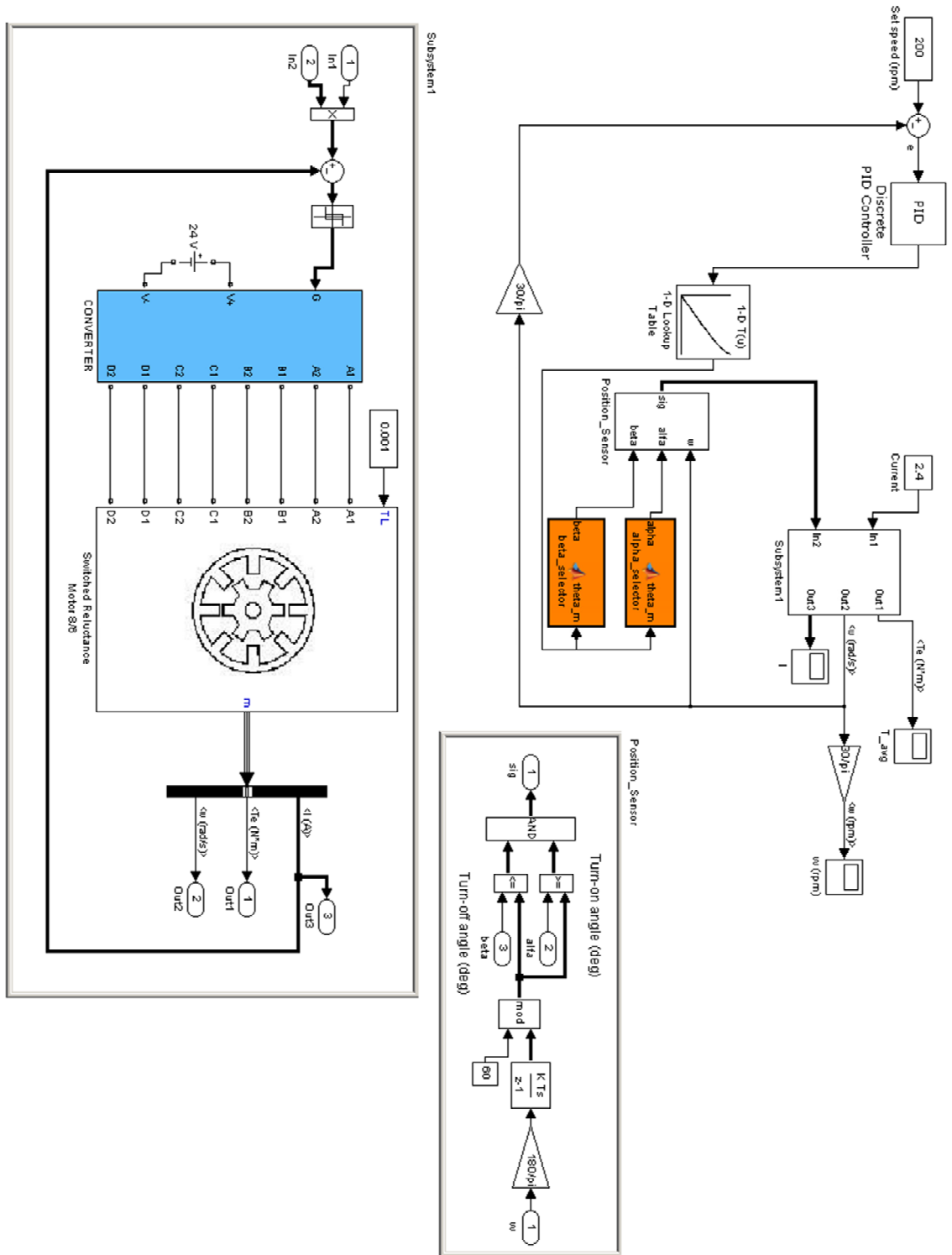


Figure A. MATLAB Simulink model with build-in SRM block and power electronics.

Appendix B: Simplified Simulink model

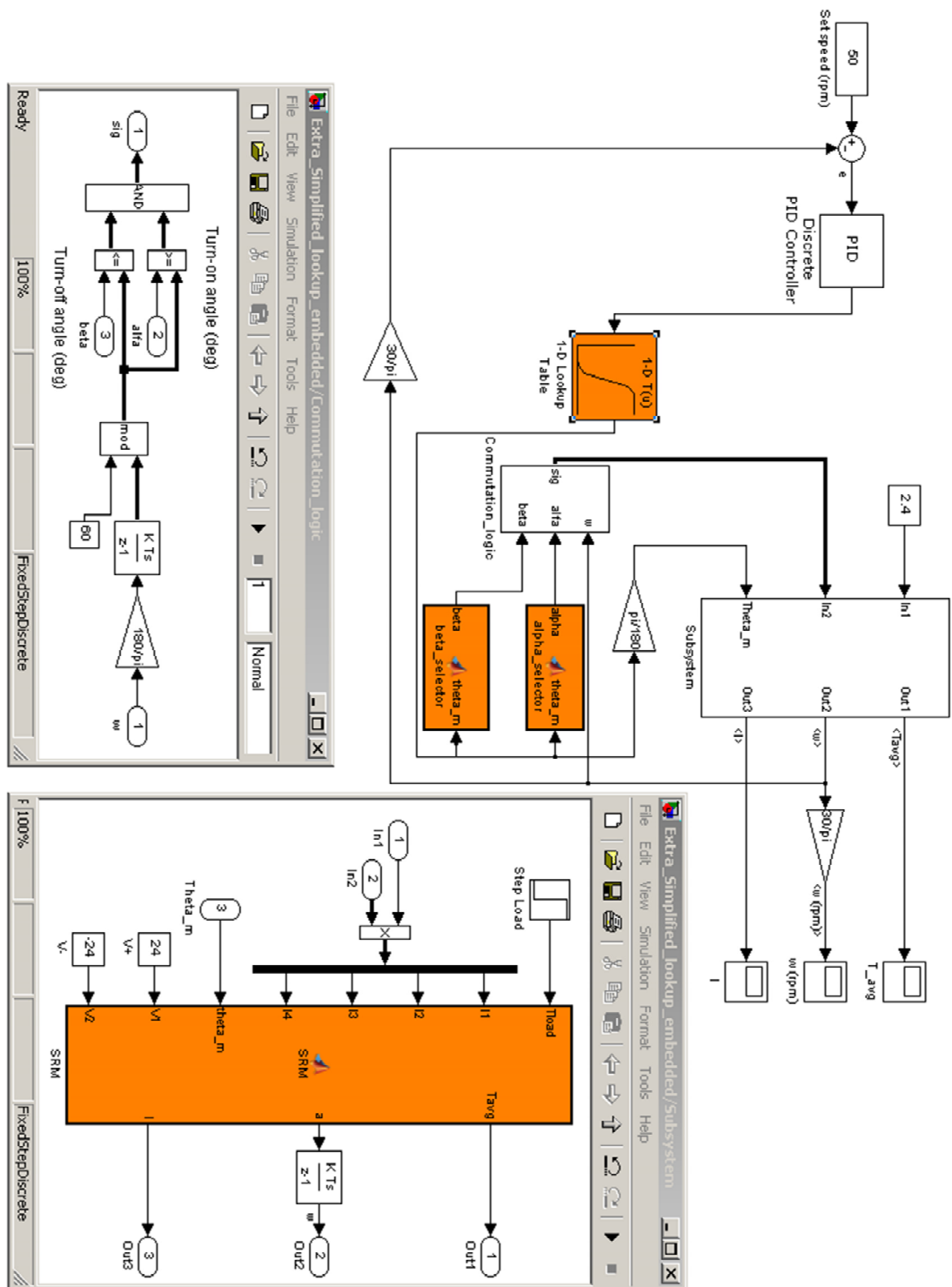


Figure B. The Simulink model of the SRM speed control. The model is simplified to make the conversion to LabVIEW possible. All the levels are visible. The darkened blocks contain source code

Appendix C: Simulink model converted to LabVIEW

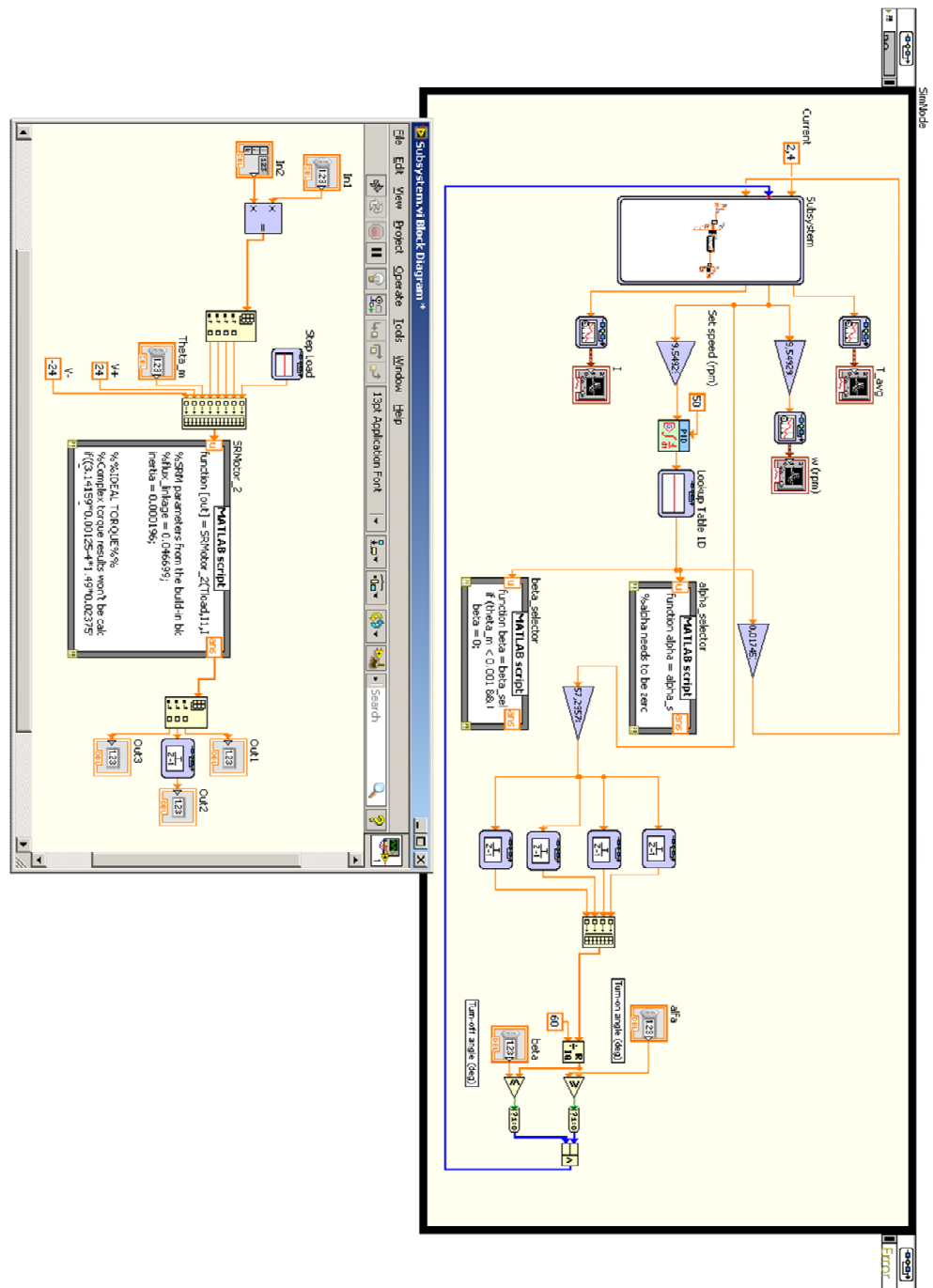
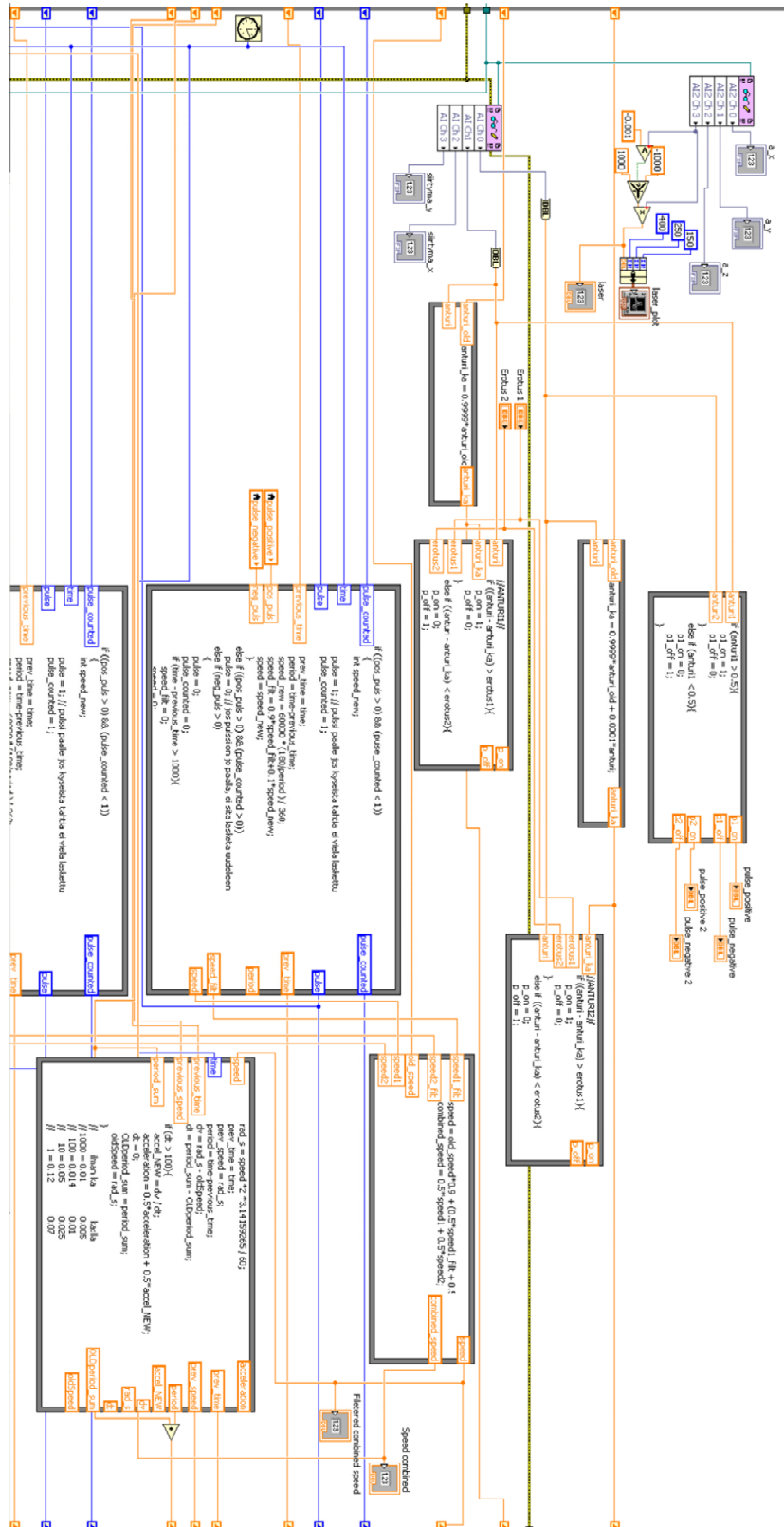
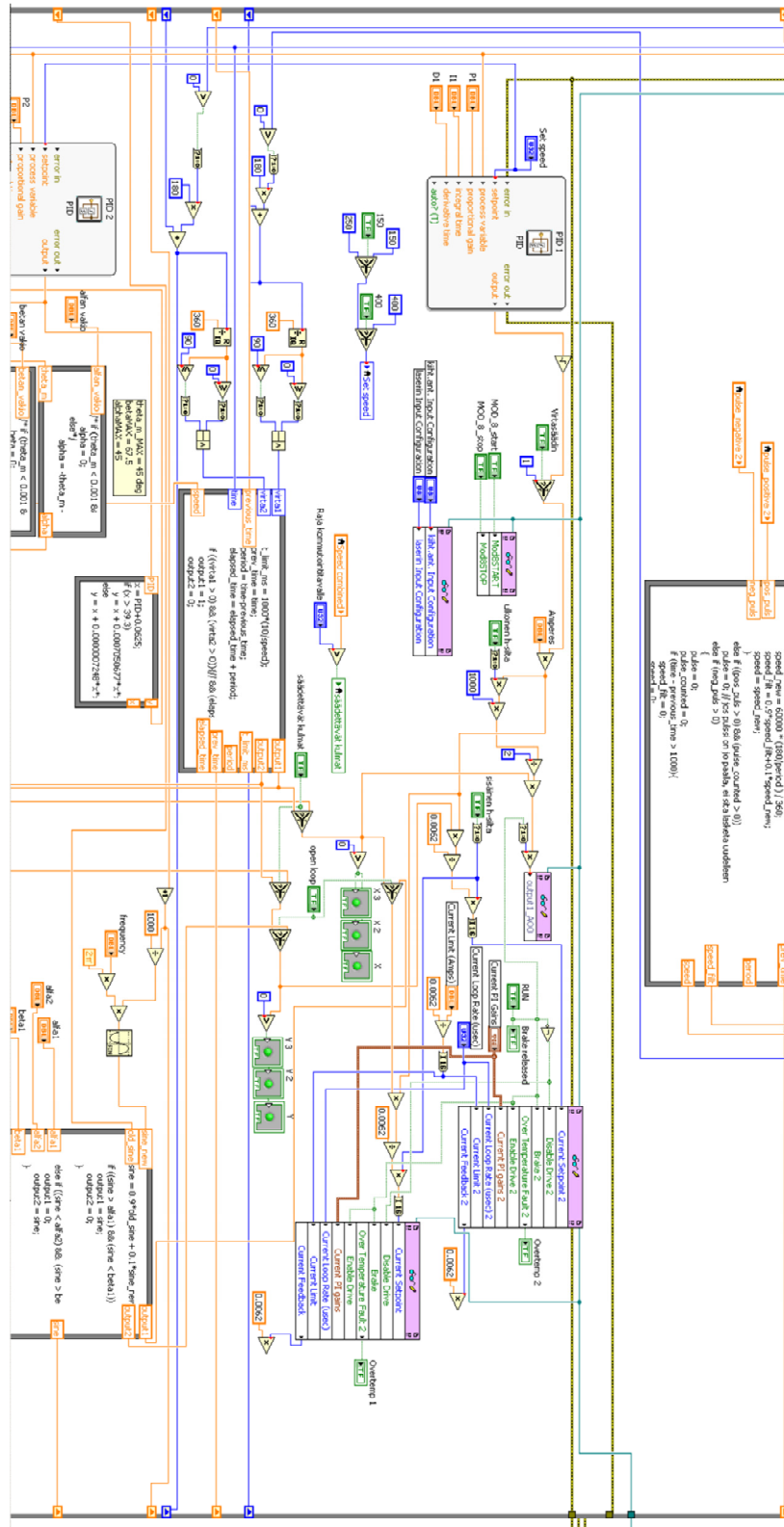


Figure C. LabVIEW VI of the simplified Simulink model after modifications in LabVIEW end to make the model to compile.

Appendix D: Real-time part of the LabVIEW VI used for controlling the SRM, page 1/3



Appendix D: Real-time part of the LabVIEW VI used for controlling the SRM, page 2/3



controlling the SRM, page 3/3

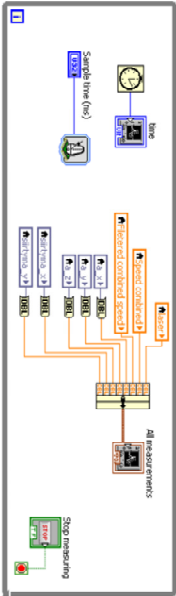
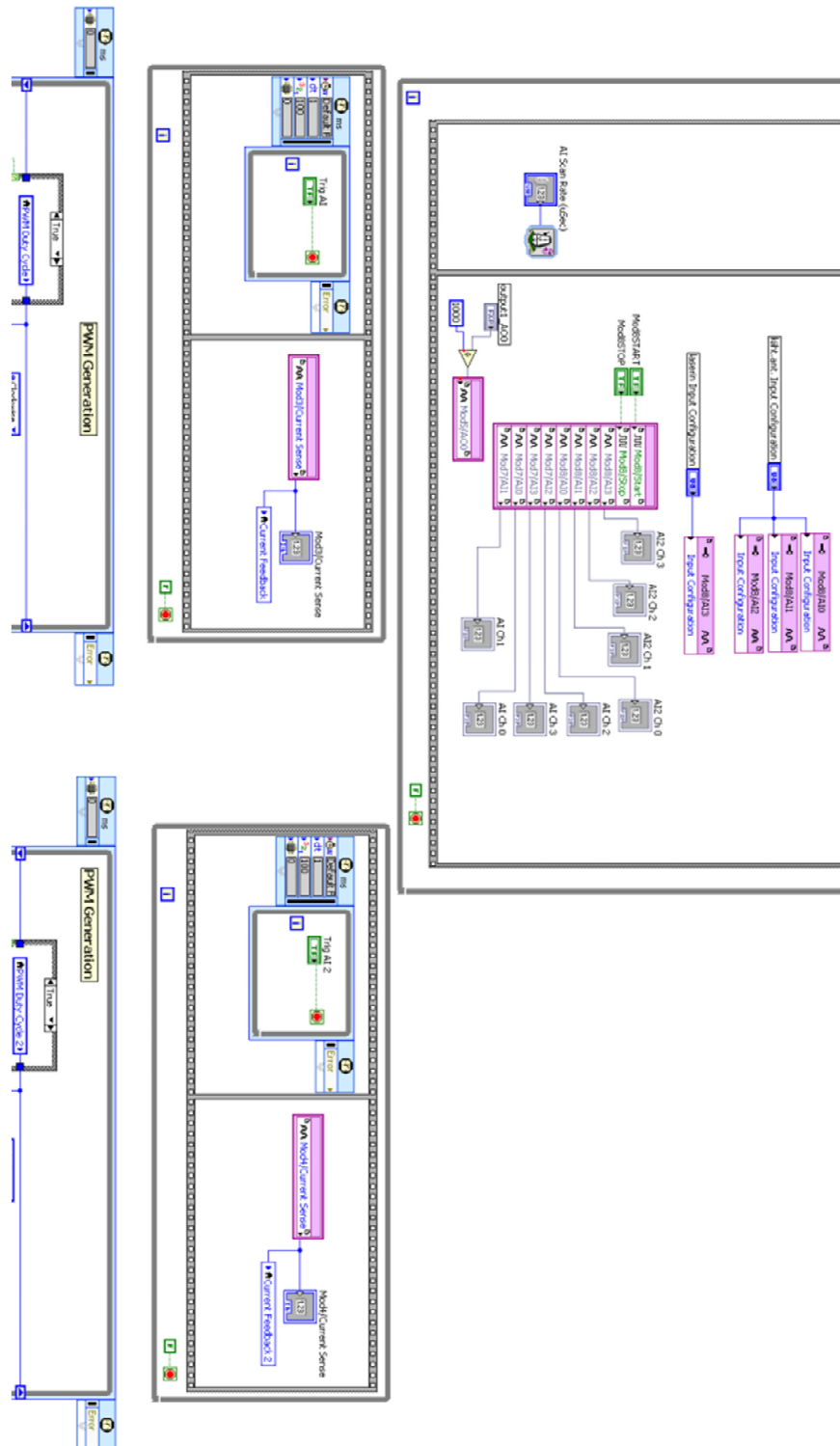


Figure D. LabVIEW block diagram that is used for controlling a 4/2 type switched reluctance motor. This is the real-time part of the control system. Most of the functionalities are implemented in here.

Appendix E: FPGA part of the LabVIEW VI used for controlling the SRM, page 1/2



Appendix E: FPGA part of the LabVIEW VI used for controlling the SRM, page 2/2

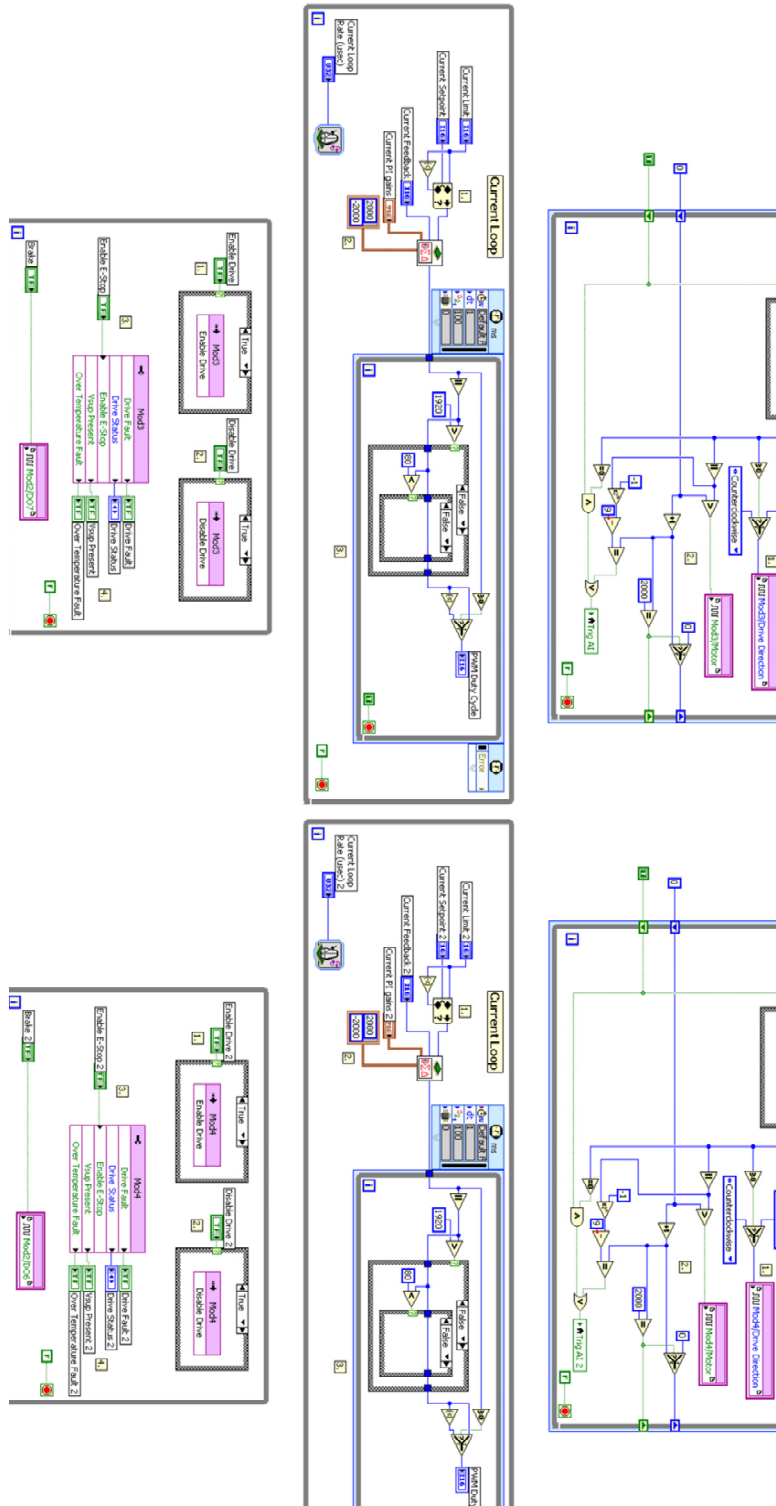


Figure E. The FPGA portion of the LabVIEW block diagram that is used for controlling a 4/2 type switched reluctance motor. In FPGA is included the most time critical tasks.

Appendix F: Error budget for pure mathematical model error, page 1/2

	Takemoto	
<i>Educational version, for training usage only!</i>		
Takemoto Matemaattisen mallin virhe. Malli ei huomioi suhteellista eroa testilaitteeseen.		
Model Equation: $T = ((2 * \text{sqr}(N_p) * \text{sqr}(i)) / \pi) * (((\mu_0 * l_{stk} * r_{gap}^2 * \theta_m * (\pi / 180)) / l_{gap}) + ((4 * \mu_0 * l_{stk}) / \pi) * (\ln((\pi * l_{gap} - 4 * c * r_{gap} * ((-\pi / 4) + \theta_m * (\pi / 180))) / ((\pi * l_{gap} - 4 * c * r_{gap} * ((-\pi / 4) - \theta_m * (\pi / 180)))))))$		
List of Quantities:		
Quantity	Unit	Definition
T	Nm	Output torque
N _p		Number of rotations in a coil
i	A	Current
π		
μ ₀	Vs/Am	Permeability of air
l _{stk}	m	Length of the stator stack
r _{gap}	m	Radius of the rotor
θ _m	rad	Advanced angle
l _{gap}	m	Length of the air gap
c		Constant of 1.49
N_p: Type B rectangular distribution Value: 30 Halfwidth of Limits: 1		
i: Type B rectangular distribution Value: 4 A Halfwidth of Limits: 0.00000001 A		
π: Constant Value: 3.1415926535898		
μ₀: Constant Value: 0.0000012566 Vs/Am		
l_{stk}: Type B rectangular distribution Value: 0.065 m Halfwidth of Limits: 0.002 m		
r_{gap}: Type B rectangular distribution Value: 0.02375 m Halfwidth of Limits: 0.001 m		
θ_m: Type B rectangular distribution Value: 45 rad Halfwidth of Limits: 0.000001 rad		
<i>Educational version, for training usage only!</i>		
Date: 05/19/2012	File: Takemoto.smu	Page 1 of 2

Appendix F: Error budget for pure mathematical model error, page 2/2

	Takemoto					
Educational version, for training usage only!						
I_{gap} :		Type B rectangular distribution Value: 0.00125 m Halfwidth of Limits: 0.0001 m				
c:		Constant Value: 1.49				
Uncertainty Budgets:						
T:		Output torque				
Quantity	Value	Standard Uncertainty	Distribution	Sensitivity Coefficient	Uncertainty Contribution	Index
N_p	30.000	0.577	rectangular	$1.2 \cdot 10^{-3}$	$710 \cdot 10^{-6}$ Nm	27.1 %
i	4.000000000000 A	$5.77 \cdot 10^{-9}$ A	rectangular	$9.2 \cdot 10^{-3}$	$53 \cdot 10^{-12}$ Nm	0.0 %
π	3.1415926535898					
μ_0	$1.2566 \cdot 10^{-6}$ Vs/Am					
l_{stk}	0.06500 m	$1.15 \cdot 10^{-3}$ m	rectangular	0.28	$330 \cdot 10^{-6}$ Nm	5.8 %
r_{gap}	0.023750 m	$577 \cdot 10^{-6}$ m	rectangular	0.90	$520 \cdot 10^{-6}$ Nm	14.5 %
θ_m	45.0000000000 rad	$577 \cdot 10^{-9}$ rad	rectangular	$-110 \cdot 10^{-6}$	$-66 \cdot 10^{-12}$ Nm	0.0 %
l_{gap}	$1.2500 \cdot 10^{-3}$ m	$57.7 \cdot 10^{-6}$ m	rectangular	-17	$-990 \cdot 10^{-6}$ Nm	52.6 %
c	1.49					
T	0.01848 Nm	$1.37 \cdot 10^{-3}$ Nm				
Results:						
Quantity	Value	Expanded Uncertainty	Coverage factor	Coverage		
T	0.0185 Nm	$2.7 \cdot 10^{-3}$ Nm	2.00	95% (normal)		
Educational version, for training usage only!						
Date: 05/19/2012	File: Takemoto.smu					Page 2 of 2

Generated with GUM Workbench Edu Version 2.4.1.384

Figure F. Error budget for pure mathematical model error.

Appendix G: Error budget for difference between the simulation model and the test setup, page 1/2

Takemoto

Educational version, for training usage only!

Takemoto

Matemaattisen mallin virhe suhteessa testilaitteeseen.

Model Equation:

$$T = ((2 * \text{sqr}(N_p) * \text{sqr}(i)) / \pi) * (((\mu_0 * l_{stk} * r_{gap}^2 * \theta_m * (\pi / 180)) / l_{gap}) + ((4 * \mu_0 * l_{stk}) / \pi) * (\ln((\pi * l_{gap} - 4 * c * r_{gap} * ((-\pi / 4) + \theta_m * (\pi / 180))) / ((\pi * l_{gap} - 4 * c * r_{gap} * ((-\pi / 4) - \theta_m * (\pi / 180)))))))$$

List of Quantities:

Quantity	Unit	Definition
T	Nm	Output torque
N _p		Number of rotations in a coil
i	A	Current
π		
μ ₀	Vs/Am	Permeability of air
l _{stk}	m	Length of the stator stack
r _{gap}	m	Radius of the rotor
θ _m	deg	Advanced angle
l _{gap}	m	Length of the air gap
c		Constant of 1.49

N_p:

Type B rectangular distribution

Value: 30

Halfwidth of Limits: 1

i:

Type B rectangular distribution

Value: 4 A

Halfwidth of Limits: 0.5 A

π:

Constant

Value: 3.1415926535898

μ₀:

Constant

Value: 0.0000012566 Vs/Am

l_{stk}:

Type B rectangular distribution

Value: 0.065 m

Halfwidth of Limits: 0.002 m

r_{gap}:

Type B rectangular distribution

Value: 0.02375 m

Halfwidth of Limits: 0.001 m

θ_m:

Type B rectangular distribution

Value: 34 deg

Halfwidth of Limits: 10 deg

Educational version, for training usage only!

Date: 05/19/2012

File: Takemoto_2.smu

Page 1 of 2

Appendix G: Error budget for difference between the simulation model and the test setup, page 2/2

Takemoto

Educational version, for training usage only!

I_{gap} :

Type B rectangular distribution

Value: 0.00125 m

Halfwidth of Limits: 0.00011 m

c:

Constant

Value: 1.49

Uncertainty Budgets:

T:

Output torque

Quantity	Value	Standard Uncertainty	Distribution	Sensitivity Coefficient	Uncertainty Contribution	Index
N_p	30.000	0.577	rectangular	$1.0 \cdot 10^{-3}$	$580 \cdot 10^{-6}$ Nm	2.9 %
i	4.000 A	0.289 A	rectangular	$7.6 \cdot 10^{-3}$	$2.2 \cdot 10^{-3}$ Nm	41.5 %
π	3.1415926535898					
μ_0	$1.2566 \cdot 10^{-6}$ Vs/Am					
l_{stk}	0.06500 m	$1.15 \cdot 10^{-3}$ m	rectangular	0.23	$270 \cdot 10^{-6}$ Nm	0.6 %
r_{gap}	0.023750 m	$577 \cdot 10^{-6}$ m	rectangular	0.71	$410 \cdot 10^{-6}$ Nm	1.4 %
θ_m	34.00 deg	5.77 deg	rectangular	$400 \cdot 10^{-6}$	$2.3 \cdot 10^{-3}$ Nm	47.1 %
l_{gap}	$1.2500 \cdot 10^{-3}$ m	$63.5 \cdot 10^{-6}$ m	rectangular	-13	$850 \cdot 10^{-6}$ Nm	6.4 %
c	1.49					
T	0.01511 Nm	$3.39 \cdot 10^{-3}$ Nm				

Results:

Quantity	Value	Expanded Uncertainty	Coverage factor	Coverage
T	0.0151 Nm	$6.8 \cdot 10^{-3}$ Nm	2.00	95% (normal)

Educational version, for training usage only!

Date: 05/19/2012

File: Takemoto_2.smu

Page 2 of 2

Generated with GUM Workbench Edu Version 2.4.1.384

Figure G. Error budget for difference between the simulation model and the test setup.